



Layer-by-layer capsules of hyaluronic acid as potential drug carriers: synthesis, characterization and manipulation the propertis

Anna Szarpak

► To cite this version:

Anna Szarpak. Layer-by-layer capsules of hyaluronic acid as potential drug carriers: synthesis, characterization and manipulation the propertis. Chemical Sciences. Université Joseph-Fourier - Grenoble I, 2009. English. NNT: . tel-00442324

HAL Id: tel-00442324

<https://theses.hal.science/tel-00442324>

Submitted on 19 Dec 2009

HAL is a multi-disciplinary open access archive for the deposit and dissemination of scientific research documents, whether they are published or not. The documents may come from teaching and research institutions in France or abroad, or from public or private research centers.

L'archive ouverte pluridisciplinaire **HAL**, est destinée au dépôt et à la diffusion de documents scientifiques de niveau recherche, publiés ou non, émanant des établissements d'enseignement et de recherche français ou étrangers, des laboratoires publics ou privés.

UNIVERSITE JOSEPH FOURIER – GRENOBLE I

THÈSE

Pour obtenir le grade de :

DOCTEUR DE L'UNIVERSITE JOSEPH FOURIER

(Arrêtés ministériels du 5 juillet 1984 et 30 mars 1992)

Spécialité: SCIENCES DES POLYMERES

Présentée par

Anna SZARPAK

Layer-by-Layer capsules of hyaluronic acid as potential drug carriers: synthesis, characterization and manipulating the properties

Date de la soutenance: 26 Mai 2009

COMPOSITION DU JURY :

Mme. Claudine FILIATRE	Rapporteur
M. Jean-Claude VOEGEL	Rapporteur
Mme. Rachel AUZELY-VELTY	Directeur de thèse
Mme. Catherine PICART	Examineur
M. Bruno De Geest	Examineur
M. Adam PRON	Examineur

ACKNOWLEDGMENTS

To my supervisor prof. Rachel Auzély-Velty for the reception in her workgroup, advice, positive feedback, giving me freedom to explore my ideas and support in the all good and difficult scientific moments.

To Serge Perez for giving the chance to do a PhD.

To director Reduane Borsali for the opportunity of work in the CERMAV laboratory.

I give special thanks to Catherine Picart for her expertise in QCM-D and many discussions and invaluable advice, also many thanks for Thomas and Claire.

To Isabelle Pignot-Paintrand, Daniele Dupeyre, Cecile Cottet, Frédéric Charlot for the help with microscopic techniques. Many hours of work, often boring hours in the dark, but what results! Thank you Isabelle. Thanks to Frédéric Dubreuil for AFM studies.

To Karim, for his reception when I first arrived in Grenoble (50 kilos of baggage, thanks for help), for teaching me molecular modelling and the coffee breaks when the PC crashed!

To Shirin Kadi and Caroline Creuzet for the introduction into the wet lab, correcting my French and help whenever I needed it.

To Helene, Carol and Eric.... for their company “in the open air”!

To Di Cui, Xia Miao and Jing Jing, the colleagues from the office, thank you my dears for each smile at the beginning of the day.

To all my friends in CERMAV: Peter, Michael, Alexandra, Karoline, Roberto, Sahra, Mialy, I will miss you all!

To my special friends from inside and outside of CERMAV: Lina, Camelia, Oznur, Elif, Joaquim and Ananda for all the time we shared, happy, sad, crazy moments, thank you for all the “attractions”, thank you for being with me.

To Charles for showing me the world different than it was in my reality.

To my family for confidence in me, for all the hours on the phone we spent together (especially my mum and Magda), by this way I could be more close to you.

To my Polish friend Malgosia, a special person who always gives me a positive energy, strength, and hope for a better future. Even if it is rainy, you know how to send me the ray of the sunshine. Thank you.

To everybody who has contributed in some way to the development of this work.
Thank you for the Marie Curie financial support.

Thank you for all who I met in CERMAV, Grenoble and France, you and this place will be always exceptional for me, I hope to come back often, see you next ski season!

Introduction (en)

The administration of drugs is often limited by problems of insolubility, inefficient distribution, enzymatic hydrolysis, lack of selectivity and side-effects leading to health concerns. During the past decades, a large variety of micro- and nanocarriers have been developed in order to improve efficiency, availability and toxicity profiles of drugs. Among the currently available carrier systems, hollow capsules prepared by the layer-by-layer (LbL) assembly of oppositely charged polyelectrolytes on a colloidal template, followed by its decomposition, have recently emerged as attractive vehicles in the field of drug delivery. These capsules possess a fascinating multicompartment structure, with the possibility to introduce a high degree of functionality within their nanoshell. This in particular may allow the development of original drug vehicles with controlled encapsulation and triggered-release properties. Indeed, the shell can be designed to efficiently respond to various environmental changes, allowing the programmed release of active substances contained within the capsule. The literature data show a large interest in the design of such systems. Hollow nano-/microcapsules with desired shape, size, shell thickness and tuned permeability properties are reported. To date, the most studied capsules are of poly(allylamine)/poly(styrenesulfonate) (PAH/PSS). In spite of the advantages of biocompatibility, biodegradability and in some cases, bioactivity that can be offered by polysaccharides for biological applications, very little research has been devoted to the design of multicompartment systems based on polysaccharides. This can be explained by the strong hydrophilic character of these polymers, difficulties related to their structural and macromolecular characterization and their tendency to lead to “soft” and highly hydrated planar films.

For drug delivery applications, a prerequisite is to use biocompatible polyelectrolytes for the construction of the nanoshell. Capsules should also be designed to exhibit drug encapsulation and release properties well-suited to the required therapeutic application. In this context, polysaccharides showing biocompatibility, biodegradability and non toxicity appear as good candidate materials. Compared to planar films made from polysaccharides, little is known about capsules made from biopolymers. A few reported examples of capsules built mainly from alginate, dextran and chitosan suggest some difficulties in the fabrication of stable capsules, by comparison with synthetic polymers. Their exposure to solvents, pH and

ionic strength can thus affect the structural integrity of the multilayer assembly. In addition, the choice of a suitable colloidal template and the dissolution protocol, are crucial in the formation of capsules from polysaccharides in order to maintain their integrity. The harsh conditions (0.1 N HCl, 1M HF, THF) generally used for the preparation of synthetic polyelectrolyte capsules are not suitable in the case where oppositely charged polysaccharides used to form the nanoshell are weak polyelectrolytes and not chemically cross-linked. Furthermore, biocompatible cores would be preferable in the case of biological applications.

In this context, the main objective of this work was to develop new LbL capsules made from hyaluronic acid, a biocompatible and biodegradable polysaccharide. Due to its natural presence in the human body and the large number of possible chemical modifications of HA for specific purposes, such as cross-linking, grafting of drugs or cage molecules, capsules made from HA possess a great potential in the controlled delivery of drugs. Research on this topic was carried out in “Structure and functions of polysaccharides” group in the CERMAV-CNRS laboratory. This team has been working on the characterization and chemical modification of hyaluronic acid for more than ten years. Combining the intrinsic properties of polysaccharides with those provided by grafted molecules may lead to new applications for such nanoshell-based systems.

Based on these considerations, the first step of this work was thus to establish the feasibility to prepare capsules from HA. For this purpose, we proposed to use PAH as the polycationic partner as much is known from its behaviour in capsules made of synthetic polyelectrolytes. Having developed suitable conditions for the synthesis of HA/PAH nanoshells, we then focused on the replacement of PAH by biocompatible cationic polymers. We thus selected a polypeptide, poly (L-lysine) (PLL), and a chitosan derivative bearing cationic groups (QCH) as partners of HA. The resulting capsules were then investigated in terms of morphology as well as model drug encapsulation and release properties.

This thesis manuscript is divided in to four sections:

The first chapter deals with the application of the LbL technique to the synthesis of micro-/nanocapsules, and especially those made of polysaccharides. Promising applications of these multicompartiment systems are demonstrated suggesting the need to develop methods for the synthesis of biopolymer microcapsules in a mild, effective and reproducible manner.

The experimental techniques used in this work are described in Chapter 2. Materials used and techniques applied to characterize the polyelectrolyte complexes, LbL planar films and hollow capsules are described.

In the third chapter the synthesis of the LbL hollow capsules based on hyaluronic acid is presented. The optimization of conditions such as the choice of suitable template, molecular weight and concentration of HA for multilayer deposition are considered. High dependence of capsule morphology on the preparation conditions is shown. The problem of core dissolution from HA/poly(allylamine) (PAH) coating without, and after, shell cross-linking is also described.

The fourth chapter compares capsules made from HA and the biocompatible polycationic partners, PLL and QCH. The sharp analysis of HA/PAH, HA/PLL and HA/QCH complexes in the bulk, on the planar surface, and porous spherical template will be shown. The key properties of these capsules as potential drug carriers i.e. permeability to small molecules and enzymatic degradation are deeply investigated. Differences related to the multilayer structures between all types of HA/PAH, HA/PLL and HA/QCH capsules are also highlighted and show that capsule formation based on HA depends strongly on the cationic partner. Chemical cross-linking of the shells allows one to improve not only their stability but also their permeability properties. After optimization of the conditions required to produce impermeable shells, the encapsulation and controlled release of small molecules of dextran at molecular size of $\sim 2\text{nm}$, as a model drug, is presented.

Introduction (fr)

L'index thérapeutique des substances médicamenteuses est souvent limité par des problèmes d'insolubilité, de sensibilité à l'hydrolyse enzymatique, de manque de sélectivité vis-à-vis du site visé ainsi que d'effets secondaires. Au cours de ces dernières décennies, divers types de micro-et nano-capsules ont été développés dans le but de modifier la pharmacodynamie de substances biologiquement actives tout en essayant de minimiser leur éventuel effet toxique. Parmi ces systèmes, les capsules creuses préparées par assemblage couche-par-couche de polymères de charges opposées sur un support colloïdal chargé, suivi de sa décomposition, suscitent un intérêt croissant depuis leur introduction il y a une dizaine d'années. La paroi de ces capsules "multicompartmentes" est donc constituée d'un film multicouche de polymères permettant d'introduire diverses fonctionnalités. La capacité de la paroi à répondre efficacement à des sollicitations environnementales diverses, peut en particulier être avantageusement mise à profit pour libérer de manière programmée des substances actives encapsulées. De nombreux exemples de nano / microcapsules multicouches différant par la forme, la taille, les constituants et fonctionnalités de la paroi ont été décrits dans la littérature. À ce jour, les capsules les plus étudiées sont préparées à partir de poly(allylamine)/poly(styrènesulfonate) (PAH/PSS). En dépit des avantages en termes de biocompatibilité, biodégradabilité, et bioactivité, que peuvent offrir les polysaccharides pour des applications biologiques, peu de travaux ont été consacrés à la conception de tels systèmes multicompartmentes, utilisant des polysaccharides. Ceci s'explique en partie par le caractère hydrophile de ces polymères, les difficultés liées à la caractérisation structurale et macromoléculaire difficile de ces macromolécules et leur tendance à former des films "mous" fortement hydratés.

L'utilisation de polymères biocompatibles s'avère nécessaire pour l'élaboration de capsules destinées à des applications pharmaceutiques. Celles-ci doivent par ailleurs présenter des propriétés d'encapsulation et de libération bien adaptées à la cible thérapeutique. Dans ce contexte, les polysaccharides apparaissent comme de bons candidats pour la conception de ces nouveaux transporteurs de principes actifs. Contrairement aux multicouches planes réalisées à partir de polysaccharides, il existe à ce jour peu de données sur les capsules préparées par assemblage couche-par-couche de polysaccharides chargés. Des

exemples de capsules construites principalement à partir d'alginate, dextrans et de chitosane suggèrent quelques problèmes de stabilité par rapport à leurs homologues constitués de polymères synthétiques. L'exposition aux solvants, au pH et à la force ionique peut affecter l'intégrité de la structure multicouche. En outre, le choix d'un support colloïdal, ainsi que le protocole de dissolution de celui-ci, sont essentiels à la formation et au maintien de l'intégrité des capsules de polysaccharides. Les conditions assez drastiques (0,1 N HCl, HF 1M, THF), généralement utilisées pour la préparation de capsules de polymères synthétiques ne sont pas appropriées à la synthèse de capsules de polysaccharides. En outre, l'utilisation de telles capsules pour des applications biologiques passe par l'utilisation de supports colloïdaux biocompatibles.

Dans ce contexte, l'objectif principal de ce travail était de développer de nouvelles capsules multicouches à partir d'acide hyaluronique, un polysaccharide biocompatible et biodégradable. Grâce à sa présence naturelle dans le corps humain et à aux nombreuses possibilités de modifications chimiques de ce polysaccharide (réticulation chimique, greffage de médicaments), des capsules issues de ce polymère laissent envisager des applications intéressantes pour le transport de principes actifs. Le travail décrit dans ce mémoire a été réalisé au sein de l'équipe "Structure et fonctions des polysaccharides" du CERMAV-CNRS. Une partie de l'activité de cette équipe concerne la caractérisation et la modification chimique de l'acide hyaluronique, activité qui a débutée il y a plus de dix ans.

Sur la base de ces considérations, la première étape de ce travail a donc consisté à mettre en évidence la faisabilité de préparer des capsules à base de HA. À cette fin, nous avons dans un premier temps utilisé le PAH en tant que partenaire polycationique puisque beaucoup de données sont disponibles sur les capsules préparées à partir de ce polymère. Nous nous sommes ensuite proposés de remplacer le PAH par des polymères cationiques biocompatibles. Nous avons donc sélectionné un polypeptide, la poly (L-lysine) (PLL), et un polysaccharide dérivé de chitosane portant des groupements cationiques (QCH) comme partenaires du HA. Les capsules ont ensuite été étudiées en ce qui concerne leur morphologie ainsi que pour leur propriétés d'encapsulation et de libération de médicaments.

Ce manuscrit de thèse est divisé en quatre chapitres :

Le premier chapitre traite des stratégies de synthèse des micro-/nanocapsules multicouches. Des applications prometteuses de ces systèmes multicompartiments montrent la nécessité de développer des méthodes de synthèse de microcapsules à base de biopolymères, efficaces et reproductibles.

Les techniques expérimentales utilisées dans ce travail sont décrites dans le chapitre 2. Nous présentons les matériaux utilisés, les techniques appliquées pour caractériser les polyélectrolytes complexes, les multicouches planes ainsi que les capsules.

Dans le troisième chapitre, la synthèse de capsules utilisant l'acide hyaluronique est présentée. L'optimisation des conditions telles que le choix du support, la masse molaire et la concentration du HA pour les dépôts multicouches sont développés. Nous montrons que la morphologie des capsules est fortement dépendante des conditions de préparation.

Le quatrième chapitre compare les capsules en fonction des partenaires polycationiques (PLL et QCH) du HA. L'analyse porte sur les complexes HA/PAH, HA/PLL et HA/QCH en solution, sur des surfaces planes et sur un support sphérique et poreux. Les principales propriétés de ces capsules comme vecteur de médicament (perméabilité aux petites molécules, dégradation enzymatique) sont étudiées. Nous montrons que les différences entre les types de capsules HA/PAH, HA/PLL et HA/QCH sont liées à la structure du film multicouche. Sa réticulation chimique permet par ailleurs d'améliorer non seulement la stabilité, mais aussi les propriétés de perméabilité des capsules. Après la mise au point de capsules imperméables aux petites molécules, l'encapsulation de petites molécules de dextrane comme modèles de médicaments est présentée.

TABLE OF CONTENTS

CHAPTER 1

LBL CAPSULES MADE FROM POLYSACCHARIDES -

BIBLIOGRAPHY REVIEW.....1

1.1. RÉSUMÉ (FR).....	3
1.2. INTRODUCTION	5
1.3. LAYER-BY-LAYER (LBL) TECHNIQUE.....	6
1.4. APPLICATION OF THE LBL TECHNIQUE TO THE SYNTHESIS OF MICROCAPSULES	9
1.4.1. Principle of synthesis	10
1.4.2. Template.....	11
1.4.3. Interactions used for multilayer construction.....	13
1.5. APPLICATIONS OF THE LBL BASED CAPSULES	15
1.5.1. Drug delivery.....	15
a) Encapsulation	15
b) Surface modification	20
c) Release	23
1.5.2. Microreactors	27
1.5.3. Microsensors	29
1.5.4. Semiconductors	32
1.5.5. Waveguides	32
1.5.6. Capsules in nutrition.....	33
1.6. CAPSULES MADE FROM POLYSACCHARIDES	33
1.7. HYALURONIC ACID	37
1.7.1. Structure	37
1.7.2. Chemical modification	39
1.7.3. Occurrence in the living organism and its functions.....	40
1.7.4. Applications	42
1.8. Conclusion.....	43
References.....	45

CHAPTER 2

MATERIALS AND METHODS.....55

2.1. CHEMICALS.....	57
2.2. LBL CAPSULES	58
2.2.1. Synthesis.....	58
2.2.2. Chemical cross-linking.....	58
2.2.3. Permeability	58
2.2.4. Enzymatic degradation.....	59
2.2.5. Encapsulation and release	60
2.3. CHARACTERIZATION METHODS AND EXPERIMENTAL PROTOCOLS	60
2.3.1. Microscopy techniques.....	60
a) Scanning Electron Microscopy (SEM)	60

b) Confocal Laser Scanning Microscopy (CLSM)	62
c) Transmission Electron Microscopy (TEM)	64
d) Atomic Force Microscopy (AFM).....	66
2.3.2. Fourier Transform Infrared Spectroscopy (FTIR) with Attenuated Total Reflectance (ATR).....	66
2.3.3. Isothermal Titration Calorimetry (ITC).....	68
2.3.4. Quartz Crystal Microbalance with Dissipation (QCM-D).....	70
2.3.5. Zeta-potential measurements	72
2.3.6. Size Exclusion Chromatography (SEC).....	74
References.....	75

CHAPTER 3

MULTILAYER ASSEMBLY OF HYALURONIC ACID/POLY(ALLYLAMINE): CONTROL OF THE BUILDUP FOR THE PRODUCTION OF HOLLOW CAPSULES..... 77

3.1. RESUME (FR).....	79
3.2. ARTICLE.....	81
3.3. SUPPORTING INFORMATION.....	89
3.4. COMPLEMENTARY RESULTS.....	95
References of CR.....	98

CHAPTER 4

EFFECT OF POLYCATIONIC PARTNER OF HA ON CAPSULE MORPHOLOGY CHARACTERIZATION AND PRELIMINARY RELEASE ASSESSMENT..... 99

4.1. RÉSUMÉ (FR).....	101
4.2. INTRODUCTION	103
4.3. RESULTS AND DISCUSSION	105
4.3.1. Synthesis of capsules based on HA, role of the polycationic partner on the morphology and stability properties	105
4.3.1.1. Analysis of HA/PAH, HA/PLL and HA/QCH complexation in the bulk and on planar surface.....	105
4.3.1.2. Synthesis of HA/PAH, HA/PLL and HA/QCH hollow capsules and their characterization.....	112
4.3.2. Cross-linking of the microcapsule shells: improvement of morphology and stability.....	121
4.3.3. Shell permeability of cross-linked and non cross-linked capsules.....	129
a) Permeability in aqueous solution without salt	129
b) Permeability in salt	132
c) Encapsulation of fluorescent molecules as model drugs	134
4.3.4. Enzymatic degradation.....	136
4.4. CONCLUSION.....	139
REFERENCES.....	140

<i>List of Figures</i>	147
------------------------------	-----

<i>List of Tables</i>	154
-----------------------------	-----

<i>Abbreviation</i>	155
---------------------------	-----

CHAPTER 1

*LbL Capsules Made from Polysaccharides
- Bibliography Review*

1.1. Résumé (fr)

Ce chapitre, situant le travail dans son contexte bibliographique, s'organise en quatre volets principaux. Les différentes approches proposées dans la littérature pour la synthèse de capsules par la technique de dépôt couche-par-couche sont tout d'abord présentées. Elles reposent sur l'utilisation de particules colloïdales sacrificielles de taille nano- ou micrométrique comme supports pour l'élaboration de films multicouches. L'analyse bibliographique met en évidence une grande variété de matériaux utilisés pour la synthèse de ces cœurs. Ceux-ci peuvent être de nature minérale ou organique et de taille variable comprise entre 30nm et 170µm. En ce qui concerne les films multicouches constituant la paroi des capsules après dissolution du cœur, ils sont généralement construits à partir de polymères synthétiques ou naturels. Dans ces films, les interactions mises en jeu peuvent être de nature électrostatique ou reposer sur la formation de liaisons hydrogène, de liaisons covalentes ou encore la complexation hôte-invité. Ces interactions peuvent être modulées par la température, le pH, la force ionique, ou la présence de biomolécules, rendant ainsi les assemblages sensibles, voire réactifs aux conditions extérieures.

L'intérêt suscité par les capsules multicouches est ainsi lié à la capacité de leur paroi à répondre efficacement à des sollicitations environnementales diverses, permettant une libération programmée des substances actives encapsulées. Ces systèmes laissent de ce fait envisager des applications intéressantes dans le domaine pharmaceutique et les biotechnologies. Celles-ci font l'objet de la deuxième partie de ce chapitre. Une attention particulière est portée aux techniques utilisées pour encapsuler des molécules actives à l'intérieur de la capsule.

Comparés aux polymères de synthèse couramment auto-assemblés, les polysaccharides présentent des propriétés intéressantes et originales qui peuvent être avantageusement mises à profit pour la synthèse de microcapsules comme transporteurs de principes actifs. L'utilisation de ces polymères naturels pour produire des capsules multicouches est discutée dans la troisième partie de ce chapitre. Celui-ci se termine par une présentation des propriétés de l'acide hyaluronique, le polysaccharide principal utilisé dans ce travail.

1.2. Introduction

Functionalized capsules are of increasing interest in a variety of fields such as cell biology, biotechnology, diagnostics, and pharmacy.

Among the different technologies for capsule fabrication, the layer-by-layer (LbL) technique introduced in 1993 for the formation of thin planar films has emerged as an interesting approach to produce micro-/nanocapsules with tailored architectures and properties.

This chapter provides an overview of research work devoted to the design and synthesis of LbL micro- and nanocapsules.

The first part of the chapter describes the LbL assembly technique as a method for the preparation of nanoscale films from polyelectrolytes of synthetic or natural origin.

Next, the focus will be on polyelectrolyte adsorption onto colloidal particles followed by core removal, resulting in the formation of hollow capsules. The different colloidal templates used and interactions stabilizing the multilayer film are described.

The potential applications of LbL capsules are discussed with a special interest in drug delivery. Several techniques to incorporate therapeutics into the capsule interior as well as functionalizing film surfaces to protect them during administration whilst directing their content to the target site are described. In general, drug release from hollow capsules can be controlled by modifications of membrane permeability based on changes in the physicochemical properties of the films. The latter can respond to stimuli such as pH, ionic strength, temperature, etc., which may improve the treatment of many diseases. There are, however, several challenges that must be addressed before this goal can be achieved.

For biomedical applications a prerequisite is to use biodegradable and biocompatible materials. The currently investigated LbL capsules made from polysaccharides, proteins and polypeptides are reviewed. This allows one to define the context of the study and the aims which were taken upon realization of this work.

The final part of this chapter focuses on the biological and physico-chemical properties of the main polysaccharide used in this work for LbL capsule fabrication; hyaluronic acid.

1.3. Layer-by-Layer (LbL) technique

The concept of constructing thin films by the deposition of two oppositely charged species was originally proposed by Iler in 1966¹, since the early 1990's this has been developed extensively by Gero Decher²⁻⁴. He introduced the concept of forming layers of oppositely charged polymers i.e. polyelectrolytes (PE) by the Layer-by-Layer (LbL) technique creating “polyelectrolyte multilayer films”. It is generally accepted that the electrostatic interactions occurring between oppositely charged PE is the principal driving force for multilayer assembly. The usual way of polyelectrolyte deposition is the following: when a solid substrate with a positively charged planar surface is immersed into a solution containing an anionic polyelectrolyte, a layer of polyanion is formed which reverses the surface charge; after a rinsing step to remove excess non-adsorbed polymer, the adsorption of polycation is carried out. One layer of polyanion deposition followed by one layer of polycation deposition is defined as a “bilayer”. Washing steps and the whole procedure is repeated until the desired number of polymer layers forming the film multilayer is achieved (**Figure 1.1**).

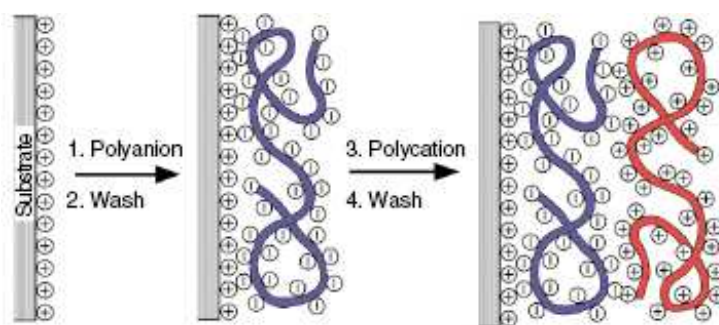


Figure 1.1. Build-up of the polyelectrolyte multilayer film by the consecutive adsorption of anionic and cationic polymers (multiple repetition of the steps for obtaining desired number of layer)⁴.

As well as other techniques like spray-coating⁵ and roll-to-roll processing⁶ have also been proposed as interesting alternatives to produce multilayer films with a higher speed of deposition.

The alternative polycation and polyanion deposition leads to the growth mechanism of the multilayer system. When the mass and thickness of multilayer increases linearly with the number of deposition steps, the film is said to exhibit a “linear growth regime”; in this case

polyelectrolytes from the solution interact exclusively with the outer layer of the film without diffusing into the architecture. If the film thickness and the amount of adsorbed polyelectrolytes increase more rapidly than linearly with the number of deposited layer pairs, the film shows an “exponential growth regime”. In this case the structure is much less organised than a linearly one, with an inter-penetration of adjacent layers. Such films were mainly observed when the LbL multilayer build-up was carried out with participation of natural polymers (polysaccharides or polypeptides)⁷⁻¹⁰, whereas it was shown that the linear growth generally appears for synthetic polymers¹⁰.

Chemical structures of principal synthetic and natural polyelectrolytes used for LbL assembly are presented in **Tables 1.1** and **1.2**, respectively.

Table 1.1. Synthetic polymers for LbL film formation.

SYNTHETIC POLYMERS		CHEMICAL STRUCTURE
POLYANIONS	Poly(styrene sodium sulfate) PSS	
	Poly(acrylic acid) PAA ¹¹⁻¹⁸	
	Poly(methacrylic acid) PMA ¹⁹⁻²⁴	
POLYCATIONS	Poly(allylamine hydrochloride) PAH ^{6,7,13,17,24-33}	
	Poly(diallyldimethylammonium chloride) PDA ^{18,34-38}	
	Poly(ethyleneimine) PEI ^{5,39-41}	

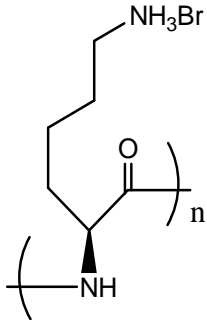
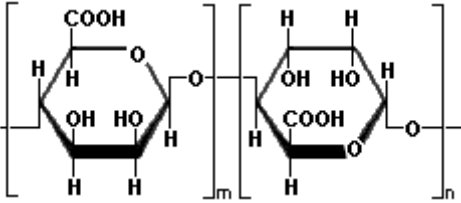
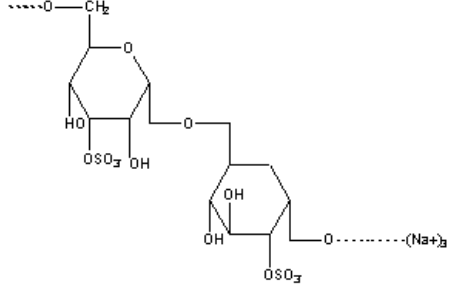
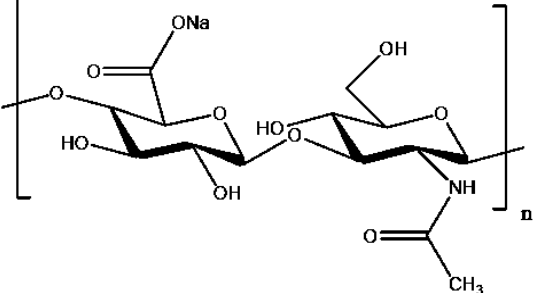
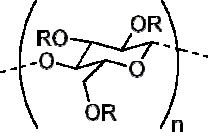
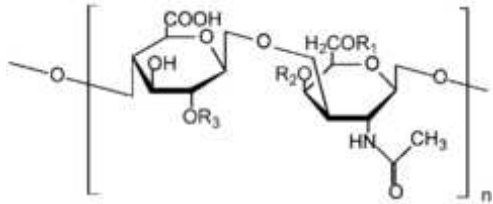
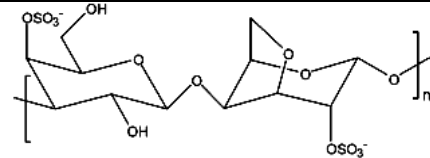
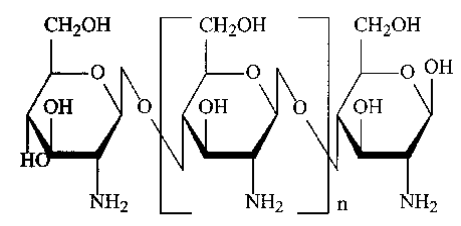
	<p>Poly(L-lysine) PLL^{5,9,42-47}</p>	
--	--	---

Table 1.2. Natural polymers used for LbL multilayer formation.

POLYSACCHARIDES		CHEMICAL STRUCTURE
POLYANIONS	<p>Alginate⁴⁸⁻⁵³ ALG</p>	
	<p>Dextran sulphate^{49,54} DEXT</p>	
	<p>Hyaluronan or hyaluronic acid^{47,55} HA</p>	
	<p>Carboxymethyl cellulose CMC⁴⁹</p>	 <p>R = H or CH₂CO₂H</p>

	Heparin ⁵⁶	
	Carrageenan ^{57,58}	
POLYCATIONS	Chitosan and its derivatives CH ^{32,48,49,51,59-62}	 Chitosan

Natural polymers generally show low or no toxicity, low immunogenicity, biodegradability and good biocompatibility. Their principal disadvantage are problems of variability in structures and properties as well as purification processes after extraction from living organisms or plants⁶³. Biopolymers are generally weak polyelectrolytes (only partially charged), lead to exponential growth of the LbL films and give soft, highly hydrated structures such as HA/CH, HA/PLL films^{55,64-66}. These properties are thus strongly different from those of films made of synthetic polyelectrolytes (such as PAH/PSS), often exhibiting linear growth with well organized layered structure and good mechanical properties^{10,67}.

1.4. Application of the LbL technique to the synthesis of microcapsules

The capsules in the micrometer to millimetre range are already fabricated by many available technologies including complex coacervation, *in situ* polymerization, solvent evaporation from emulsions, spray drying, prilling, extrusion, gelation, etc...⁶⁸

These micro-/millicapsules find applications in various fields such as pharmaceuticals, agriculture, food, textile and cosmetics for cell immobilization, beverage production, drug release, soil inoculation, nutrition, etc...(see **Figure 1.2**)^{68,69}.

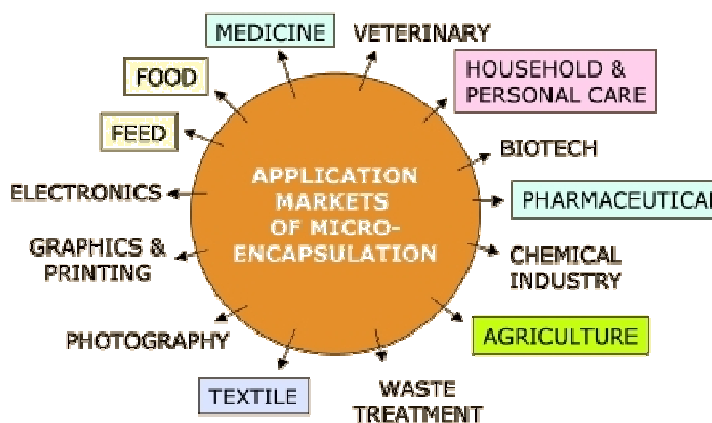


Figure 1.2. Areas of applications of polymer capsules ⁷⁰.

LbL technique allows the preparation of capsules in which the wall structure can be precisely controlled. Capsules are thus characterized by well-controlled shape and size, thickness and roughness of the shell which may be made of various material compositions. Incorporation of functional species at the surface of the “nanoshell” such as biomacromolecules, lipids, dyes, nanoparticles enables tuning their physicochemical properties with high precision. The modification of the inner walls ensures a micro-/nanoenvironment for specific materials.

The LbL approach for capsulation is a promising challenge in the high technology field ^{71,72}.

1.4.1. Principle of synthesis

Microcapsules prepared by the LbL polyelectrolyte deposition were introduced in 1998 by Sukhorukov *et al.*⁷³. The principle of preparation was similar to already well known LbL PE deposition on planar surfaces, but oppositely charged polyelectrolytes were adsorbed onto colloidal particles as a template instead of a planar support.

The general procedure for preparation of LbL hollow capsules is presented in **Figure 1.3**. The colloidal particles are alternatively immersed into the oppositely charged polyelectrolyte solutions, with washing steps before the new PE layer is adsorbed. After deposition of the desired number of layers, the core can be removed resulting in the formation of hollow capsules.

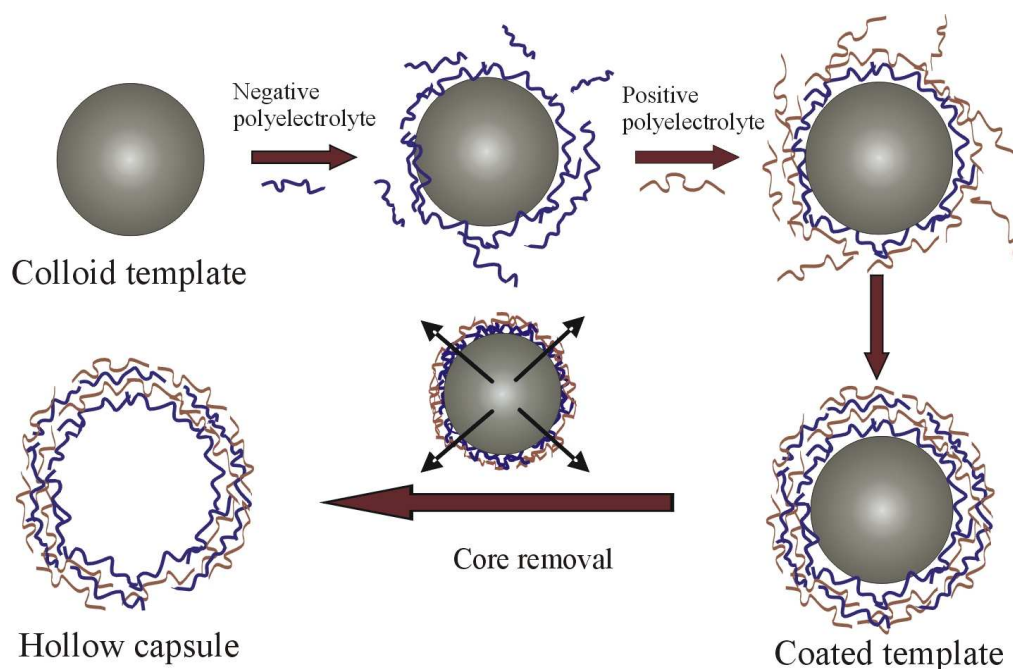


Figure 1.3. Polyelectrolyte multilayer deposition process and subsequent core dissolution resulting in the formation of hollow capsules.

1.4.2. Template

The choice of the colloidal particle is a key step in fabrication of hollow capsules. Many aspects like stability of the core during LbL process, conditions required for template dissolution and particle size and shape should be carefully considered. Commercially available colloidal particles, as well as particles synthesized in research laboratories can be used as organic, inorganic or biological templates for the synthesis of hollow capsules. **Table 1.3** presents different templates together with their main properties, which have been used for LbL formation of capsules.

Table 1.3. Templates used for the preparation of hollow polyelectrolyte capsules.

Particles	Size [μm]	Shape	Monodispersity	Problem upon dissolution
Polystyrene latex PS 13,25,73,74	0.1-5	spherical	excellent	Mechanical stress, residues, organic solvent for decomposition
Melamine formaldehyde (MF) 25,35,75	0.3-10	spherical	excellent	Mechanical stress, residues, low pH conditions for decomposition
Silica (SiO₂) 20,23,76	4-100	spherical	Good-excellent	Aggregation, harsh conditions for decomposition (HF)
Gold nanoparticles 77-79	0,030-0.05	spherical	low	Aggregation, toxic solvent for decomposition
Liquid droplets 28,80-82	1-35	spherical	Very low	-
Liquid crystal droplets ⁸³	1-10	Spherical	low	Ethanol for decomposition
Gas bubbles ²⁸	1-20	spherical	low	Dissolution of template is not required, but bubbles of the gas present low stability
CaCO₃, MnCO₃, CdCO₃ ^{31,84}	3-8	Spherical, crystalline	medium	There is no osmotic pressure, since small ions easily diffuse across multilayer membrane
Biological cells 32,62,81	5.5-7.5	Biconcave shape	good	Red cells are removed by treatment with strong oxidizing agent (NaOCl) which can cause wall destruction
Drug crystals 41,85	0.1-45	Squares, triangles, rectangles	low	-
Magnesium oxalate microcrystals (MgC₂O₄ × 2H₂O) 26	1-3	Squares, rectangles	good	No osmotic pressure, but the shell shrinkage is observed
Hydrogel beads 47,86	16-170	spherical	Very low	-

As can be seen from **Table 1.3**, none of the templates meet all requirements in terms of size monodispersity, mild conditions for core dissolution or colloidal stability. Each of the

sacrificial cores has certain limitations associated with its applications. The use of PS particles requires solvents such as tetrahydrofuran (THF) for decomposition. Moreover, the swelling of the PS cores during removal can lead to rupture of the polymer capsules⁸⁷. MF particles are chemically decomposed under acidic conditions (pH 1.5) or in organic solvents e.g. dimethylsulfoxide. Some of the oligomers produced during MF dissolution are generally retained within the polymer capsule walls, which is not desired because of their biological incompatibility^{35,51,54,88}. Inorganic cores like SiO₂ particles completely disappear in a few seconds under dissolution but require the use of hazardous HF acid⁷¹. Gold nanoparticles are removed upon exposure to toxic potassium cyanide^{77,78}. The dissolution of inorganic crystals such as CaCO₃, MnCO₃, CdCO₃ can be performed under mild conditions. If the formed ions do not form a complex with the shell polyelectrolytes they easily diffuse through the membrane, eliminating osmotic problem^{24,84}. However, these templates are often porous, and during deposition of the layers, the polyelectrolyte can diffuse inside forming inter-complexes^{84,89} similar to the case of silica particles¹¹. Gas bubbles²⁸ do not require specific solvent, but they show low stability, lower than biological cells⁷¹ with mechanically sensitive walls. Often too large size and non regular shape of the templates excludes them from potential applications, since the use of hollow capsules as potential drug vehicles requires small size and allow homogenous diffusion through the membrane; in case of cubes, the release velocity through the edges in comparison to walls is different.

1.4.3. Interactions used for multilayer construction

Most of the interactions between adjacent layers are created by using electrostatic attractions[28, 32, 40, 91-93], but there are many other kinds of interactions which can be used to form multilayers: hydrogen bonding^{22,23,90,91}, host/guest interactions⁹², specific biomolecular recognitions⁹³, or covalent bonds^{12,94}. The examples of each type of bonding are illustrated in **Figure 1.4**.

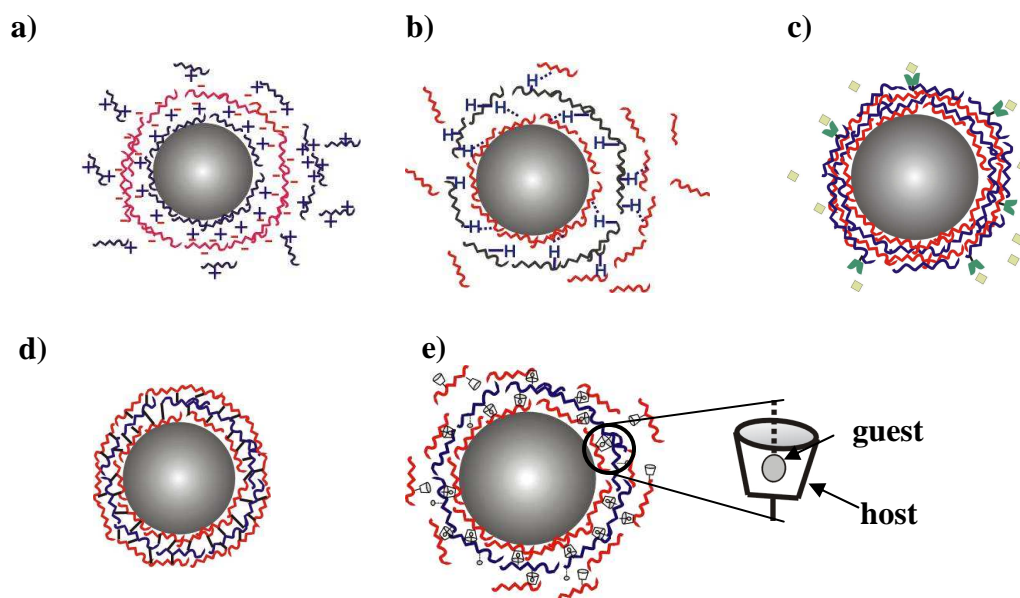


Figure 1.4. The illustration of different interactions within the LbL shell: electrostatic (a), hydrogen bonding (b), specific (c), covalent bonds (d), and host-guest (e).

Hydrogen bonded multilayers^{22,23,90,91} can be formed when the hydrogen present in one polymer gets associated with an electronegative atom in the second polymer of the next deposited layer. Large number of such weak hydrogen bonds between adjacent polymers enables formation of polymer film sensitive to pH changes, such as PVPON/PMAA capsules²³. Capsules functionalized with *biotinlated* PLL-g-PEG adsorb streptavidin as a consequence of specific biotin-streptavidin interactions⁹³.

The formation of covalent bonds between layers allows the use of neutral polymers with the same charge. It has thus been shown the possibility to obtain capsules from PAA copolymer with either alkyne or azide functionality using click chemistry¹². The covalent bonds between epoxides of PGMA and amine groups of PAH were stable in extreme pH and high temperature capsule conditions⁹⁴. The formation of stable borate-glucose complexes as a result of charge transfer has been advantageously applied to capsules which are sensitive and reversible as a function of glucose concentration^{95,96}.

The other type of capsules involve host-guest interactions between cyclodextrins (CD) and ferrocene^{97,98} showing multi-responsiveness to environmental stimuli and the specific base-pair interactions of individual DNA strands have been recently exploited to produce functional, biodegradable, biocompatible molecule sensors^{99,100}.

1.5. Applications of the LbL based capsules

Creation of new LbL nano-/microengineering capsules is established as a relatively easy way to produce vehicles which can find application in many fields, among which the largest interest is found in biotechnology and medicine.

Up to now, there are no commercially available capsules fabricated by the LbL technique. However, the promising perspectives bring continuous development in this direction. Large possibility of modifications of capsule properties including their size and shape, composition, shell thickness, permeability, stiffness and stability makes these assemblies an object of a great interest.

1.5.1. Drug delivery

The multicompartiment structure of microcapsules as well as their potential to change their behaviour in response to external stimuli makes them interesting candidates as drug delivery system.

Delivery and controlled release of drugs requires “intelligent systems” which first enclose an active substance, then go to the required region of the body and liberate the content with preserved bioactivity. The role of such systems is to obtain the maximum efficiency of the drug without unwanted side-effects. To achieve this goal, it is necessary to overcome many “obstacles” related to fabrication of suitable capsules, their functionalization, and analysis of their properties before introducing them at a commercial level.

a) Encapsulation

As shown by **Figure 1.5**, different strategies have been proposed to load materials (macromolecules, nanoparticles) into the LbL capsules.

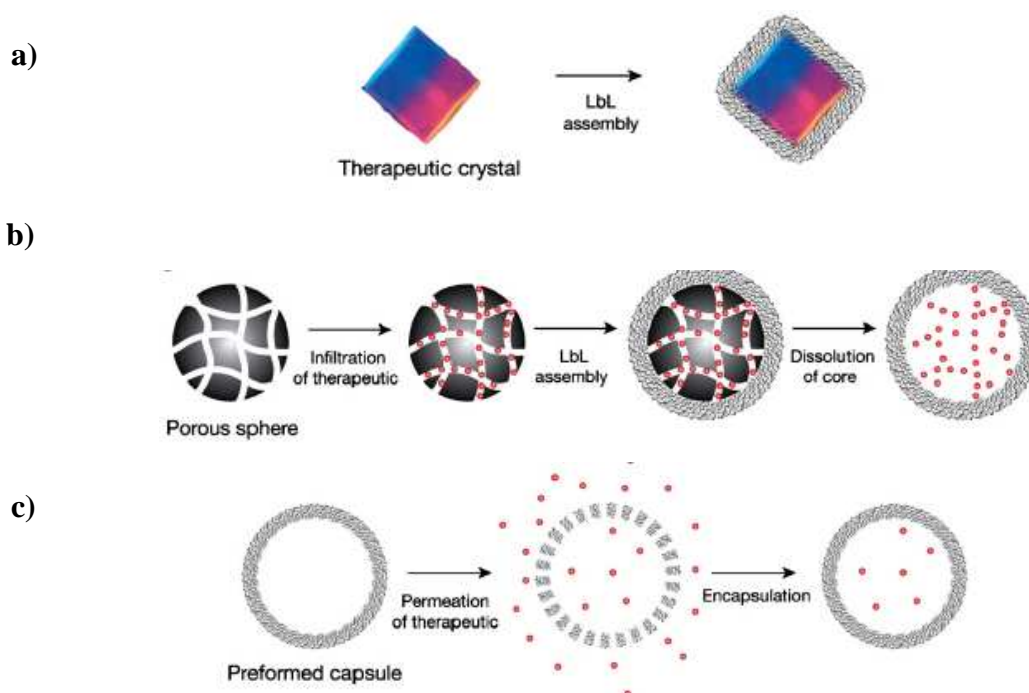


Figure 1.5. Different methods for encapsulating materials: encapsulation of crystalline particles (a), incorporation in porous materials (b), and loading preformed capsules (c)¹⁰¹.

- **Assembly of multilayers on crystal, or aggregates of the desired substances**

Perhaps, the simplest method consists of coating crystals or agglomerates of the desired compounds with a multilayer film. However, application is limited to compounds which are insoluble under conditions used for multilayer deposition and forming crystals of the same size^{41,71,85}.

- **Pre-adsorption or co-precipitation of a substance with template**

Another technique to encapsulate compounds is their coprecipitation during template synthesis or adsorption onto the surface of highly porous templates, followed by coating the template with polyelectrolyte layers^{11,89,102}.

For non-porous particles, a possible strategy is to use “transitional complex”. Molecules possessing a multivalent charge can form transitional complexes with some macromolecules. Such a temporary precipitated complex is deposited on the particle and then covered by stable polyelectrolyte multilayers. After core dissolution, the precipitated transitional complex, as a first bilayer, can be decomposed under conditions where the outer polyelectrolyte shell is

stable. Multivalent ions are small enough to diffuse out of the shell and leave the capsule, whereas the macromolecules of the temporary complex polymer have too high molecular weight to be able to escape from the multilayer. The latter, thus, stays in the interior of the capsule. This method gives one more possibility to load the capsules with desired macromolecules¹⁰³.

- **Loading pre-formed capsules**

Finally, it may also be possible to load hollow capsules by diffusion of materials through the walls from the exterior to the interior of the capsules. In this case we can apply the “sucking” of the substances from outside into the interior, or “switching permeability”.

In 2005 Liu et al.¹⁰⁴ published a relatively fast and high-yield method for loading of anti-cancer drugs (doxorubicin, DNR) into the interior of hollow capsules. This phenomenon is attributed to the presence of traces of negatively charged PSS/MF complexes within the capsule interior, formed by PSS polyelectrolyte (component of the capsules) and the rest of MF after its dissolution. The positively charged substance present outside of the capsule is “sucked-up” into the interior by the negative charge of PSS/MF complex species resulting in an interior concentration several times higher than bulk solution, this method was called “spontaneous deposition”. The spontaneous accumulations of the charged substances leading to high concentrations of the biomolecule inside the capsules was also observed by other authors^{48,51}.

A more general technique of loading substances involves reversible opening and closing of the capsules. This approach requires a multilayer whose permeability can be varied in response to external stimuli. This is based on the disruption of the multilayer assembly in response to changes in environmental conditions. The capsule shells can be opened to allow diffusion of material from the surrounding medium; when the active substance is in the capsule interior, the pores are then closed to retain the compound (**Figure 1.5.c**). Such stimuli-responsive multilayers for encapsulation have attracted a lot of interest among other approaches, since this method can also be exploited for content release. The “intelligent” closing and opening of the pores in multilayer structures take place under pH changes of solutions containing suspended capsules, salt concentration, solution polarity, and temperature.

Encapsulation by the change of environmental pH can be applied when the multilayer contains at least one weak polyelectrolyte of which charge density strongly depends on the pH conditions. When the pH of the environment increases above the pKa in case of a polybase, or becomes lower than pKa in case of a polyacid, the polyelectrolytes lose the charge reducing electrostatic interactions. This may lead to the swelling of capsules and their subsequent disruption as illustrated in **Figure 1.6**.

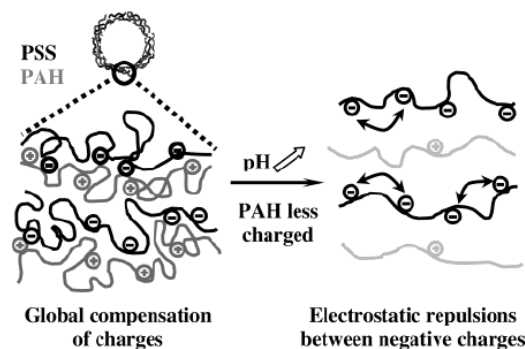


Figure 1.6. Swelling of the capsule in basic conditions due to electrostatic repulsion between negative charges of PSS¹⁰⁵.

The switchable permeability of capsules as a function of pH has been reported by several authors^{30,106,107}.

From a pharmaceutical point of view, it is necessary to take into account the pH of the target object where capsules should deliver the bioactive substances. The pH of such objects such as vagina, extracellular matrix of tumours, inflammatory regions or intracellular vesicles is slightly lower (except of the stomach where pH=1-2) than the pH of serum i.e., pH=7.4. Creation of capsules which are stable in blood but release their payload at pH just a half unit lower is a big challenge. Until now, there are not any capsules meeting this requirement¹⁰⁸.

Similarly to pH, the variation of salt concentration can also be used to encapsulate materials. When a polymer participates in multilayer formation, variation of the overall charge occurs as a result of interactions between two oppositely charged polymers and electrolyte ions in the polymer films. The salt added to the external solution of capsules can cause some swelling of the multilayer due to the screening of electrostatic interactions and if the concentration of the salt is relatively high, the swelling can lead to decomposition of multilayers into individual initial components. For example, the PSS/PAH capsules remain impermeable for labelled PAH polymer at $M_w \sim 70 \times 10^3$ g/mol when they are incubated in solution with low salt concentration up to 5.20 mM, above this value they became

permeable¹⁰⁹. Considering physiological conditions, the concentration of NaCl in the blood plasma is approximately 0,15M and there is little variation of ionic strength in the human body¹⁰⁸, thus the tuning of the capsules which are able to open/close their pores as a function of small changes of salt concentration is an issue of challenge.

The incubation of the polyelectrolyte capsules at various temperatures influences the chain diffusion in the multilayer shell, changing the structure and properties of the capsules.

Koheler et al.³⁷ observed changes in multilayer thickness and shell permeability after incubation of PDADMAC/PSS capsules at temperature between 25-50°C. Upon heating, the capsules became impermeable to dextran^{FITC} ($M_w \sim 10 \times 10^3$ g/mol), since the shells shrink and simultaneously thicken and more dense. It has been shown that heat incubation can be used for encapsulation of both neutral and charged molecules inside the capsules (**Figure 1.7**).

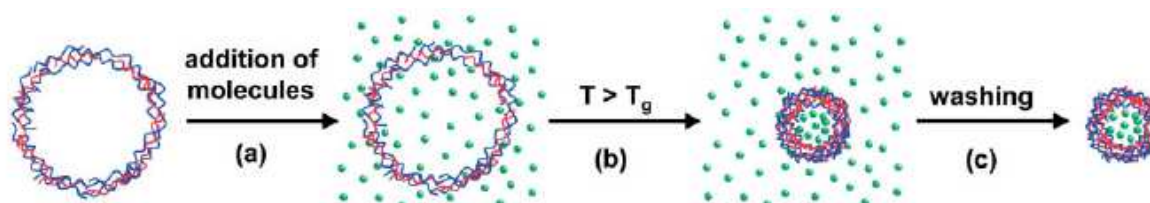


Figure 1.7. a) Incubation of polyelectrolyte multilayer capsules in a solution of the desired compound, b) The mixture is heated until the capsules shrink so much that the shells become impermeable for the molecules leading to entrapment; c) Removal of surrounding molecules by subsequent washing steps³⁷.

If the multilayer shrinks, it is possible to enclose bioactive molecules as a result of more densely packed chains and densify. The molecules can no longer move out and thus remain encapsulated inside. Improved mechanical stability can protect the filled capsules from external forces e.g., shear or compression and also can effect cell adhesion behaviour.

Similarly, an increase in layer thickness with a decrease in capsule diameter upon heating was also observed by other authors^{32,34}.

Since some polyelectrolyte complexes are insoluble in water and soluble in ethanol, by changing the ratio water/ethanol of solution for incubation of LbL capsules, one can observe changes in their structure and hence in their permeability. PSS/PAH capsules were placed in ethanol solution to allow the diffusion of model polymers (Dextran ($M_w \sim 77 \times 10^3$ and 2000×10^3 g/mol, proteins, PSS and PAH) into the interior of the capsules, and then the pores were closed by washing with water¹¹⁰.

b) Surface modification

Encapsulated medicines should be transported to a particular site or specific cell type in the body and then released without affecting the other tissues or cells.

Two strategies can be used for drug targeting: non-specific targeting and specific targeting.

In the non-specific or passive targeting, the carrier-drug complex is often delivered to macrophages or the other cells of monocyte-phagocytic system, which leads to gradual degradation of the drug-carrier complex during circulation in the blood or tissue environment.

Specific or active targeting involves release at the site of action, avoiding earlier degradation.

In order to avoid non-specific uptake of the capsules after their administration into the body and to be later delivered to specific cells or tissue, the immobilization of specific recognition groups has been reported.

- **Control of non-specific adsorption**

Drug carriers after introduction in to the blood plasma interact with proteins which lead to uptake by phagocytic cells and degradation, losing their activity. Hereby, it is important to protect the carriers from unspecific interactions with macrophages and undesirable phagocytosis to keep bioactivity of the entrapped drug.

Zahr et al.¹¹¹ modified the surface of the PSS/PAH capsules by covalent bonding of poly(ethylene glycol) (PEG) with PAH as an outermost layer. PEG coatings create a cloud of solvated hydrophilic and neutral chains at the particle surface which can repel approaching plasma and blood proteins. In the reports of Textor^{44,93}, PSS/PAH capsules was covered by layer of copolymer of poly(ethylene glycol) grafted poly-L-lysine (PLL-g-PEG).

Comparison of the capsules adhesion by serum cells is presented in **Figure 1.8**.

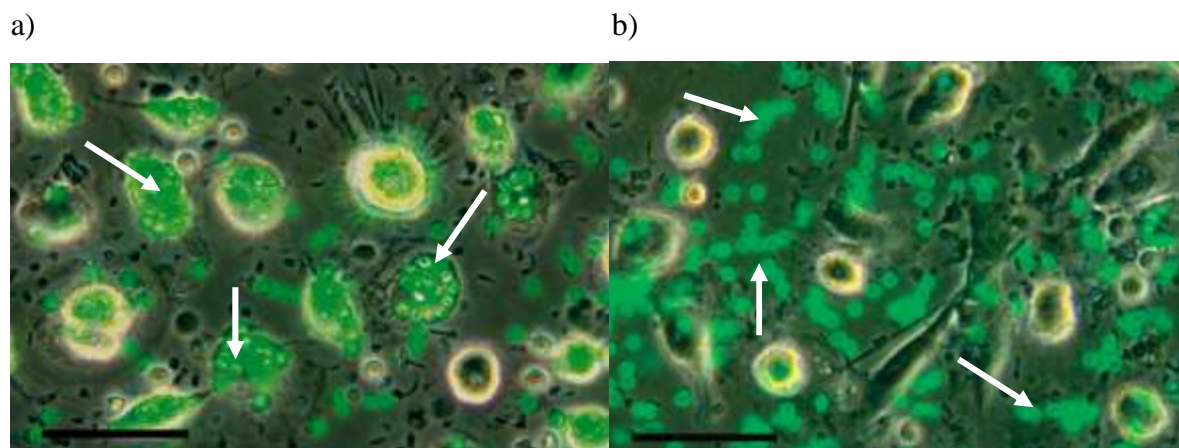


Figure 1.8. Phagocytosis of coated LbL microcapsules by dendritic cells, capsules made from PSS/PAH polyelectrolytes: (a) PSS-coated microcapsules; (b) PLL-g-PEG coated microcapsules. FITC labelled PAH was used for capsule synthesis to enable CLSM visualization. Arrows indicate the sites of capsule placement. Scale bar=50 μm ⁴⁴.

From the figure, it can be observed, that capsules made from PSS/PAH with PSS as the outermost layer were efficiently adhered on the cells while the same capsules protected by (PLL-g-PEG) “corona” largely resisted internalization.

The incorporation of some proteins onto the particle surface can also reduce non-specific uptake. Fischlechner *et al.*¹¹² constructed PSS/PAH particles coated with lipid membrane with incorporated protamine sulphate particles. This system could avoid undesirable interactions.

• Targeting

Various types of groups such as antibodies, viruses and carbohydrates have been incorporated onto the surface of capsules to achieve specific recognition of appropriate object.

Antibodies

It has been observed, that glycoproteins present on the cancer cells differ from those from healthy cells. They can play the role of an antigen, which should be recognized by specific antibodies. The biofunctionalization of particles with specific antibodies determined as “huA33 mAb” which are able to bind cancer antigen “A33” allowed the transport of therapeutic-loaded vehicles to infected tissues without non-specific uptake by healthy organs/cells leading to side effects¹¹³.

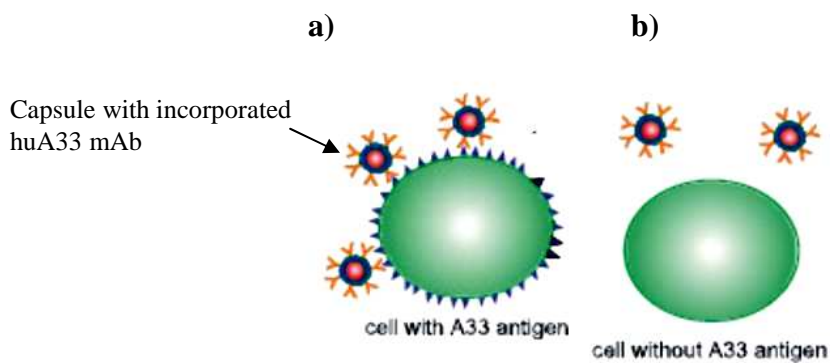


Figure 1.9. Model of the cells with a) and without b) “A33” antigen. Capsules with incorporated antibody are able to recognize only the cell with specific antigen¹¹³.

Viruses

For reproduction, specific binding between viral proteins and specific receptors on the host cellular surface is used; it is a potential strategy to introduce these viral proteins on LbL capsule surfaces to recognize a host cell/tissue.

PSS/PAH particles coated lipid membrane with incorporated “rubella-like” virus particles (Figure 1.10) were constructed to bear the functionality for the facilitation of cell membrane passage. The results showed that the capsules with immobilized viruses found target cells contrary to capsules coated with only lipid membrane¹¹².

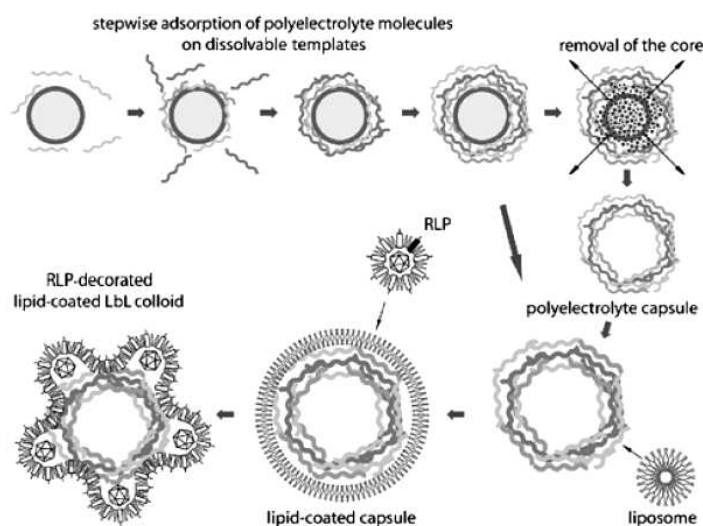


Figure 1.10. Protocol for engineering virus functionality. The PSS/PAH coated particles were incubated in the liposome vesicles solution to accomplish the lipid membrane and incorporate viruses particles¹¹².

Carbohydrates

D-Galactose is a well known targeting molecule directing to the hepatic cells. PNA (peanut agglutinin) lectin binds preferentially to β -D-galactose or galactosyl-(β -1,3)-*N*-acetylgalactosamine. Thus, the poly(vinyl galactose ester-*co*-methacryloxyethyl trimethylammonium chloride) PGEDMC was synthesized to obtain PGEDMC/PSS capsules which have shown to specifically interact with PNA lectin¹¹⁴.

The same capsules can be functionalized to avoid non-specific uptake by serum proteins and on other hand they can also be functionalized to allow specific interaction with other required proteins. These capsules covered by grafted poly-L-lysine (PLL-*g*-PEG) have been additionally functionalized with biotin for specific recognition and complexation of the required protein – streptavidin⁹³.

c) Release

The release of the drugs can occur according to different mechanisms which depend on the requirements of diseased organs.

The loaded substance can quickly leave the capsule as a result of a sudden break of the film structure (burst release). Due to the fact that the fast release of drug in a burst stage can be pharmacologically dangerous, the sustained release (extended release) system which implies slow release of the drug over a time period is desired.

• Burst release

Medicines are sometimes most effective when they treat rapidly and directly the diseased organs/cells. From this reason it is desired that the filled capsules are first internalized by the cells to spontaneously release the content in a later step.

Burst release of the capsule content can be achieved by physical and chemical stimuli.

One of the processes involves the irradiation technique^{88,115-118}. Near infrared (IR) laser light was applied to open PAH/PSS polyelectrolyte shells with gold⁸⁸ or PDADMAC/PSS capsules with silver nanoparticles¹¹⁵ incorporated within multilayer. Upon irradiation, the nanoparticles infiltrated into the polyelectrolyte shell absorb the energy and transform it into heat, leading to local destruction of the multilayer system. The substance can thus leave the interior of the

capsule (**Figure 1.11**)^{115,118}. The bioactive encapsulated material can be released by a laser pulse without damaging their activity⁸⁸.

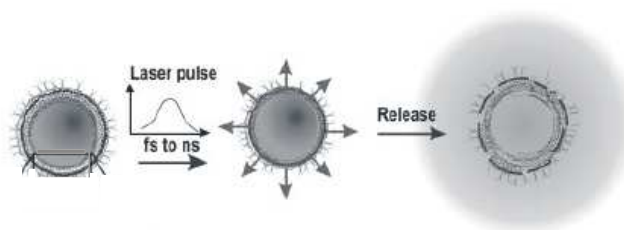


Figure 1.11. The capsules under laser irradiation⁸⁸.

Following the laser irradiation damage of the capsules is presented below (**Figure 1.12**)

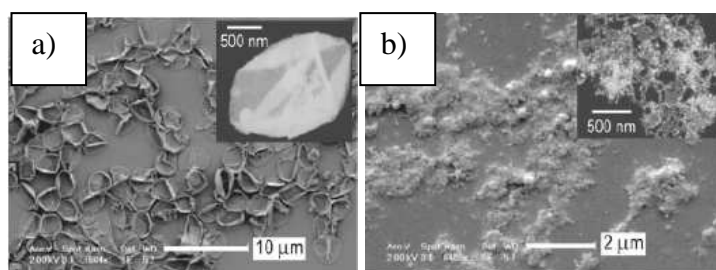


Figure 1.12. Irradiation of capsules with laser pulses. SEM images of capsules: (a) before irradiation, (b) after radiant exposure⁸⁸.

This opening method is promising for the treatment of tumour cells. Chemotherapy generally tends to kill diseased cells, at the same time damaging other cells in the body. To avoid the destruction of the healthy cells, it is important to transport the drug to targeted cells and release the substance there. Preliminary studies performed on cancer cells established the feasibility for the capsules to deliver their content in cancer cells by the use of laser light¹¹⁶.

Gold coated cobalt nanoparticles were incorporated into the PSS/PAH multilayers and nanoparticles were then disrupted by applying an oscillating magnetic field thereby allowing diffusion of macromolecules. The vibrating magnetic nanoparticles induce opening of the polymer matrix¹¹⁹.

An easy and fast release of the substance can also be achieved by ultrasound irradiation that breaks up filled capsules^{120,121}.

Besides physical stimuli, we can distinguish chemical strategies^{21,95,122} for destruction of the interactions between the layers or degradation of used polymers^{47,76}.

The disulfide cross-linked PMA/PVPON capsules, which chemically decomposed after contact with dithiothreitol (thiol-disulfide exchange)²¹. Glucose-sensitive polyelectrolyte shells, fabricated from PSS and a polycationic polymer modified with phenylboronic acid, were decomposed in the presence of sugars (**Figure 1.13**⁹⁵. Phenylboronic acid became negatively charged in the presence of glucose.

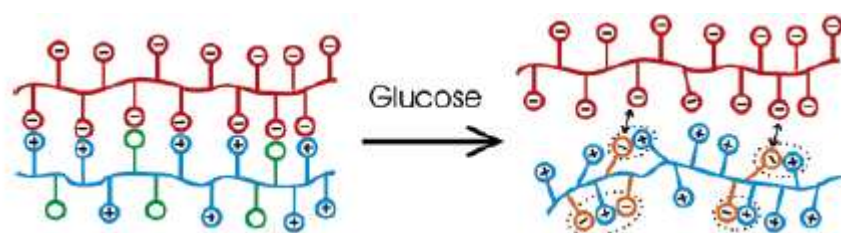


Figure 1.13. Mechanism of the glucose-induced decomplexation of a polyelectrolyte bilayer. The red circles represent the negatively charged PSS, and the blue circles represent the amino groups with uncharged phenylboronic acid (green circles). After treatment with glucose the repulsion occurs as the result of negative charge of borate⁹⁵.

Enzymatic degradation of films on the planar surface has been applied to multilayers constructed from chitosan or hyaluronic acid^{47,76}.

In the case of capsules, CH/DEXS multilayer destructions was observed after contact with enzyme responsible for chitosan cleavage - chitosanase. Degradation of the polysaccharide capsule was shown after 4 days, while in the presence of chitosanase enzyme (37°C) it was much more rapid (after 5min visible changes). Low temperature was less effective⁷⁶. The other, cross-linked HA/PLL capsules showed higher protein release in contact with hyaluronidase (an enzyme which degrades HA by random hydrolysis of β -N-acetyl-hexosamine-(1 \rightarrow 4) glycosidic bonds leading to oligosachcarides)⁴⁷.

• Sustained release

The release of the payload from LbL capsules can be provided by simple diffusion through the wall pores of which size can be varied at different conditions^{26,49,51,104,108-110,123}. For this aim we can distinguish external and intrinsic parameters which influence the multilayer structure, then permeability of the walls can be used to control the rate of drug release.

As discussed above, external parameters such as salt, pH and temperature can largely influence the permeability of capsules. This capsule responsiveness can be used for encapsulation of material as well as for its release¹⁰⁴.

Moreover, intrinsic parameters such as wall thickness and its chemical structure can also have strong effects on the rate of diffusion of molecules encapsulated in the capsules. The additional deposition of layers slow down the substance release^{26,51,52,110,124}. As illustrated in Figure 1.14, adding further layers to the shell lead to a reduced rate of release for the enclosed insulin molecules. The additional layers thus act as an extra barrier which hinders diffusion of molecules through the wall.

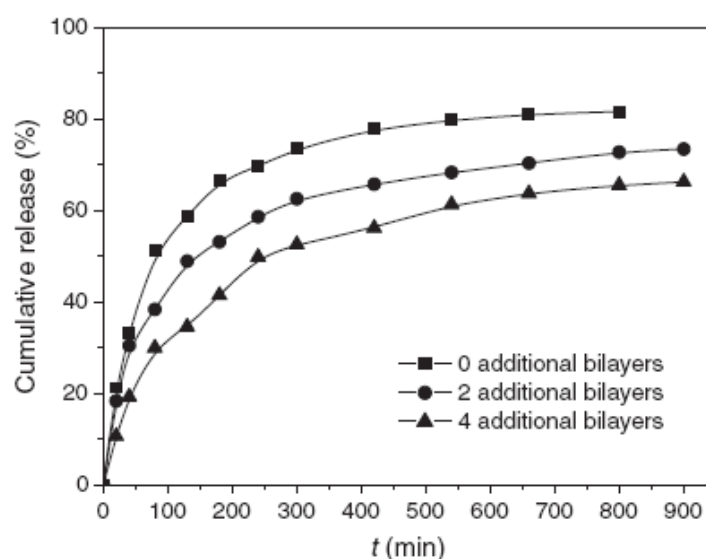


Figure 1.14. Release profile of insulin from (ALG/CH)5 microcapsules coated with additional layers after loading⁵¹.

Cross-linking through condensation reaction of complementary groups located on adjacent layers constitutes another possible way to stabilize the structure of the capsule walls, thereby, limiting the release. The relatively high permeability in the case of non cross-linked capsule walls becomes limited after formation of covalent bonds, which causes a compact structure^{31,125}. Furthermore, it has been observed, that cross-linking protects capsules against enzymatic degradation which can be a promising perspective in retarding drug release as a result of naturally occurring enzymes in the body.

In conclusion, several strategies have been proposed to control the release of drugs from capsules. However, in all cases, it is important to study the behaviour of the permeability *in vitro*, which gives the essential useful information for later introduction into the body.

1.5.2. Microreactors

In 2002, Dähne et al. carried out a copolymerization reaction inside of the PSS/PAH capsules (diameter 5.94 μ m). The hollow capsules were permeable to monomers - reactants such as styrene sulfonate (SS) and methacroyloxyethylthiocarbamoyl rhodamine B (MRho). The reaction in the presence of $K_2S_2O_8$ (temp. 80°C) as initiator yielded polystyrene with $M_w \sim 120 \times 10^3$ g/mol labelled with MRho.

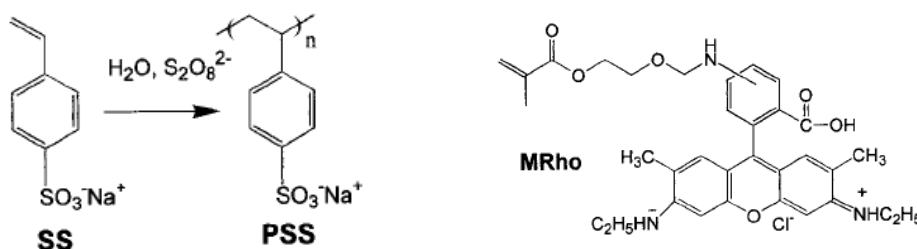


Figure 1.15. Structures of the monomers used for the synthesis of polystyrene labelled with rhodamine B, reaction occurs inside the capsules¹²⁶.

The capsules were separated from excess of polymer by centrifugation and oligomers were removed by dialysis. They were not permeable for high M_w of synthesized polystyrene polymer in the capsules¹²⁶.

Bioreactions in multicompartiment capsules has been performed by introducing various components into the same microcapsule separated by inner wall and then their mixing and leaving of the content. The capsules were based on an outer compartment built up around the inner one. The shell-in-shell capsules had a total size ranging from 8–10 μ m with an inner shell diameter of 3–4 μ m.

The last outer shell was formed by re-precipitation of $CaCO_3$ on the inner shell which contains the metal nanoparticles adsorbing the laser light. Destruction of the barrier between contents of the two separate compartments occurred by laser impulses, allowing the mixing of two substances (**Figure 1.16**). It is a promising method to initiate bioreactions in very small microcompartments¹²⁷.

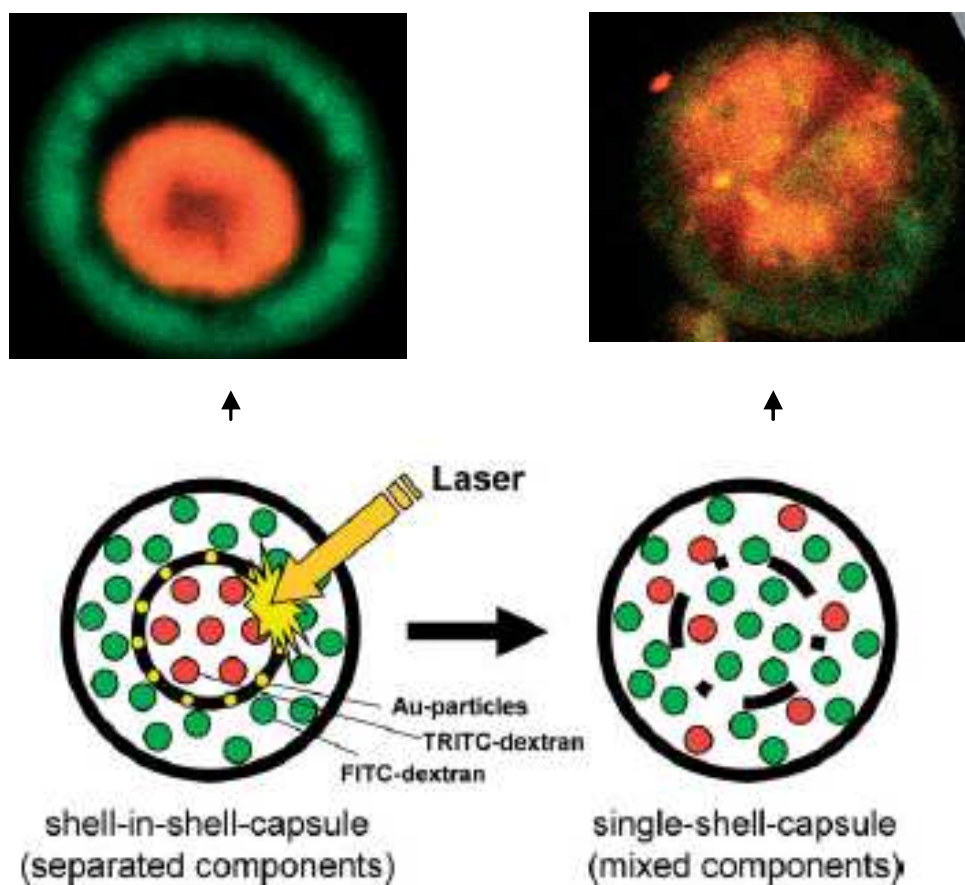


Figure 1.16. Schematics of the shell-in-shell polyelectrolyte multilayer capsule and laser induced inter-compartmentalized mixing and above their equivalent CLSM images¹²⁷.

The capsules can also play the role of protectors for bioactive substances which should often be “temporarily inactive” during travel time to the targeted cell. When they have reached their target, they can be activated and released.

Bacterial alkaline phosphatase (AP) (hydrolase enzyme responsible for removing phosphate groups from many types of molecules) is known to be able to convert the doxorubicin (DOX) precursor in order to kill cancer cells. Sukhorukov *et al.*¹²⁸ showed an example as a model, how to use AP to convert a nonfluorescent substrate into fluorescein. AP, included between the PSS/PAH multilayer shells, transformed non-active into active fluorescein (**Figure 1.17**)

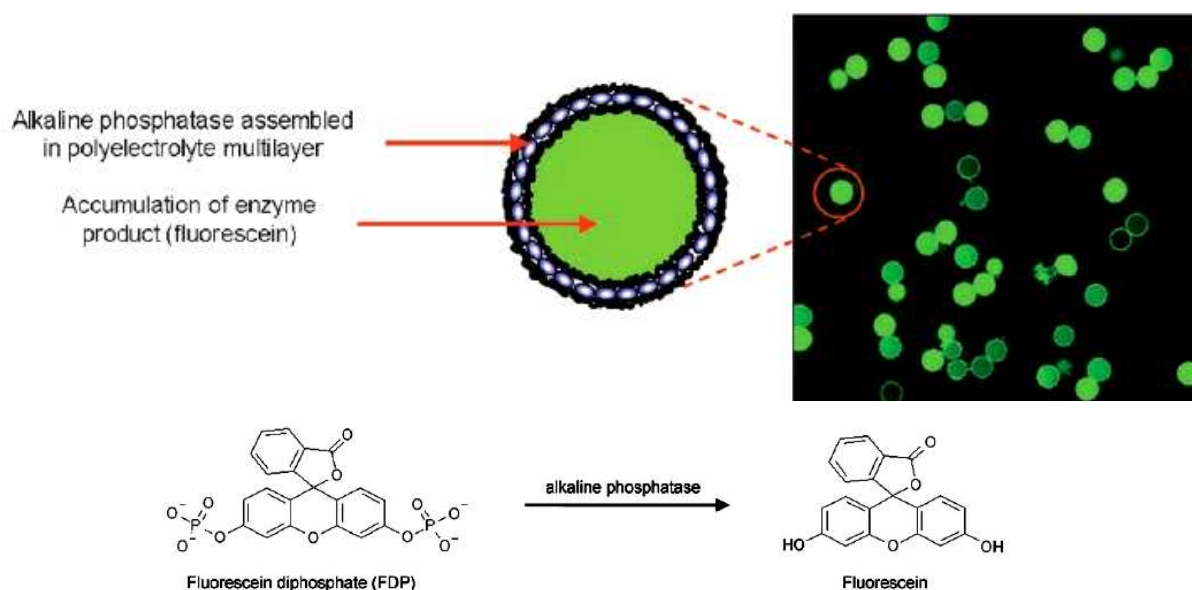


Figure 1.17. Enzymatic formation of fluorescein within polyelectrolyte microcapsules catalyzed by an encapsulated bacterial alkaline phosphatase¹²⁸.

In the perspectives, the localization of capsules in desired locations and drug production *in situ* is considered.

Mak et al.⁸⁶ performed different LbL capsules from different strong and weak polyelectrolytes (PSS, Dextran sulphate, PAA, PAH, PEI, PDA) studying their ability to be potentially used as microreactors. The multilayers deposited on highly hydrated agarose hydrogels provide excellent conditions for biochemical reactions, e.g. they show growth of *E.coli* bacterium encapsulated within the microcapsules. The use of small volumes for biochemical reactions is desirable because it reduces reaction time and reagent consumption, thus reducing reaction costs. Microcapsules suspended in a solution would allow possibility of a very high number of individual reactions.

1.5.3. Microsensors

DNA is a natural, biodegradable and biocompatible polymer of which reaction with other components can be controlled by the composition of the chain. It is possible to arrange DNA bases in such a way that the DNA polymer adopts a “loop” conformation. A fluorophore and quencher were attached at positions on such a DNA polymer allowing controlled intensity of fluorescence emission as a function of conformation (on **Figure 1.18**

red and grey ball). The moment, when the place of the “loop” will be fulfilled by another matching object, the DNA will change its conformation causing change in position of the fluorophore and quencher. Depending on the distance between the fluorophore and quencher, a fluorescent signal may be induced⁹⁹.

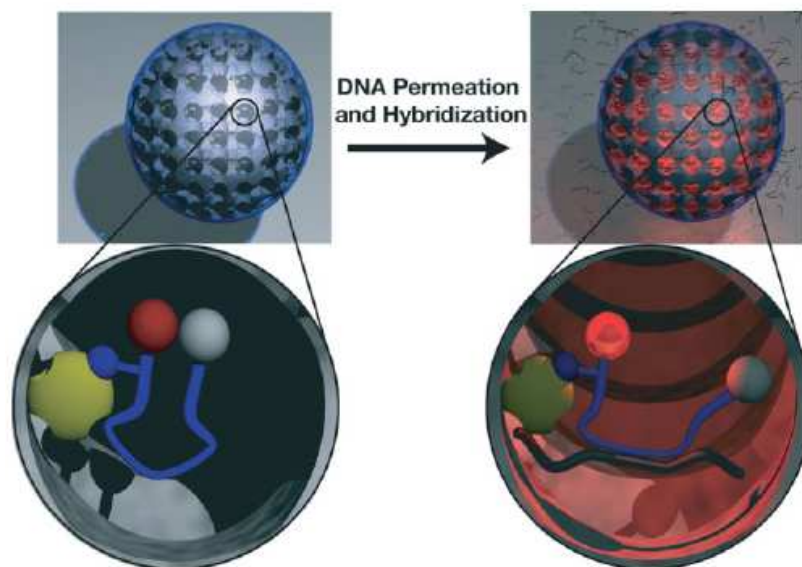


Figure 1.18. Biotin-functionalized system immobilized inside avidin-modified polyelectrolyte multilayer-covering nanoporous silica particles. By complexation with a DNA sequence complementary to the loop, a change of conformation occurred resulting in a fluorescent signal⁹⁹.

The versatile nature of DNA as a functional, biocompatible, biodegradable and site-specific building block paves the way to engineer new materials for biomedical applications, ranging from therapeutics (e.g., targeted drug delivery, gene therapy, vaccine delivery) to diagnostics (e.g., biosensing and imaging).

LbL based capsules are promising micro-tool for detecting low molecule concentrations. There is interest in developing biosensors for monitoring glucose level in relation to diabetes treatment. Recently, glucose sensitive complexes (FITC-dextran/ TRITC-apo-GOx, where apo-GOx is a glucose oxidase enzyme sensitive to β -D-glucose) was enclosed inside the capsules. In the presence of glucose inside the capsules, the dextran was replaced from the complex leading to changes in the transmitted energy; this was expressed in terms of FITC/TRITC fluorescence percentage ratio. By calculation of suitable fluorescence one can estimate the level of the glucose in a given living system¹²⁹.

In order to generate a capsule-based pH sensor “seminaphthorhodafluor” dye (“SNARF-1”) was employed. The SNARF-1 dye was covalently attached to dextran species (70 kDa) and coprecipitated with $\text{Na}_2\text{CO}_3/\text{CaCl}_2$. The resulting CaCO_3 particles were then coated with PSS/PAH layers. After carbonate dissolution, the capsules filled with SNARF-1 were incubated in solutions at various pH values. The above-mentioned dye exhibits a significant pH-dependent emission shift from yellow/orange to deep-red fluorescence under acidic and basic conditions. After capsule uptake by the cells, monitoring of the local pH inside living cells is possible (**Figure 1.19**)⁷².

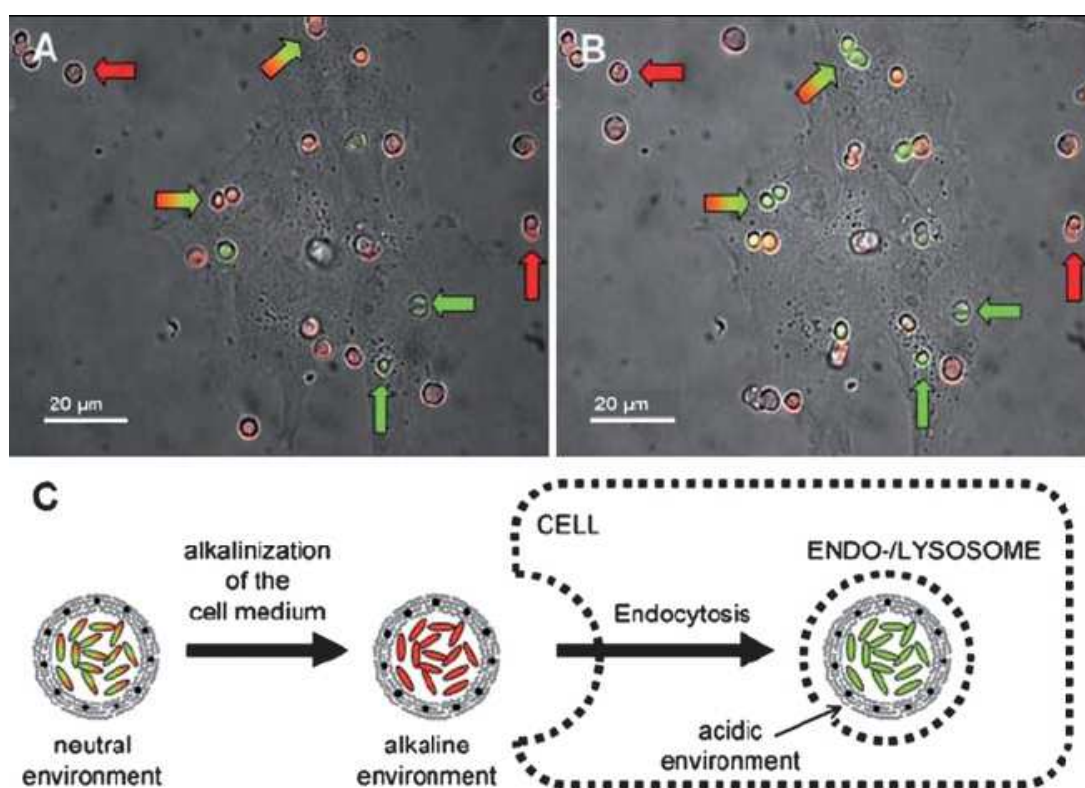


Figure 1.19. SNARF-loaded capsules change from red to green fluorescence upon internalization by cells. The capsules outside of the cells exhibit red fluorescence due to the basic pH of the environment. Capsules remaining in the cell medium retain their red fluorescence (red arrows). Capsules incorporated in the acidic endosome retain their green fluorescence (green arrows). Some capsules were incorporated in endosomal/lysosomal compartments inside cells which is indicated by their change in fluorescence from red to green (red to green arrows)⁷².

1.5.4. Semiconductors

Semiconductor nanocomposites have recently emerged as promising nanomaterials in electronic technology. The incorporation of functional nanoparticles into multilayer films deposited on colloidal particles is an interesting object for optic and electronic properties.

For example, CdTe is a highly useful material for the development of solar cells (photovoltaics). Its drawback is the toxicity of CdTe nanocrystal in case of inhalation or ingestion. Once properly and securely captured and encapsulated, it can be used in manufacturing process.

In regard to this problem, it has been shown that nanoparticles such CdTe(S) (cadmium telluride with a trace amount of sulphide) can be incorporated into the PSS/PAH capsules¹³⁰.

1.5.5. Waveguides

Polymerization of the porphyrin monomers in the polyelectrolyte multilayer capsules leads to the formation of interesting satellite-like structures consisting of hollow capsules with cylindrical, radially directed nanotubes¹³¹.

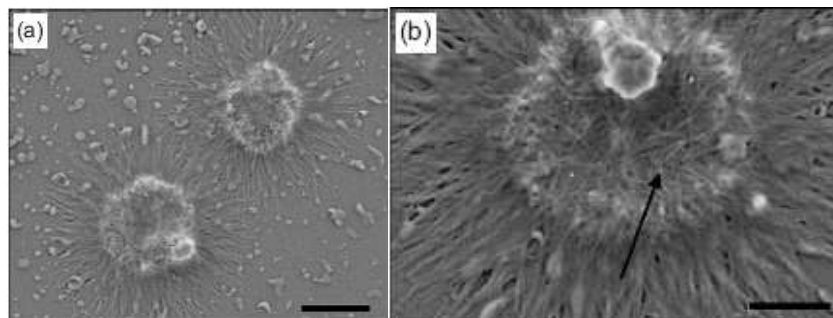


Figure 1.20. SEM images showing satellite-like structures with central capsule core and porphyrin fibers (scale bar = 2 μ m).

Porphyrins are heterocyclic macrocycles, aromatic compounds; they are components of haemoglobin and myoglobin; they are known for applications as a dye, as catalyst in organic chemistry and use in solar cells for converting solar energy into electricity. As optical waveguide they have already found applications as catalysts in chemical, biological and medical fields.

The porphyrin nanotubes protruding from the capsule surface can act as optical waveguides to diffuse light from one end of the tube to the capsule interior; such delivered energy can be used for specific applications in the centre of capsule¹³¹.

1.5.6. Capsules in nutrition

In food industry, there is an interest in the use of microcapsules to protect, isolate or control the release of a given substance. The encapsulated substances can be flavours, vitamins, polyunsaturated fatty acids, minerals, antioxidants or functional ingredients.

The LbL capsules with significant mechanical stability were fabricated from food-grade components. For this aim, the capsules prepared by LbL adsorption of positively charged protein fibrils and negatively charged high methoxyl pectin (HMP) were adsorbed on oil droplets which, were removed by freeze drying in a later step. The size and strength of the capsules can be controlled by emulsification processes and by varying the number of layers⁸².

1.6. Capsules made from polysaccharides

To date, most of the studies on LbL capsules have been carried out on synthetic polyelectrolytes such as PSS and PAH. Owing to the potential applications of the LbL nano-/microcapsules in the field of biotechnology and drug delivery, natural polysaccharides have the advantages of biocompatibility, biodegradability and bioactivity and are promising candidates for capsule wall building.

Today, even if there are some reports with examples of polysaccharides multilayer on the planar surface^{5,33,43,46,55-57,64,66,132-137}, only little is known about the properties of polysaccharide capsules.

The reason of some difficulties with capsules fabrication is related with the physico-chemical properties of the natural polysaccharides: variability of the structures, high dispersion of molecular weight of the chains as well as hydrophilic properties.

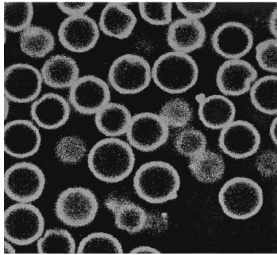
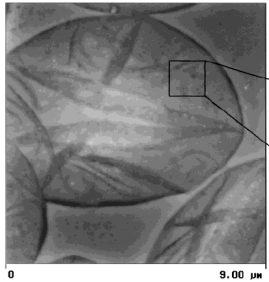
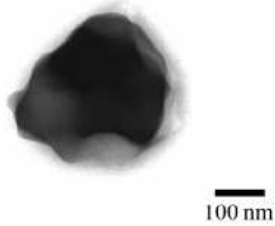
Films containing polysaccharides exhibit exponential growth of the thickness^{5,10}. They are more hydrated and mechanically softer than their synthetic counterparts with linear growth. The fact that natural polysaccharides are generally weak polyacids/polybases (low charge density along backbone) leads to the formation of weak complexes¹³⁸. Additionally, contrary

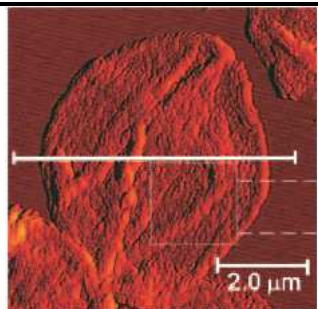
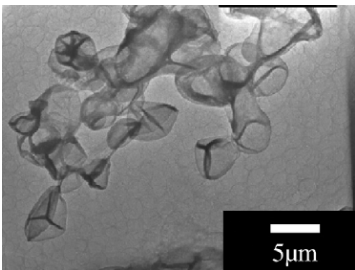
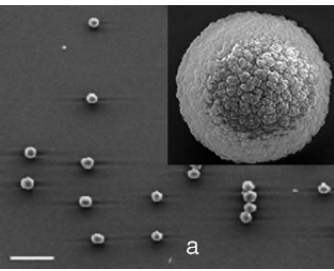
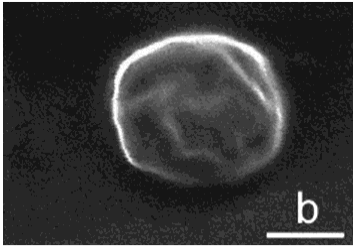
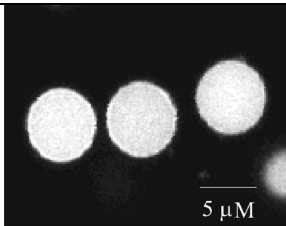
to films formed on planar surfaces, the fabrication of the capsules requires the use of a solvent for template dissolution which, especially in case of polysaccharides, can cause multilayer destruction.

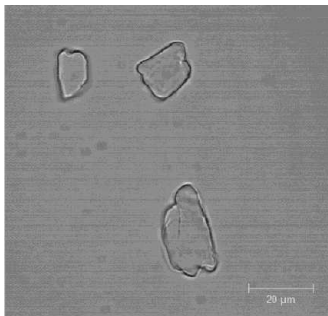
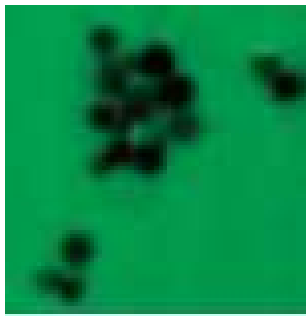
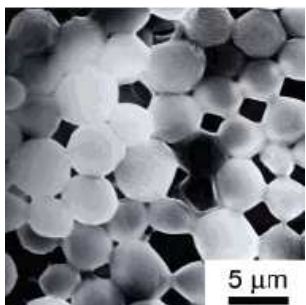
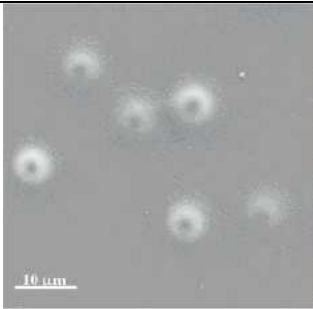
Current research work on polysaccharide LbL capsules provides information on conditions for capsule synthesis and some of their properties.

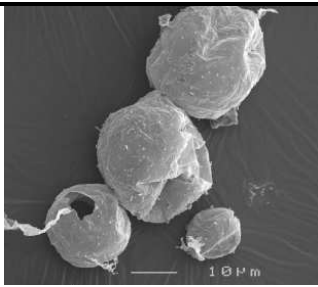
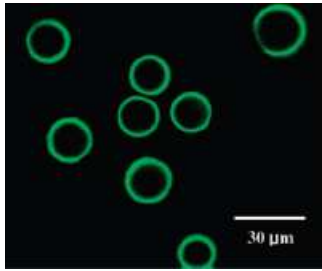
The table below lists different capsules made from polysaccharides and derivatives, as well as their principle properties.

Table 1.4. Polysaccharides in LbL capsules.

Components of the LbL capsule	Template	Studied properties	Microscopy images
Chitosan/Chitosan sulfate ⁵⁹	MF	Permeability as a function of pH, salt concentration and various substances	 <p>CLSM</p>
Chitosan/Chitosan sulfate ⁶²	Erythrocytes	Wall texture	 <p>SFM</p>
Cross-linked chitosan ⁶⁰	SiO ₂	pH behaviour (swelling, shrinking)	 <p>TEM</p>

Chitosan/Tannic acid ¹³⁹	MnCO ₃	pH responsive properties	 <p>AFM</p>
Chitosan/Alginate ^{48,61}	CaCO ₃	DOX - anticancer drug release studies (different pH corresponding to gastric and intestinal conditions respectively; <i>in vitro</i> and <i>in vivo</i> study)	 <p>TEM</p>
Chitosan/Alginate ⁵¹	MF	pH responsive properties, influence of heating, increase of the layer number, chemical cross-linking (release of the insuline)	 <p>SEM</p>
Chitosan/Alginate ¹⁴⁰	PS	Influence of cross-linking on drug release	 <p>SEM</p>
Protamine/Alginate ⁵²	MF	Release of entrapped biological macromolecules in two various pH imitating the stomach and intestinal conditions	 <p>CLSM</p>

Chitosan/Dextran sulfate ⁴⁹	Ibuprofen crystals	Drug release as a function of multilayer thickness, crystal size, at two different pH: 1,4 and 7,4	 <p>SEM</p>
Chitosan/Dextran sulfate ^{76,141}	SiO ₂	pH-responsive properties of the film, enzymatic degradation, shell permeability, encapsulation	 <p>CLSM ¹⁴¹</p>  <p>SEM ⁷⁶</p>
Protamine/Dextran sulphate ⁵⁴	MF	Permeability of the macromolecules at various molecular weight and charge, permeability as a function of various pH and wall thickness	 <p>SEM</p>

Protein/HMP ⁸²	Oil template	Mechanical resistance	 <p>SEM</p>
Poly (L-lysine)/Hyaluronic acid ⁴⁷	HA disulfide cross-linked hydrogel	Behaviour on freezing and thawing, permeability in different pH, enzymatic degradation, cross-linking	 <p>CLSM</p>

As it has been observed, the most often used polysaccharides for LbL capsule fabrication are chitosan and alginate. There is only one example of the capsules based on HA, however the multilayers are chemically cross-linked to obtain more stable shells⁴⁷.

In this context, the studies on the synthesis of the capsules made from hyaluronic acid with its unique properties are desired and they are demonstrated in the next paragraph.

1.7. Hyaluronic acid

1.7.1. Structure

Hyaluronic acid (sodium hyaluronate, HA) is a linear natural polysaccharide composed of repeating disaccharide units of (1→4) - β linked D-glucuronic and (1→3)- β linked *N*-acetyl-D-glucosamine residues, **Table 1.2**. The weight average molecular weight of HA can vary from 10^5 to $\sim 5\text{-}6 \times 10^7$ g/mol.

In the solid state, different helical conformations were demonstrated in which intramolecular H-bonds stabilize the single- or double- helical conformation depending on the counterion (H^+ , Na^+ , K^+ , Ca^{2+})¹⁴².

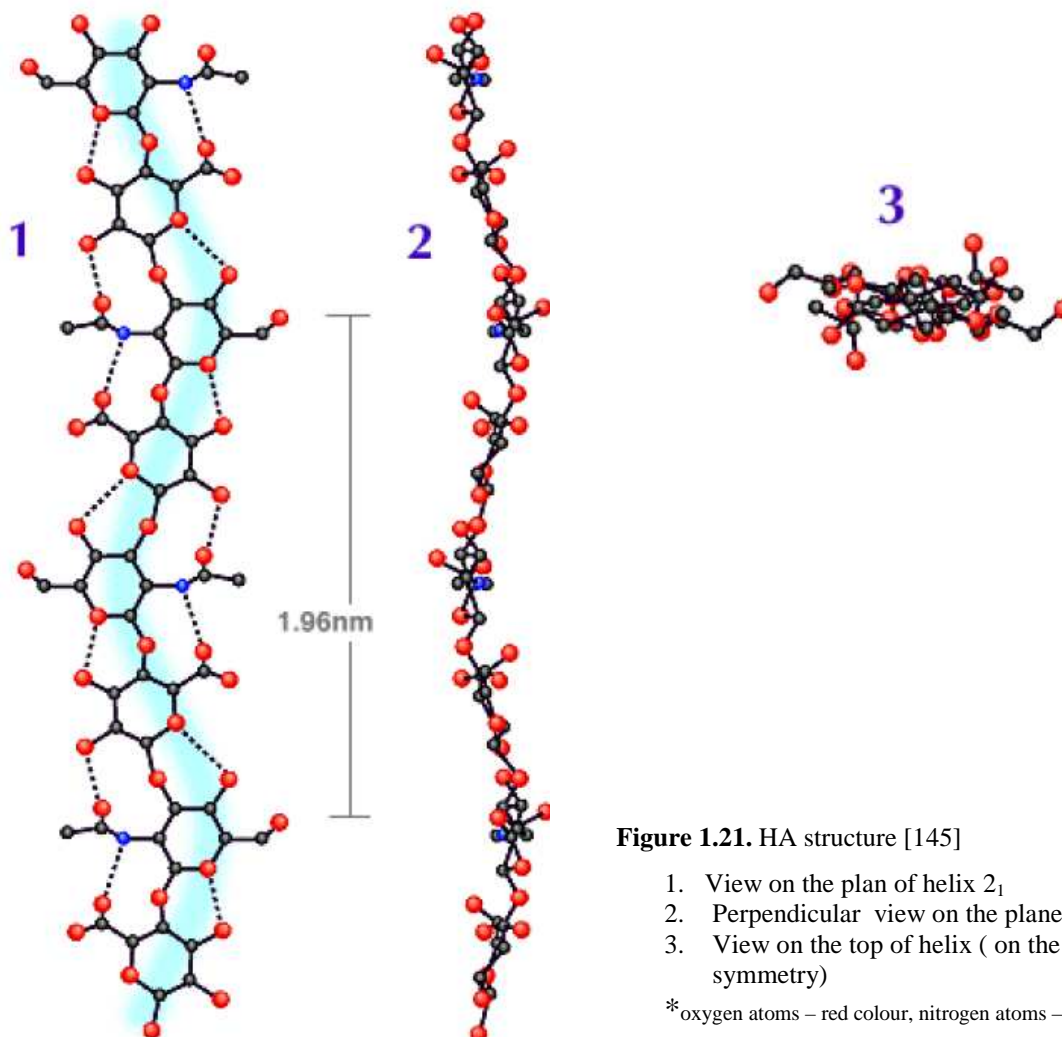


Figure 1.21. HA structure [145]

The exact conformation in aqueous solution is not yet established. It is said that the individual HA molecules are present in solution in random coil conformation, but it is possible that for the polymeric chain, dynamic hydrogen bonded regions exist, controlling the average stiffness of the molecule. It was shown that the stiffness of the chain decreases when the temperature increases due to the dissociation of the hydrogen bonds.

The hyaluronan is a charged acid polyelectrolyte, with the distance between two ionic carboxylic groups equal to 9.8 Å from the chemical structure in the extended coiled conformation, but from the helical structure the distance is estimated as 8.5 Å¹⁴².

Its intrinsic pK (pKa) is estimated by pH titration and is equal to 2.9 ± 0.1 ^{142,143}. When decreasing pH by progressive addition of HCl, a gel is formed around pH 2.5 since degree of dissociation of carboxylic acid groups decreases, favouring intermolecular interactions and H-bond network formation. Further decrease of the pH causes the gel-sol transition related to the protonation of the acetamide groups leading to electrostatic repulsions.

Important characteristics for a polymer are its molecular weight distribution, the average molecular weights and the related intrinsic viscosity. Molecular weight distribution is related to chain dimension in solution (i.e. the radius of gyration, R_g). The Size Exclusion Chromatography (SEC) technique allows a very complete characterization of the polymer from which it is possible to determine the relation between molecular weight, and the gyration radius or viscosity (in the solvent used for the SEC analysis 0.1M NaNO₃)^{142,144}:

$$R_g(\text{nm}) = KM^v \quad \text{eq. 1.1}$$

R_g – radius of gyration

M- molecular weight

K, v – known parameters: K=0.049, v=0.55

1.7.2. Chemical modification

HA presents few functional groups which can be chemically modified: primary hydroxyl, acetamide, and carboxyl groups (**Figure 1.22**).

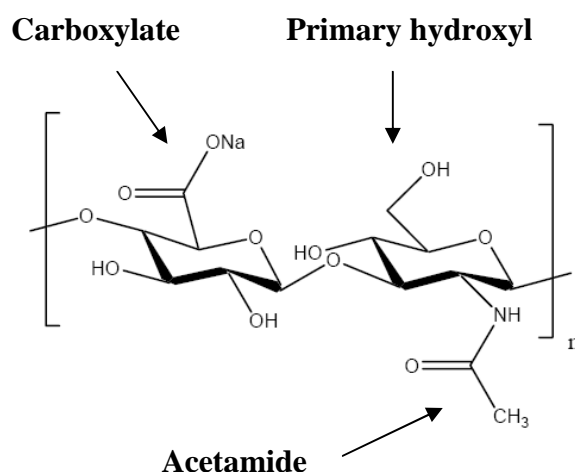


Figure 1.22. The repeating unit of HA with its functional groups.

Acetamide can react only under harsh conditions creating reactive -NH_2 group. The drawback of this reaction is depolymerisation. The -OH are suitable for sulfatation or esterification reactions¹⁴⁵.

The main chemical modifications of HA take a place on the carboxyl groups. An important reaction is modification of HA via adipic acid dihydrazide (ADH) in the presence of a water soluble carbodiimide (*N*-(3-Dimethylaminopropyl)-*N'*-ethylcarbodiimide hydrochloride, EDC) to obtain derivatives with reactive pendant hydrazide groups, HA-ADH¹⁴⁶. For instance, HA-ADH can be further modified by methacrylic anhydride to be later chemically cross-linked to produce hydrogels¹⁴⁶.

1.7.3. Occurrence in the living organism and its functions

Hyaluronic acid is present in the human body and other vertebrates, in some bacteria, for example *Streptococci*. It has been found at high concentration in rooster combs. Occurrence of HA in different animal tissues is presented in **Table 1.5**.

Table 1.5. Occurrence of HA in different animal tissues and its content¹⁴⁷.

Tissue or body fluid	Concentration (µg/ml)
Rooster comb	7500
Human umbilical cord	4100
Human joint (synovial) fluid	1400–3600
Bovine nasal cartilage	1200
Human vitreous body	140–340
Human dermis	200–500
Human epidermis	100
Rabbit brain	65
Rabbit heart	27
Human urine	0.1–0.3
Human serum	0.01–0.1

HA is found naturally in most cells in the human body and occurs in high concentrations in specific body locations.

The half-life of HA in tissues is less than 3 days. HA undergoes enzymatic degradation by hyaluronidase enzymes present in the human body in organs such as testes, spleen, skin, eye, liver, kidney, uterus and placenta and body liquids (tear liquid, blood and sperma)^{144,148}.

Besides enzymatic scission of hyaluronic acid chains, there are other non-enzymatic reactions that degrade HA¹⁴⁹ such as free radical degradation, acidic and alkaline hydrolysis¹⁵⁰, photodegradation involving microwave, UV or γ -irradiation, thermal and ultrasonic degradation. It is assumed that degradation of HA in human body is an effect of few agents. However, the body constantly replenishes itself with HA.

Below is demonstrated the areas of the human body where hyaluronic acid is present and plays an important structural and biological function. It exist in many forms, circulating freely, tissue-associated, inserted into the extracellular matrix, thereby participating in the preservation of the form and in the spatial arrangement of tissue components.

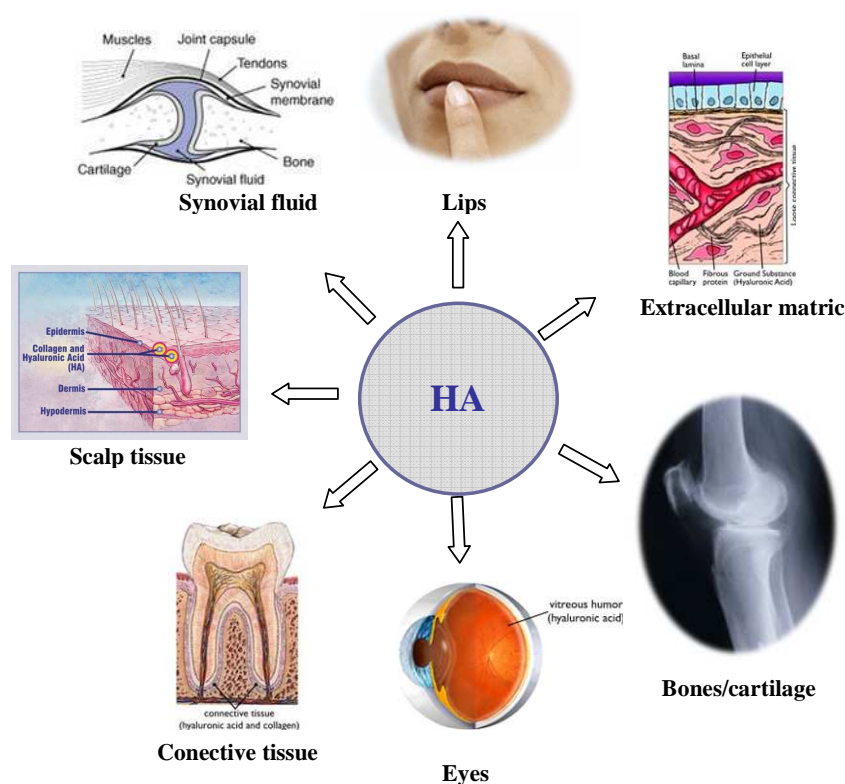


Figure 1.23. Occurrence of HA in human body¹⁵¹.

The presence of high molar weight of HA at high concentration in the synovial fluid provides necessary lubrication for the joint and shock absorption. The HA molecules can absorb a large volume of water which expands in the extracellular space, hydrates tissues and finally maintains the moisture of the skin. In the lips, HA with collagen gives shape and plumpness. The fluid inside the eye, called the vitreous humor, is composed almost completely of hyaluronic acid. HA is responsible for the gel-like property of the fluid inside the eye which acts as a “shock absorber”.

Young skin contains a large amount of HA. With age, the ability of the skin to produce HA decreases leaving the skin unhealthy and wrinkled.

Besides its structural role in the connective tissue, HA has many other functional activities. Due to its specific binding to proteins and receptors, it plays important roles in embryogenesis, signal transduction and cell motility, and is associated with cancer diseases and metastasis^{147,152}.

Commercially available HA samples can come from animal sources (rooster combs) or produced by bacterial fermentation. HA was previously extracted from bovine vitreous humour, rooster combs and umbilical cords. HA is produced, on a large scale, by the bacteria *Streptococcus zooepidemicus* and *Streptococcus equi* with high purity and good yields.

1.7.4. Applications

HA is used in various fields in medicine. Since it is biodegradable and biocompatible and highly hydrophilic it is ideal for application in human tissues.

HA and derivatives find application in:

- 1) viscosurgery, to protect delicate tissues and provide space during surgical manipulations;
- 2) viscoaugmentation, to fill tissue spaces, as in skin, muscles, vocal and pharyngeal tissues;
- 3) viscoseparation, to separate connective tissue surfaces traumatized by surgical procedures or injury, in order to prevent adhesion and excessive scar formation;
- 4) viscosupplementation, to replace or supplement tissue fluids, such as replacement of synovial fluid in painful arthritis, to relieve pain;
- 5) viscoprotection, to protect healthy, wounded, or injured tissue surfaces from dryness or noxious environmental agents¹⁵³.

1.8. Conclusion

The main aim of this chapter was to review the recent research activities developed in the field of LbL hollow capsules.

The versatility of the LbL approach has allowed a broad range of materials to be assembled on various substrates, on the basis of not only electrostatic interactions but also hydrogen bonding, covalent bonding, and other driving forces such as host-guest, base-pair or other specific interactions. The properties of the LbL films, such as composition, thickness, and function, can be readily tuned by simply varying the type of adsorbed material, the number of deposited layers, and the conditions employed during the assembly process.

The unique advantage of multifunctional microcapsules in comparison to other systems is that they can be simultaneously loaded/functionalized with different components, allowing for a combination of their properties in a single object.

The LbL microcapsules with integrated multifunctionalities have a high capacity for loading a wide range of substances and a sensitive response to diverse stimuli, thus they are highly attractive for applications in biotechnology and pharmacy. The suitable surface coating of the particle may control the specific and unspecific uptake mechanisms into the cell. The ability to remotely release the encapsulated material at the site of interest makes capsules very attractive in drug delivery. Their multifunctional properties can be also used to diagnostics i.e. biosensing or imaging. Due to their small internal volume, they can be useful as microreactors in order to reduce reagent consumption for many biochemical reactions. They can also produce drugs *in situ*, upon reaching their destination, which would prevent the random release of potentially toxic material before reaching the target.

For drug delivery, capsules made from biocompatible and biodegradable polymers are desired. To date, only a few examples of LbL capsules made from such materials are reported. Capsules made from polysaccharides such as chitosan, alginate and dextran are mainly described. The permeability properties as a function of external stimuli such as pH and salt concentration have been characterized. These capsules often show non stable structures. Current research in polysaccharide capsule synthesis still requires development in the construction and application of viable capsules.

References:

- (1) Iler, R. K. *Journal of Colloid and Interface Science* **1966**, *21*, 569-594.
- (2) Decher, G.; Lvov, Y.; Schmitt, J. *Thin Solid Films* **1994**, *244*, 772-777.
- (3) Lvov, Y.; Haas, H.; Decher, G.; Moehwald, H.; Mikhailov, A.; Mtchedlishvily, B.; Morgunova, E.; Vainshtein, B. *Langmuir* **1994**, *10*, 4232-4236.
- (4) Decher, G. *Science* **1997**, *277*, 1232-1237.
- (5) Porcel, C., Lavalle, P., Ball, V., Decher, G., Senger, B., Voegel, J.-C., and Schaaf, P. *Langmuir* **2006**, *22*, 4376-4383.
- (6) Fujimoto, K.; Fujita, S.; Ding, B.; Shiratori, S. *Japanese Journal of Applied Physics, Part 2: Letters & Express Letters* **2005**, *44*, L126-L128.
- (7) Boulmedais, F., Ball, V., Schwinte, P., Frisch, B., Schaaf, P., and Voegel, J.-C. *Langmuir* **2003**, *19*, 440-445.
- (8) Picart, C.; Mutterer, J.; Richert, L.; Luo, Y.; Prestwich, G. D.; Schaaf, P.; Voegel, J. C.; Lavalle, P. *Proceedings of the National Academy of Sciences of the United States of America* **2002**, *99*, 12531-12535.
- (9) Richert, L., Boulmedais, F., Lavalle, P., Mutterer, J., Ferreux, E., Decher, G., P., Schaaf, Voegel J.-C., and Picart, C. *Biomacromolecules* **2004**, *5*, 284-294.
- (10) Laugel, N.; Betscha, C.; Winterhalter, M.; Voegel, J.-C.; Schaaf, P.; Ball, V. *Journal of Physical Chemistry B* **2006**, *110*, 19443-19449.
- (11) Wang, Y.; Angelatos, A. S.; Dunstan, D. E.; Caruso, F. *Macromolecules (Washington, DC, United States)* **2007**, *40*, 7594-7600.
- (12) Such, G. K.; Tjinto, E.; Postma, A.; Johnston, A. P. R.; Caruso, F. *Nano Letters* **2007**, *7*, 1706-1710.
- (13) Schuetz, P.; Caruso, F. *Advanced Functional Materials* **2003**, *13*, 929-937.
- (14) Schlenoff, S. T. D. a. J. B. *Macromolecules* **2001**, *34*, 3736-3740.
- (15) Li, Q.; Quinn, J. F.; Wang, Y.; Caruso, F. *Chemistry of Materials* **2006**, *18*, 5480-5485.
- (16) Mendelsohn, J. D., Yun Yang, S., Jeri'Ann Hiller, Hochbaum, A.I., and Rubner, M.F. **2003**, *4*, 96-106.
- (17) Jinhua Dai, A. W. J., Dillip K. Mohanty, Jason Erndt and Merlin L. Bruening. *Langmuir* **2001**, *17*, 931-937.

- (18) Petrov, A. I., Antipov, A.A., and Sukhorukov, G.B. *Macromolecules* **2003**, 36, 10079-10086.
- (19) Biesheuvel, P. M.; Mauser, T.; Sukhorukov, G. B.; Moehwald, H. *Macromolecules* **2006**, 39, 8480-8486.
- (20) Zelikin, A. N.; Becker, A. L.; Johnston, A. P. R.; Wark, K. L.; Turatti, F.; Caruso, F. *ACS Nano* **2007**, 1, 63-69.
- (21) Zelikin, A. N.; Quinn, J. F.; Caruso, F. *Biomacromolecules* **2006**, 7, 27-30.
- (22) Ok, S.; Kozlovskaya, V.; Sousa, A.; Libera, M.; Sukhishvili, S. A. *Abstracts of Papers, 227th ACS National Meeting, Anaheim, CA, United States, March 28-April 1, 2004*.
- (23) Kozlovskaya, V.; Kharlampieva, E.; Mansfield, M. L.; Sukhishvili, S. A. *Chemistry of Materials* **2006**, 18, 328-336.
- (24) Mauser, T., Dejuguat, C., Mohwald, H., and Sukhorukov, G.B. *Langmuir* **2006**, 22, 5888-5893.
- (25) Radtchenko, I. L., Sukhorukov, G.B., Leporatti, S., Khomutov, G.B., Donath, E., and Mohwald, H. *Journal of Colloid and Interface Science* **2000**, 230, 272–280.
- (26) Petrov, A. I.; Gavryushkin, A. V.; Sukhorukov, G. B. *Journal of Physical Chemistry B* **2003**, 107, 868-875.
- (27) Feng Wang, J. F., Weijun Tong and Changyou Gao. *J. Mater. Chem.*, **2007**, 17, 670-676.
- (28) Shchukin, D. G.; Koehler, K.; Moehwald, H.; Sukhorukov, G. B. *Angewandte Chemie, International Edition* **2005**, 44, 3310-3314.
- (29) Poptoshev, E.; Schoeler, B.; Caruso, F. *Langmuir* **2004**, 20, 829-834.
- (30) Shutava, T., Prouty, M., Kommireddy, D., and Lvov, Y. *Macromolecules* **2005**, 38, 2850-2858.
- (31) Weijun Tong, C. G., and Helmuth Mohwald. *Chemical Materials* **2005**, 17, 4610-4616.
- (32) S. Leporatti, C. G., A. Voigt, E. Donath, H. Mohwald. *The European Physical Journal E* **2001**, 5, 13-20.
- (33) Burke, S. E.; Barrett, C. J. *Biomacromolecules* **2005**, 6, 1419-1428.
- (34) Mueller, R.; Koehler, K.; Weinkamer, R.; Sukhorukov, G.; Fery, A. *Macromolecules* **2005**, 38, 9766-9771.

- (35) Gao, C., Leporatti, S., Donath, E., Mohwald, H., *J. Phys. Chem.B* **2000**, *104*, 7144-7149.
- (36) Miller, M. D.; Bruening, M. L. *Langmuir* **2004**, *20*, 11545-11551.
- (37) Koehler, K.; Sukhorukov, G. B. *Advanced Functional Materials* **2007**, *17*, 2053-2061.
- (38) Kohler Karen, S. D., G. Mohwald, Helmuth, Sukhorukov Gleb, B. *J Phys Chem B* **2005**, *109*, 18250-18259.
- (39) Celine Brunota, L. P., Christelle Lagneaua, Pierre Farge, Catherine Picarte, Brigitte Grosogoeat. *Biomaterials* **2007**, *28*, 632-664.
- (40) Meyer, F.; Dimitrova, M.; Jedrzejenska, J.; Arntz, Y.; Schaaf, P.; Frisch, B.; Voegel, J.-C.; Ogier, J. *Biomaterials* **2007**, *29*, 618-624.
- (41) Qiu, X.; Donath, E.; Mohwald, H. *Macromolecular Materials and Engineering* **2001**, *286*, 591-597.
- (42) De Vos, P.; Hoogmoed, C. G.; Busscher, H. J. *Journal of Biomedical Materials Research* **2002**, *60*, 252-259.
- (43) Collin, D.; Lavalle, P.; Garza, J. M.; Voegel, J.-C.; Schaaf, P.; Martinoty, P. *Macromolecules* **2004**, *37*, 10195-10198.
- (44) Wattendorf, U.; Kreft, O.; Textor, M.; Sukhorukov, G. B.; Merkle, H. P. *Biomacromolecules* **2008**, *9*, 100-108.
- (45) Vodouhe, C., Le Guena, E., Garzaa, J.M., Franciusa, G., Dejognat, C., Ogiera, J., Schaaf, P., Voegel, J.-C., Lavalle, P. *Biomaterials* **2006**, *27*, 4149–4156.
- (46) Ball, V.; Huebsch, E.; Schweiss, R.; Voegel, J.-C.; Schaaf, P.; Knoll, W. *Langmuir* **2005**, *21*, 8526-8531.
- (47) Lee, H., Jeong, Yongho, Park, Tae Gwan. *Biomacromolecules* **2007**, *8*, 3705-3711.
- (48) Qinghe Zhao, B. H., Zhaohai Wang, Changyou Gao, Chenghong Peng, Jiacong Shen. *Nanomedicine* **2007**, *2007*, 63-74.
- (49) Xingping Qiu, S. L., Edwin Donath, Helmuth Mohwald. *Langmuir* **2001**, *17*, 5375-5380.
- (50) Strand, B. L.; Morch, Y. A.; Espevik, T.; Skjak-Braek, G. *Biotechnology and Bioengineering* **2003**, *82*, 386-394.
- (51) Shiqu Ye, C. W., Xinxing Liu, Zhen Tong , Beye Ren, Fang Zeng. *Journal of Controlled Release* **2006**, *112*, 79-87.
- (52) Tiourina, O. P., Sukhorukov, G.B. *International Journal of Pharmaceutics* **2002**, *242*, 155-161.

- (53) Caruso, C. S. a. F. *Biomacromolecules* **2001**, 2, 921-926.
- (54) Balabushevich, N. G.; Tiourina, O. P.; Volodkin, D. V.; Larionova, N. I.; Sukhorukov, G. B. *Biomacromolecules* **2003**, 4, 1191-1197.
- (55) Schneider, A., Richert, L., Francius, G., Voegel, J.-C., and Picart, C. *Biomedical materials* **2007**, 2, S45-S51.
- (56) Wood, K. C.; Boedicker, J. Q.; Lynn, D. M.; Hammond, P. T. *Langmuir* **2005**, 21, 1603-1609.
- (57) Schoeler, B.; Delorme, N.; Doench, I.; Sukhorukov, G. B.; Fery, A.; Glinel, K. *Biomacromolecules* **2006**, 7, 2065-2071.
- (58) Jung, B. D.; Hong, J. D.; Voigt, A.; Leporatti, S.; Dahne, L.; Donath, E.; Mohwald, H. *Colloids and Surfaces, A: Physicochemical and Engineering Aspects* **2002**, 198-200, 483-489.
- (59) Berth, G.; Voigt, A.; Dautzenberg, H.; Donath, E.; Moehwald, H. *Biomacromolecules* **2002**, 3, 579-590.
- (60) Zhang, Y.; Guan, Y.; Zhou, S. *Biomacromolecules* **2005**, 6, 2365-2369.
- (61) Qinghe Zhao, Z. M., Changyou Gao, Jiacong Shen. *J. Biomater. Sci. Polymer Edn*, **2006**, 17, 997-1014.
- (62) Leporatti, S., Voigt, A., Mitlohner, R., Sukhorukov, G.B., Donath, E., and Mohwald, H. *Langmuir* **2000**, 16, 4059-4063.
- (63) Angelova, N.; Hunkeler, D. *Trends in Biotechnology* **1999**, 17, 409-420.
- (64) Picart, C.; Schneider, A.; Etienne, O.; Mutterer, J.; Schaaf, P.; Egles, C.; Jessel, N.; Voegel, J.-C. *Advanced Functional Materials* **2005**, 15, 1771-1780.
- (65) Catherine Picart, B. S., Kheya Sengupta, Frederic Dubreuil, Andreas Fery. *Colloids and Surfaces A: Physicochem. Eng. Aspects* **2007**, 303, 30-36.
- (66) Schneider, A.; Vodouhe, C.; Richert, L.; Francius, G.; Le Guen, E.; Schaaf, P.; Voegel, J.-C.; Frisch, B.; Picart, C. *Biomacromolecules* **2007**, 8, 139-145.
- (67) Mertz, D.; Hemmerle, J.; Boulmedais, F.; Voegel, J.-C.; Lavalley, P.; Schaaf, P. *Soft Matter* **2007**, 3, 1413-1420.
- (68) P. M. M. Schrooyen, R. v. d. M. a. C. G. D. K. *Proceedings of the Nutrition Society* **2001**, 60, 475-479.
- (69) Uludag, H.; De Vos, P.; Tresco, P. A. *Advanced Drug Delivery Reviews* **2000**, 42, 29-64.
- (70) <http://www.karmat.com/document.aspx?documentID=12>.

- (71) Peyratout, C. S.; Daehne, L. *Angewandte Chemie, International Edition* **2004**, *43*, 3762-3783.
- (72) Tong, W.; Gao, C. *Journal of Materials Chemistry* **2008**, *18*, 3799-3812.
- (73) Sukhorukov, G. B., Donath, E., Lichtenfeld, H., Knippel, E., Knippel, M., Budde, A., Mohwald, H. *Colloids and Surfaces A: Physicochemical and Engineering Aspects* **1998**, *137*, 253-266.
- (74) Caruso, F., Caruso, R.A., Möhwald, H. *Science* **1998**, *282*, 1111-1114.
- (75) Gao, C.; Moya, S.; Lichtenfeld, H.; Casoli, A.; Fiedler, H.; Donath, E.; Moehwald, H. *Macromolecular Materials and Engineering* **2001**, *286*, 355-361.
- (76) Yuki Itoh, M. M., Toshiyuki Kida, Mitsuru Akashi. *Biomacromolecules* **2006**, *7*, 2715-2718.
- (77) Gittins, D. I.; Caruso, F. *Advanced Materials (Weinheim, Germany)* **2000**, *12*, 1947-1949.
- (78) Decher, G. S. a. G. *Nano Letters* **2004**, *4*, 1833-1839.
- (79) Angelatos, A. S.; Katagiri, K.; Caruso, F. *Soft Matter* **2006**, *2*, 18-23.
- (80) Gu, Y. S.; Decker, A. E.; McClements, D. J. *Langmuir* **2005**, *21*, 5752-5760.
- (81) Voigt, A.; Buske, N.; Sukhorukov, G. B.; Antipov, A. A.; Leporatti, S.; Lichtenfeld, H.; Baumler, H.; Donath, E.; Mohwald, H. *Journal of Magnetism and Magnetic Materials* **2001**, *225*, 59-66.
- (82) Leonard M. C. Sagis, R. I. d. R., Francisco J. Rossier Miranda, Jolet de Ruiters, Karin Schroe, A. C. v. A., Henk Kieft, Remko Boom, and; Linden, E. v. d. *Langmuir* **2008**, *24*, 1608-1612.
- (83) Tjipto, E.; Cadwell, K. D.; Quinn, J. F.; Johnston, A. P. R.; Abbott, N. L.; Caruso, F. *Nano Letters* **2006**, *6*, 2243-2248.
- (84) Antipov, A. A., Shchukin, D., Fedutik, Y., Petrov, A.I., Sukhorukov, G. B., Mohwald, H. *Colloids and Surfaces A: Physicochemical and Engineering Aspects* **2003**, *224*, 175-183.
- (85) Agarwal, A.; Lvov, Y.; Sawant, R.; Torchilin, V. *Journal of Controlled Release* **2008**, *128*, 255-260.
- (86) Mak, W. C.; Cheung, K. Y.; Trau, D. *Chemistry of Materials* **2008**, *20*, 5475-5484.
- (87) Park, M.-K.; Deng, S.; Advincula, R. C. *Langmuir* **2005**, *21*, 5272-5277.
- (88) Radt, B.; Smith, T. A.; Caruso, F. *Advanced Materials (Weinheim, Germany)* **2004**, *16*, 2184-2189.

- (89) Dmitry V. Volodkin, N. I. L., and Gleb B. Sukhorukov. *Biomacromolecules* **2004**, 5, 1962-1972.
- (90) Elsner, N.; Kozlovskaya, V.; Sukhishvili, S. A.; Fery, A. *Soft Matter* **2006**, 2, 966-972.
- (91) Veronika Kozlovskaya, S. O., Alioscka Sousa, Matthew Libera, and Svetlana A. Sukhishvili. *Macromolecules* **2003**, 36, 8590-8592.
- (92) Van der Heyden, A.; Wilczewski, M.; Labbe, P.; Auzely, R. *Chemical Communications (Cambridge, United Kingdom)* **2006**, 3220-3222.
- (93) Heuberger, R.; Sukhorukov, G.; Voeroes, J.; Textor, M.; Moehwald, H. *Advanced Functional Materials* **2005**, 15, 357-366.
- (94) Zhiqiang Feng, Z. W., Changyou Gao, Jiacong Shen. *Advanced Materials* **2007**, 19, 3687-3691.
- (95) De Geest, B. G.; Jonas, A. M.; Demeester, J.; De Smedt, S. C. *Langmuir* **2006**, 22, 5070-5074.
- (96) Levy, T., Déjugnat, C., Sukhorukov, G.B. *Advanced Functional Materials* **2008**, 18, 1586-1594.
- (97) Iwao Suzuki, Y. E., Yosuke Mizukawa, Tomonori Hoshi and Jun-ichi Anzai. *Chemical Communications* **2002**, 164-165.
- (98) Crespo-Biel, O., Dordi, B., Reinhoudt, D.N., and Huskens, J. *Journal of the American Chemical Society* **2005**, 127, 7594-7600.
- (99) Johnston, A. P. R.; Zelikin, A. N.; Caruso, F. *Advanced Materials (Weinheim, Germany)* **2007**, 19, 3727-3730.
- (100) Johnston, A. P. R.; Caruso, F. *Small* **2008**, 4, 612-618.
- (101) Johnston, A. P. R.; Cortez, C.; Angelatos, A. S.; Caruso, F. *Current Opinion in Colloid & Interface Science* **2006**, 11, 203-209.
- (102) Petrov, A. I.; Volodkin, D. V.; Sukhorukov, G. B. *Biotechnology Progress* **2005**, 21, 918-925.
- (103) Radtchenko, I. L.; Sukhorukov, G. B.; Mohwald, H. *Colloids and Surfaces, A: Physicochemical and Engineering Aspects* **2002**, 202, 127-133.
- (104) Xingyu Liu, C. G., Jiacong Shen, Helmuth Mohwald. *Macromol. Biosci.* **2005**, 5, 1209 –1219.
- (105) Dejugnat, C.; Sukhorukov, G. B. *Langmuir* **2004**, 20, 7265-7269.

- (106) Antipov, A. A., Sukhorukov, G.B., Leporatti, S., Radtchenko, I.L., Donath, E., Mohwald, H. *Colloids and Surfaces A* **2002**, 198-200, 535-541.
- (107) Sukhorukov, G. B., Antipov, A.A., Voigt,A., Donath, E., and Mohwald, H. *Macromol. Rapid Commun* **2001**, 22, 44-46.
- (108) De Geest, B. G.; Sanders, N. N.; Sukhorukov, G. B.; Demeester, J.; De Smedt, S. C. *Chemical Society Reviews* **2007**, 36, 636-649.
- (109) Ibarz, G.; Dahne, L.; Donath, E.; Mohwald, H. *Advanced Materials (Weinheim, Germany)* **2001**, 13, 1324-1327.
- (110) Antipov, A. A.; Sukhorukov, G. B. *Advances in Colloid and Interface Science* **2004**, 111, 49-61.
- (111) Alisar S. Zahr, M. d. V., and Michael V. Pishko. *Langmuir* **2005**, 21, 403-410.
- (112) Fischlechner, M., Zschornig, O., Hofmann, J., and Donath, E. *Angew. Chem. Int. Ed.* **2005**, 44, 2892 –2895.
- (113) Cortez, C.; Tomaskovic-Crook, E.; Johnston, A. P. R.; Radt, B.; Cody, S. H.; Scott, A. M.; Nice, E. C.; Heath, J. K.; Caruso, F. *Advanced Materials (Weinheim, Germany)* **2006**, 18, 1998-2003.
- (114) Zhang, F.; Wu, Q.; Chen, Z.-C.; Li, X.; Jiang, X.-M.; Lin, X.-F. *Langmuir* **2006**, 22, 8458-8464.
- (115) Radziuk, D.; Shchukin, D. G.; Skirtach, A.; Moehwald, H.; Sukhorukov, G. *Langmuir* **2007**, 23, 4612-4617.
- (116) Skirtach, A. G.; Munoz Javier, A.; Kreft, O.; Kehler, K.; Piera Alberola, A.; Moewald, H.; Parak, W. J.; Sukhorukov, G. B. *Angewandte Chemie, International Edition* **2006**, 45, 4612-4617.
- (117) Skirtach, A. G.; Dejugnat, C.; Braun, D.; Susha, A. S.; Rogach, A. L.; Parak, W. J.; Moehwald, H.; Sukhorukov, G. B. *Nano Letters* **2005**, 5, 1371-1377.
- (118) Skirtach, A. G.; Karageorgiev, P.; Bedard, M. F.; Sukhorukov, G. B.; Mohwald, H. *Journal of the American Chemical Society* **2008**, 130, 11572-11573.
- (119) Zonghuan Lu, M. D. P., Zhanhu Guo, Vladimir O. Golub, Challa S. S. R. Kumar, and Yuri M. Lvov. *Langmuir* **2005**, 21, 20042-22050.
- (120) De Geest, B. G.; Skirtach, A. G.; Mamedov, A. A.; Antipov, A. A.; Kotov, N. A.; De Smedt, S. C.; Sukhorukov, G. B. *Small* **2007**, 3, 804-808.
- (121) Skirtach, A. G.; De Geest, B. G.; Mamedov, A.; Antipov, A. A.; Kotov, N. A.; Sukhorukov, G. B. *Journal of Materials Chemistry* **2007**, 17, 1050-1054.

- (122) Zelikin, A. N.; Li, Q.; Caruso, F. *Angewandte Chemie, International Edition* **2006**, 45, 7743-7745.
- (123) Antipov, A. A., Sukhorukov, G. B., Mohwald, H. *Langmuir* **2003**, 19, 2444-2448.
- (124) Antipov, A. A., Sukhorukov, G. B., Donath, E., and Mohwald, H. *Journal of Physical Chemistry B* **2001**, 105, 2281-2284.
- (125) Kyeongsoon Park a, J.-H. K., Yun Sik Nam, Seulki Lee, Hae Yun Nam, ; Kwangmeyung Kim, J. H. P., In-San Kim, Kuiwon Choi, Sang Yoon Kim, Ick Chan Kwon. *Journal of Controlled Release* **2007**, 122, 305-314.
- (126) Dahne, L., Leporatti, S., Donath, E., and Mohwald, H. *J. Am. Chem. Soc.* **2001**, 123, 5431-5436.
- (127) Kreft, O.; Skirtach, A. G.; Sukhorukov, G. B.; Moehwald, H. *Advanced Materials* **2007**, 19, 3142-3145.
- (128) Sukhorukov, G. B.; Rogach, A. L.; Garstka, M.; Springer, S.; Parak, W. J.; Munoz-Javier, A.; Kreft, O.; Skirtach, A. G.; Sussha, A. S.; Ramaye, Y.; Palankar, R.; Winterhalter, M. *Small* **2007**, 3, 944-955.
- (129) Chinnayelka, S.; McShane, M. J. *Analytical Chemistry* **2005**, 77, 5501-5511.
- (130) Sussha, A. S.; Caruso, F.; Rogach, A. L.; Sukhorukov, G. B.; Kornowski, A.; Mohwald, H.; Giersig, M.; Eychmuller, A.; Weller, H. *Colloids and Surfaces, A: Physicochemical and Engineering Aspects* **2000**, 163, 39-44.
- (131) Sadasivan, S.; Koehler, K.; Sukhorukov, G. B. *Advanced Functional Materials* **2006**, 16, 2083-2088.
- (132) Garza, J. M.; Jessel, N.; Ladam, G.; Dupray, V.; Muller, S.; Stoltz, J.-F.; Schaaf, P.; Voegel, J.-C.; Lavalle, P. *Langmuir* **2005**, 21, 12372-12377.
- (133) Hahna S. Kwang., H. A. S. *International Journal of Biological Macromolecules* **2005**, 37, 227-231.
- (134) Burke, S. E., Barrett C. J. *Biomacromolecules* **2003**, 4, 1773-1783.
- (135) Porcel, C., Lavalle, P., Decher, G., Senger, B., Voegel, J.-C., and Schaaf, P. *Langmuir* **2007**, 23, 1898-1904.
- (136) Volodkin, D.; Arntz, Y.; Schaaf, P.; Moehwald, H.; Voegel, J.-C.; Ball, V. *Soft Matter* **2008**, 4, 122-130.
- (137) Elbert, D. L.; Herbert, C. B.; Hubbell, J. A. *Langmuir* **1999**, 15, 5355-5362.
- (138) A. Denuziere, D. F., and A. Domardb. *Carbohydrate Polymers* **1996**, 29, 317-323.

- (139) Shutava, T., and Lvov, Y. *Journal of Nanosciences and Nanotechnology* **2006**, 6, 1655-1661.
- (140) Ye, S.; Wang, C.; Liu, X.; Tong, Z. *Journal of Biomaterials Science, Polymer Edition* **2005**, 16, 909-923.
- (141) Itoh, Y.; Matsusaki, M.; Kida, T.; Akashi, M. *Biomacromolecules* **2008**, 9, 2202-2206.
- (142) Dumitriu, S. *Polysaccharides. Structural diversity and functional versatility.*, Second edition ed.: Quebec, Canada, 2005.
- (143) Rinaudo, M. *Polymer International* **2008**, 57, 397-430.
- (144) Rinaudo, M. *Corrosion Engineering, Science and Technology* **2007**.
- (145) Tomihata, K.; Ikada, Y. *Journal of Biomedical Materials Research* **1997**, 37, 243-251.
- (146) Hahn, S. K.; Park, J. K.; Tomimatsu, T.; Shimoboji, T. *International Journal of Biological Macromolecules* **2007**, 40, 374-380.
- (147) Kogan, G., Soltes, L., Stern, R., Gemeiner, P. *Biotechnol. Lett.* **2007**, 29, 17-25.
- (148) Menzel, E., and Farr, C. *Cancer Letters* **1998**, 131, 3-11.
- (149) Stern, R., Kogan, G., Jedrzejewski, M. J., Šoltés, L. *Biototechnology Advances* **2007**, 25, 537-557.
- (150) Tokita, Y.; Okamoto, A. *Polymer Degradation and Stability* **1995**, 48, 269-273.
- (151) http://www.natural-coral-calcium.com/hyaluronic-acid/synthovial_seven_faq.htm.
- (152) Kogan, G., Soltes, L., Stern, R., Schiller, J., Mendichi R. In *Studies in Natural Products Chemistry*; Atta-ur-Rahman, F., Ed.: Pakistan, 2008; Vol. 34, pp 789-782.
- (153) Kogan, G., Soltes, L., Stern, R., Mendichi, R. In *Handbook of Polymer Research: Monomers, Oligomers, Polymers and Composites*, 2007; pp 393-439.

CHAPTER 2

Materials and Methods

2.1. Chemicals

Hyaluronic acid samples having weight-average molecular weights: $M_w = 11 \times 10^3$, 200×10^3 , 820×10^3 and 1100×10^3 g/mol described as HA11, HA200, HA820 and HA1100 respectively, were provided by ARD (Pomacle, France). They were produced by bacteria fermentation (bacteria *Spectrococcus zooepidemicus*), available as the sodium salt. Polyelectrolyte polymers such as poly(allylamine hydrochloride), PAH ($M_w \sim 70 \times 10^3$ g/mol) and poly(L-lysine hydrobromide), PLL ($M_w 15 \times 10^3 - 30 \times 10^3$ g/mol) were purchased from SIGMA. Chitosan at $M_w = 180 \times 10^3$ g/mol from Pronova (Norway) was used for the synthesis of quaternized chitosan (QCH) according to the literature¹. The calcium chloride dihydrate ($\text{CaCl}_2 \times 2\text{H}_2\text{O}$), sodium carbonate (Na_2CO_3), ethylenediaminetetraacetic acid (EDTA), citric acid, *N*-(3-Dimethylaminopropyl)-*N'*-ethylcarbodiimide hydrochloride (EDC), *N*-Hydroxysulfosuccinimide sodium salt (sulfo-NHS), fluorescein isothiocyanate (FITC), and FITC labelled dextrans (dextran^{FITC}) with molecular weights of 4×10^3 , 500×10^3 , and 2000×10^3 g/mol described as dextran-4, dextran-500 and dextran-2000 respectively, hyaluronidase enzyme (Hase) extracted from bovine testes (type VIII, $\sim 337\text{U/mg}$) were purchased from Sigma-Aldrich-Fluka.

The synthesized products such as PAH^{FITC} , HA^{FITC} are described in Experimental Section of the publication situated in Chapter 3.

Buffers: Tris (Hydroxymethyl) Aminomethane (TRIS buffered saline) was prepared by dissolution of salt in deionized water to obtain a concentration of 0.01M, the pH was adjusted using 0.1M HCl. 0.02M 2-(*N*-Morpholino) ethanesulfonic sodium (MES sodium salt, SIGMA) was prepared by titrating the free acid with NaOH. Water used in all experiments was purified by a Millipore Milli-Q Plus purification system, with a resistivity of $18.2 \text{ M}\Omega \cdot \text{cm}$.

2.2. LbL capsules

2.2.1. Synthesis

The procedure for the multilayer assembly on the calcium carbonate template followed by the core dissolution is described in detail in Chapter 3.

2.2.2. Chemical cross-linking

EDC/sulfo-NHS mixture was dissolved in 0.15M NaCl (pH 6.5), the film coated template was incubated in freshly prepared solution overnight. Different EDC concentrations were tested (EDC/sulfo-NHS: 100/25, 400/100, 800/200mM/mM, v/v).

2.2.3. Permeability

To demonstrate the permeability of capsule shells, the studies were performed using dye samples having different hydrodynamic radius (R_h) obtained from literature data²⁻⁴.

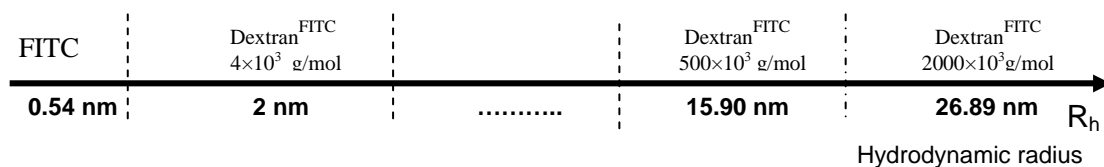


Figure 2.1. The hydrodynamic radius of FITC and FITC labelled dextran molecules at different M_w ²⁻⁴.

Depending on the size of diffusing dextran, the different concentration of molecules inside and within the shells can be obtained, as illustrated in **Figure 2.2**.

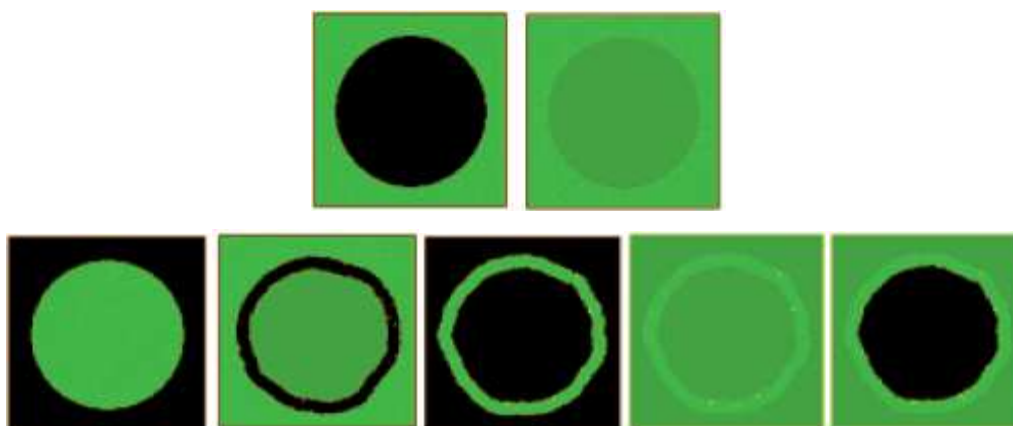


Figure 2.2. Scheme of principally obtainable images for a single suspended shell in the presence of fluorescent probes. The green color indicates regions of lower or higher fluorescent intensity according to the local concentration distribution of the probe (outside/shell wall/inside). Black regions mean the absence of fluorescent probes⁵.

In our permeability experiment, before mixing with diffusing molecules, the hollow capsules were suspended in MES buffer (pH 6.5) overnight. The fluorescent molecules were dissolved in buffer at concentrations of 1mg/mL (FITC) and of 2mg/mL (FITC-labelled dextrans). For permeability test in presence of salt, NaCl was added into the MES to obtain a concentration of 0.15M. Typically, 20 μ L of dextran solution was mixed with 20 μ L of capsule suspension on a glass slide. After 20min, the capsules were observed by a confocal microscope (CLSM).

The images were analyzed using Leica Confocal Software by the measurement of the light emitted by the capsule interior (I_{int}) and surrounding solution (I_{ext}). The permeability coefficient ($I_{\text{int}}/I_{\text{ext}} \times 100\%$) was estimated as an average value from 7-10 capsules.

Apart from permeability tests, fluorescent dextran allowing visualisation of capsules gives information about their morphology as aqueous suspension.

2.2.4. Enzymatic degradation

25 μ L of hollow capsule suspension (in water) was added to 25 μ L of hyaluronidase solution (0.02M MES buffer, pH 6.5) or MES buffer without hyaluronidase. The mixtures with final concentration of enzyme of 10, 50 and 500U/mL were stored overnight at 37°C.

The permeability changes after enzyme treatment were tested as described earlier.

2.2.5. Encapsulation and release

To encapsulate dextran in polyelectrolyte capsules, the CaCO_3 microparticles were suspended in solution of dextran^{FITC} (4×10^3 , and 2000×10^3 g/mol) with concentration of 2mg/mL (MES buffer at pH 6.5). After 40 min of incubation (gentle stirring), the microparticles were washed 3 times (each for 15min) with distilled water to remove non adsorbed dextran (centrifugation, 200g, 5min). Next, the adsorption of polyelectrolytes was performed, followed by shell cross-linking (EDC/NHS 400/100 mM/mM, v/v) in some cases. To core decomposition, non cross-linked capsules were dialyzed against EDTA, while centrifugation (1500g, 5min) was applied for cross-linked capsules. After 3-fold incubation (3×2 h) of coated particles with new portion of EDTA (0.1M, pH 7.2), the capsules were washed with water.

Microcapsules containing encapsulated dextran were dispersed in MES (or MES with 0.15M NaCl) for 4 hours. The amount of dextran^{FITC} released during this time was calculated following the measurements of fluorescence intensity outside/inside capsules ($I_{\text{ext}}/I_{\text{int}} \times 100\%$).

2.3. Characterization methods and experimental protocols

2.3.1. Microscopy techniques

a) Scanning Electron Microscopy (SEM)

The Scanning Electron Microscopy is a technique used for characterization of the surface morphology of a given object. In the SEM, the image is formed and presented by an electron beam, which is focused on the surface of the specimen. A scheme of a typical scanning electron microscope is shown in **Figure 2.3**.

The electron beam follows a vertical path through the column of the microscope. The electromagnetic lenses focus and direct the beam down towards the sample. The specimen is bombarded with electrons over a very small area. Once the electrons reach the sample, they

may be elastically reflected from the specimen, with no loss of energy, they may be absorbed by the specimen and give rise to secondary electrons of very low energy, together with X-rays, or absorbed and give rise to the emission of visible light. All these effects can be used to produce an image. Detectors collect the secondary or backscattered electrons, and convert them to a signal that is sent to a viewing screen producing an image.

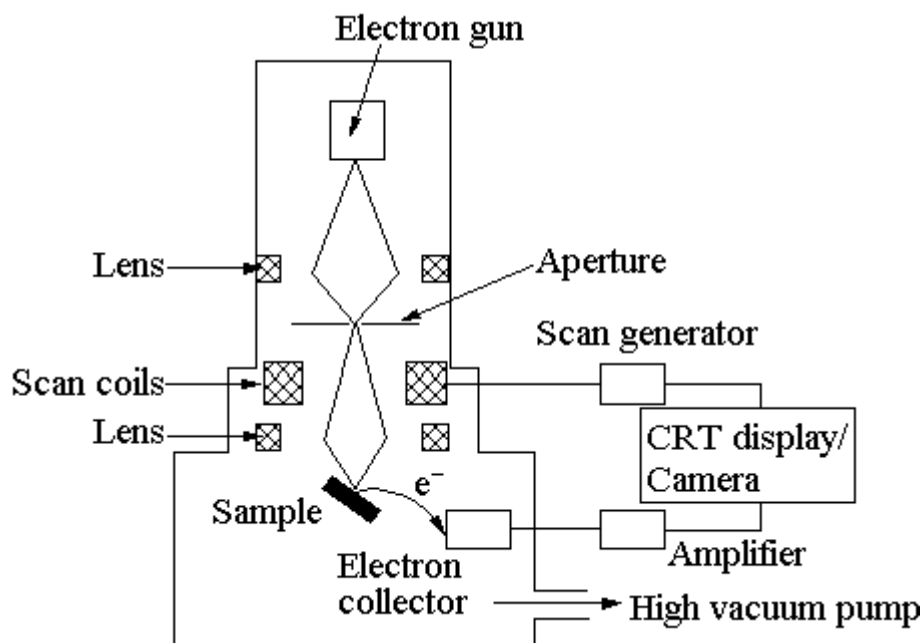


Figure 2.3. Schematic diagram of a Scanning Electron Microscope.

The sample surface must be electrically conducting, otherwise the electron beam would charge up the surface. All metals are conductive and require no preparation to be viewed using SEM. In order to view non-conductive samples such as polymer made capsules, we must cover the sample with a thin layer of a conductive material. The sputter coater uses argon gas and a small electric field. The sample is placed in a small chamber under vacuum. Argon gas is then introduced and an electric field is used to cause an electron to be removed from the argon atoms. The Ar^+ ions are then attracted to a negatively charged piece of gold foil. The Ar^+ ions act like sand in a sandblaster, knocking gold atoms from the surface of the foil which then settle onto the surface of the sample, producing a gold coating.

- Experimental protocol

For our observation the Jeol JSM6100 microscope using an accelerating voltage of 8 kV was used (Figure 2.4)

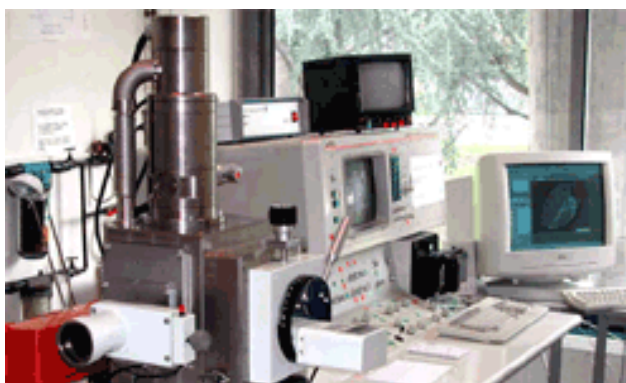


Figure 2.4. Jeol JSM6100 at CERMAV, Grenoble.

The drops of capsule suspensions were deposited onto copper stubs and allowed to air dry. The samples were sputtered with Au/Pd and observed in secondary electron imaging mode. For high resolution SEM analysis, the specimens were coated by 2 nm of electron beam evaporation carbon and observed in secondary electron imaging mode with a Zeiss ultra 55 FEG-SEM (CMTC-INPG, Grenoble) at an accelerating voltage of 3 kV, using an in-lens detector.

b) Confocal Laser Scanning Microscopy (CLSM)

Confocal Laser Scanning Microscopy is a technique that allows us to see a thin section of the entire specimen. For this aim the fluorescent properties of the sample are used. Fluorescent molecules in the ground state adsorb energy from photons which causes an increase in energy and move the molecule to an excited state. The part of this energy is lost internally within the molecule. The molecules come back rapidly to the ground state, but for this they have to emit the rest of adsorbed energy, with different colour light. When fluorescent molecules are exposed to a light source of one colour, the observed light of a different colour is emitted (**Figure 2.5**). The excitation light and the emission light are both dependent upon the molecules being examined.

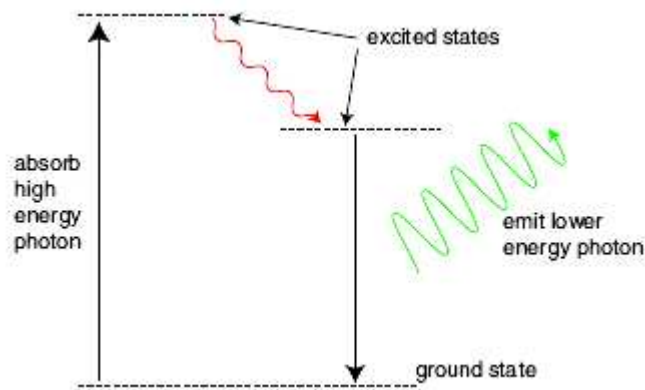


Figure 2.5. Mechanism of fluorescence.

In the CLSM, a laser beam (excitation source) passes through a pinhole aperture and then is focused by an objective lens into a small focal volume within a fluorescent specimen (**Figure 2.6**). Fluorescence emitted from points on the specimen pass back through the dichromatic mirror, then a pinhole, and are detected by a photodetection device transforming the light signal into an electrical signal that is recorded by a computer.

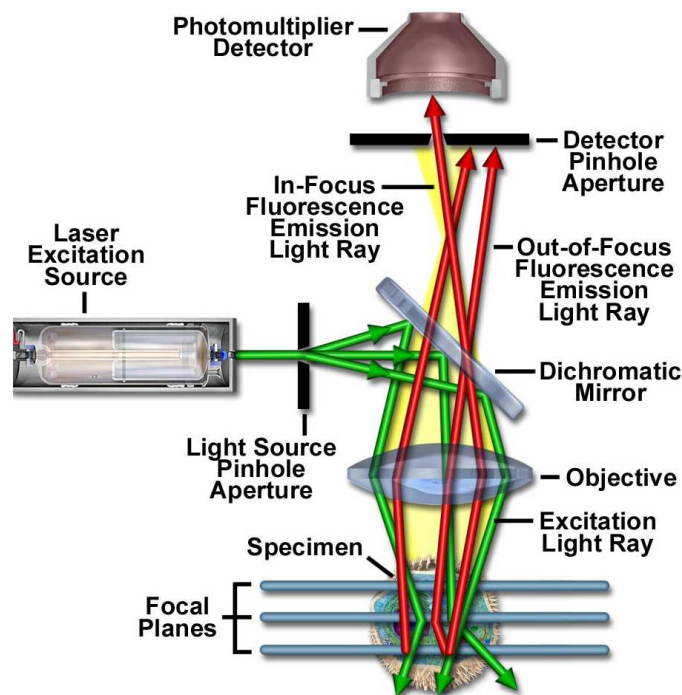


Figure 2.6. Schematic diagram of the optical pathway and principal components in a laser scanning confocal microscope⁶.

The most popular lasers for confocal microscopy are air-cooled argon and krypton-argon ion lasers and a variety of helium-neon systems. These lasers are able to provide excitation at 10-12 specific wavelengths between 400 and 650 nanometers. Also, many fluorophores needed for visualisation are available and described according to wavelengths of maximum absorbance and emission.

- Experimental protocol

Leica TCS SP2 AOBS (Acoustico Optical Beam Splitter) confocal laser scanning system and an inverted fluorescence microscope equipped with an oil immersion objective lens 63x was used in our experiments.



Figure 2.7. Confocal Microscope Leica TCS SP2 AOBS.

FITC-labelled PAH, HA or dextrans were visualized by excitation of the fluorochrome with a 488 nm Argon/Krypton laser and the emitted fluorescence was collected between 497 and 576 nm precisely defined by the AOBS.

The analysed sample (capsule suspension) was deposited on the glass slide and placed in the holder of the confocal microscope. The laser beam moves until the entire X-Y plane is scanned. The specimen is taken to different Z position following each X-Y scan. Further layers “z-series” could be acquired to form 3-D visualisation.

The experimental protocol of sample preparation is described in **paragraph 2.2**.

c) Transmission Electron Microscopy (TEM)

TEM gives the possibility to obtain high magnification of 2000 to 1000 000 \times , high resolution and ability to observe internal structure. Images are recorded by detecting the

electrons that pass through the sample to a system of electromagnetic lenses which focus and enlarge the image on a fluorescent screen, photographic film or digital camera.

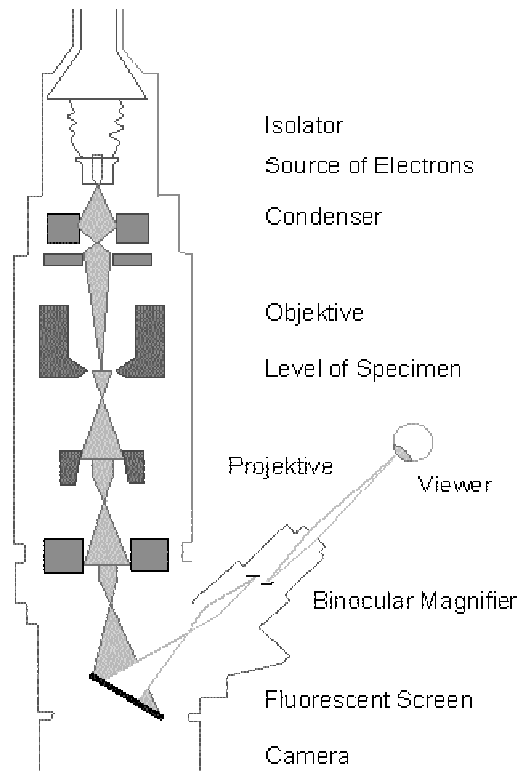


Figure 2.8. Scheme of principal components of Transmission Electron Microscope (TEM).

In **Figure 2.8**, the scheme of a conventional Transmission Electron Microscopy is presented. At the top, the cathode heated by a current, produces a stream of electrons. This stream is focused to a small, thin, coherent beam by the use of condenser lenses which strikes the specimen and part of it is transmitted. The degree of deflection depends on the electron density of the object. The greater the mass of the atoms, the greater is the degree of deflection. Often, the sample requires treatment with a special contrast agent (heavy metals). After passing the object the scattered electrons are collected by an objective. The image is formed by an additional lens-system. The darker areas of the image represent those areas of the sample that only fewer electrons were transmitted through (they are thicker or denser). The lighter areas of the image represent those areas of the sample that more electrons were transmitted through (they are thinner or less dense).

- Experimental protocol

To observe the LbL film deposited on the carbonate particles, the samples were post-fixed with 1% osmium tetroxide in water for 2 h at 4°C, in order to enhance differential contrast between the resin, particles and multilayers. After dehydration by incubation for 20 min in ethanol/water mixtures (7/3, 95/5) and finally twice in ethanol, the samples were infiltrated with ethanol/Lowicryl HM20 resin mixtures (2/3-1/3, 1/3-2/3), for 90 min each. The resin was polymerized at 22°C, allowing preservation the morphology of particles and multilayered assembly, under indirect UV light for 72 h, using the Automatic Freeze-substitution System (AFS Leica). Ultrathin sections (70 nm) were prepared with a diamond knife on an UC6 Leica ultramicrotome and collected on carbon-coated 200 µm mesh copper grids. Ultrathin sections were viewed at 80 kV with a Philips CM200 transmission electron microscope. In order to avoid modification of the morphology of particles and multilayers, we used a resin for the preparation of ultramicrotome sections which can be polymerized under mild conditions, i.e. at room temperature.

d) Atomic Force Microscopy (AFM)

The capsule wall thickness was determined for each batch by AFM imaging of dried capsules by using a Molecular Imaging PicoPlus AFM (now Agilent) in Tapping mode® using Silicon cantilevers (Mikromash NSC15 $f_c = 325$ kHz) from the Nanobio facility in Grenoble. This method was also used to ensure that the core dissolution was complete and no residuals were found inside the capsules.

2.3.2. Fourier Transform Infrared Spectroscopy (FTIR) with Attenuated Total Reflectance (ATR)

FTIR spectroscopy provides specific information about chemical structure of analyzed substances.

The technique works on the base that bonds vibrate at various frequencies depending on the elements and the type of bonds. For any given bond, there are several specific frequencies at which it can vibrate (**Figure 2.9**)

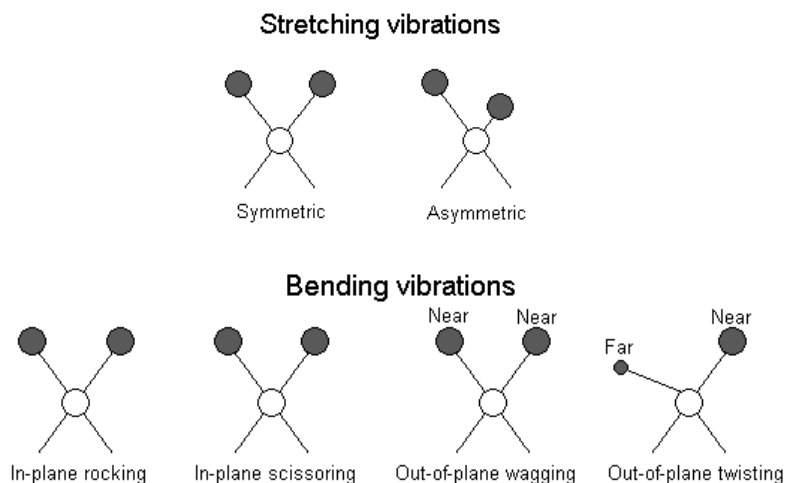


Figure 2.9. Illustration of stretching and bending vibration.

A molecule is exposed to infrared rays absorbing infrared energy at frequencies characteristic to that molecule. Infrared radiation (IR) passes through a sample. Some of the IR is absorbed by the sample and some of it is transmitted. The resulting spectrum represents the molecular absorption and transmission, creating a molecular fingerprint of the sample. By interpreting the infrared absorption spectrum, the chemical bonds in a molecule can be determined.

Sample for FTIR analysis can be prepared by different methods depending on the sample nature. Solid sample can be mixed with the potassium bromide (KBr) to form homogenous powder followed by compressing into a thin pellet, or dissolved and vaporized to obtain the film.

The second method, the solid sample can be placed in an Attenuated Total Reflectance (ATR) cell and analyzed directly without previous preparation.

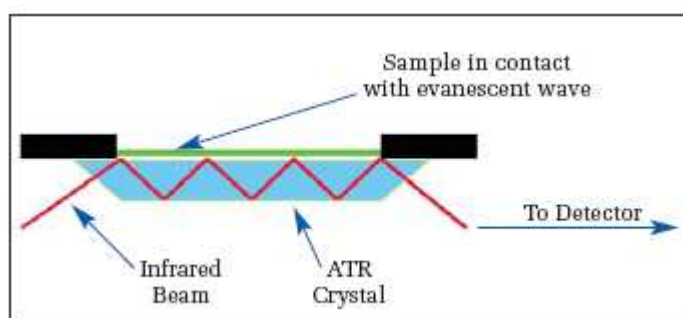


Figure 2.10. A multiple reflection ATR system⁷.

In attenuated total reflectance, an infrared beam enters a crystal made from materials that transmits IR. The wave enters into the sample that is held in close contact with crystal. The penetration depth of the beam is typically of the order of a few micrometers. Pressure up to

5.1 atm is applied to the sample lying on the diamond micro-ATR crystal during sample analysis, ensuring excellent contact of sample and crystal surfaces.

- Experimental protocol

Spectrum RX1 spectrometer, Perkin Elmer, UK with Horizontal ATR accessory was used for the FTIR analysis of the hollow freeze dried capsules deposited on the diamond crystal. For each sample 32 scans were recorded between 4000 and 400 cm^{-1} with a resolution of 2 cm^{-1} using Spectrum software V 5.0.0. The spectrum analysis was performed by using Origin 7.0 software.

2.3.3. Isothermal Titration Calorimetry (ITC)

Isothermal Titration Calorimetry (ITC) is a thermodynamic technique for measuring binding affinities and mechanisms of reaction. This method has been already largely applied for characterization of molecular interactions of small molecules, proteins, antibodies, nucleic acids, lipids and other biomolecules⁸.

The usual experimental set up has a syringe containing a “ligand” solution which then is titrated into a cell containing a solution of the “macromolecule” at constant temperature. When ligand is injected into the cell, the two materials interact, and heat is released or absorbed in direct proportion to the amount of binding. Each peak represents a heat change associated with the injection of a small volume of sample into the ITC reaction cell.

The Calorimeter VP-ITC (Nothampon, USA) uses a cell feedback network to differentially measure and compensate for heat produced or absorbed between the sample and a reference cell. Win coin-shaped cells are mounted in a cylindrical adiabatic environment, and connect to the outside through narrow access tubes (**Figure 2.11**). The temperature difference between the two cells and difference between the cells and the jacket is measured. The temperature difference between the sample and reference cells is kept at a constant value (baseline) by the addition or removal of heat to the sample cell. The integral of the power required to maintain the temperature differences constant over time is a measure of total heat resulting from the process being studied.

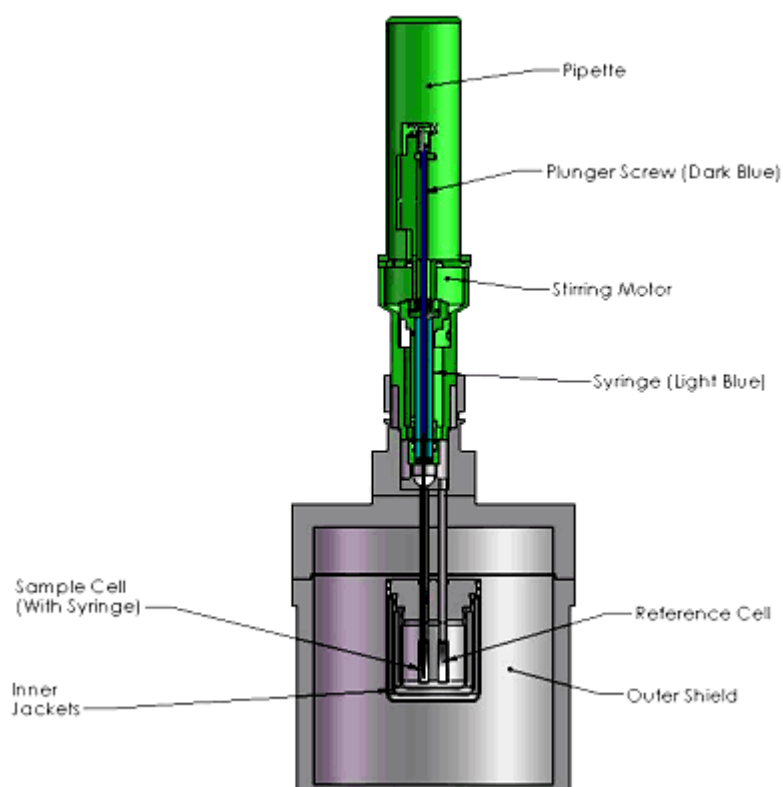


Figure 2.11. ITC cells and syringe. The syringe rotates during the ITC experiment. The system is controlled by computer and injects precise volumes of ligand⁹.

- Experimental protocol

The polycation solution (PAH, PLL, QCH) is placed in the cell, while polyelectrolyte of opposite charge (HA) is injected in successive injection steps by means of automatic microsyringe. For all the experiments HA and PAH, PLL, CH polyelectrolytes were dissolved in 10mM TRIS buffer at pH 7.4 or in this buffer with addition of NaCl with its final concentration 0.15M. HA solution was prepared to 3mg/ml concentration, PAH 2g/L, PLL at 2g/L and QCH at 5g/L. The polyanion solution was injected from the calibrated microsyringe into the cell with polycation solution. 10 μ L of the polyanion solution was injected 5 times with a time interval of 600s to allow the microcalorimeter trace to come back to a baseline, corresponding to the absence of any heat flow between the sample cell and reference cell.

The measurements of the dilution heat were also considered and measured by the same procedure as the polyanion/polycation complexation heat, but instead of the polycation solution in the cell, only TRIS buffer was placed, the same in which HA polymer was

dissolved. The values of dilution heat were considered during the calculation of reaction enthalpy.

2.3.4. Quartz Crystal Microbalance with Dissipation (QCM-D)

QCM is an electro acoustic method suitable for mass and viscoelastic analysis of adsorbed biomolecules such as proteins, vitamins, antibodies, DNA but also polyelectrolyte, particle, cell layers at the solid/liquid interface¹⁰⁻¹³. A typical QCM sensor consists of a disk-shaped piezoelectric quartz crystal sandwiched between two gold electrodes (**Figure 2.12**). The crystal is excited at its fundamental (or an overtone) resonant frequency, f , by applying a suitable current between the electrodes. Adsorbed polymer gives the growth of the mass to the electrodes that decreases the resonant frequency.

The changes in resonant frequency are proportional to the adsorbed mass on the crystal through the Sauerbrey relationship:

$$\Delta f = -k \times \Delta m \quad \text{eq.II.1}$$

where k is the quartz crystal microbalance constant.

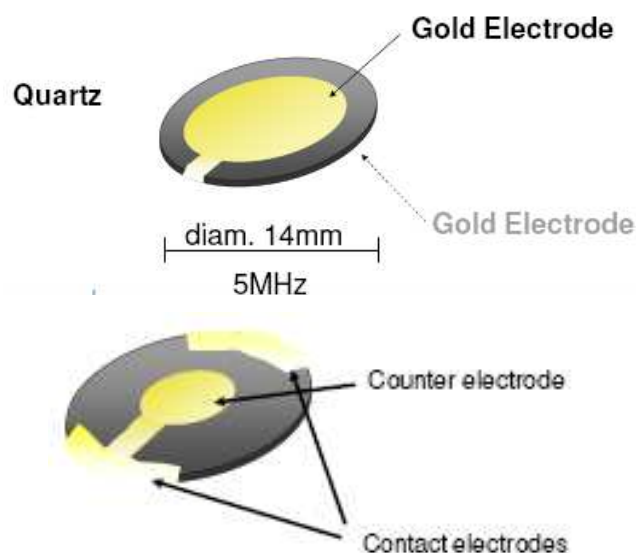


Figure 2.12. A standard QCM-crystal with electrodes on both sides of the disc¹⁴.

When the mass is adsorbed, the changes of frequency are the response not only to the mass changes, but also to changes in the rate of energy dissipation with regard to the viscoelastic

properties of the adsorbed molecules. By measuring the dampening of the shear wave recorded simultaneously with the resonant frequency of the crystal (**Figure 2.13**), one can determine if the adsorbed film is rigid or viscoelastic (soft). Raw data can be fitted to a model included in the computer software. The Sauerbrey model is valid for rigid and thin adsorbed layers. Applying a Voigt-based viscoelastic model, the mass, the swelling/hydration and viscoelastic information can be obtained.

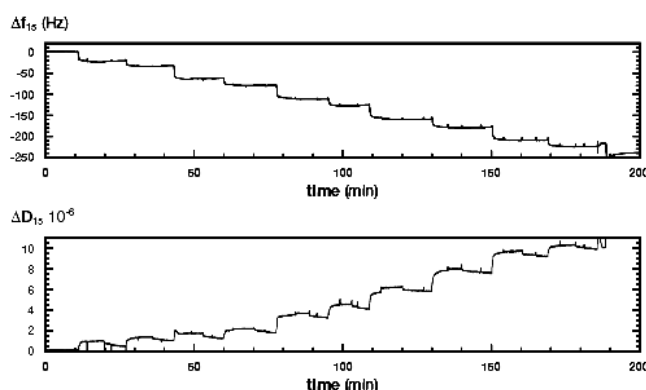


Figure 2.13. The typical graph of the frequency changes (Δf) and dissipation changes (ΔD) during adsorption process as a function of time¹⁴.

In this work, QCM-D data were analyzed using the Voigt model¹⁵ included in the Qtools software (Q-Sense, Göteborg, Sweden) by assuming and fixing the values of film density, buffer density and viscosity. Film thickness could be deduced.

The QCM-D system is shown below (**Figure 2.14**). The measurement cell is connected to computer controlled electronics that excites the crystal and records changes in resonance frequency and dissipation.



Figure 2.14. The QCM-D system¹⁴.

- Experimental protocol

The film build-up was followed by *in situ* quartz crystal microbalance (QCM with dissipation monitoring, D300, Qsense, Sweden).

The solutions for multilayer formation were prepared at concentrations of HA: 1 or 5g/L and PAH, PLL, CH solutions at 2g/L each in 0.15M NaCl at pH 6.5 (pH was checked before experiment and adjusted by 0,1M HCl or 0,1M NaOH).

First, we injected 1 mL of 0.15 M NaCl solution into the measurement cell. After stabilization of the signal, 1 mL of a polycation solution at 2 mg/mL in 0.15M NaCl is injected, left for 10 min and rinsed for 10 min with 0.15 M NaCl solution. During these time periods, the shifts Δf are continuously recorded. The same procedure is then used for the deposition of HA by introducing 1 mL of a HA solution. The build-up process is then continued by the alternate polycation and HA addition up to desired pair of layers. Solutions from the feeding container are introduced into the measurement chamber by means of a plastic tube, and it is regulated by cut-off for liquid flow. Temperature of the solutions is stabilized at 25°C.

The film was attached to the sensor quartz crystal. The crystal was excited at its fundamental frequency (5 MHz, $\nu = 1$) as well as at the third, fifth and seventh overtones ($\nu = 3, 5$ and 7 corresponding to 15, 25 and 35 MHz, respectively). Changes in the resonance frequencies Δf and in the relaxation of the vibration once the excitation is stopped were measured at the four frequencies. The observation takes place at the third, fifth and seventh overtones (corresponding to 15, 25, and 35 MHz, respectively).

Before use, a cleaning process was applied by dipping the surface in a solution of 0.01 M SDS for 10 min followed by an extensive rinse with water.

2.3.5. Zeta-potential measurements

The particle in suspension is surrounded by the liquid layer consisting of two parts; an inner region where the ions are strongly bound, and an outer (diffuse) region where they are less bound. Within the diffuse layer there is a notional boundary inside which the ions and particles form a stable entity. When a particle moves, the bounded ions follow it. The ions beyond the boundary area stay in the bulk. The potential at this boundary (surface of hydrodynamic shear) is the zeta potential¹⁶ (**Figure 2.15**).

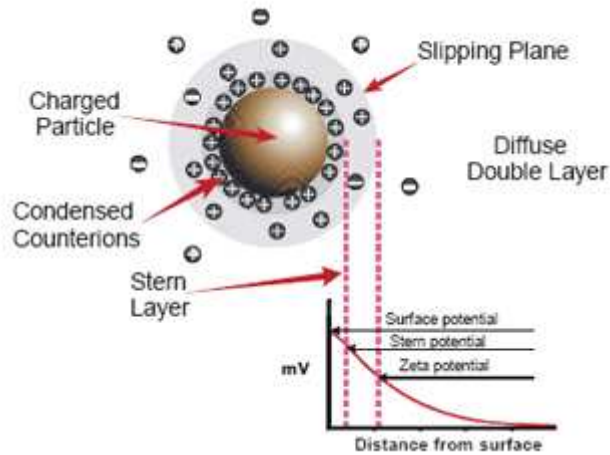


Figure 2.15. Schematic distribution of ions around charged particle¹⁷.

The value of zeta potential gives details about the stability of the colloidal system. If all particles with adsorbed polyelectrolyte layer are highly negative (when adsorbed polyelectrolyte is negative) or positive (positive polyelectrolyte), one can suppose that the particles have a sufficiently high repulsion and the colloidal system is stable. If the zeta potential is reduced towards zero, it is an indication that particles in the dispersion may adhere to one another and form aggregates with possible sedimentation.

When an electric field is applied, charged particles suspended in the electrolyte are attracted towards the electrode of opposite charge. The velocity is measured using the technique of laser Doppler anemometry. The laser ray is split onto incident and reference beam. The incident beam passes through the sample cell and the scattered light is detected. The intensity of detected light fluctuates with a frequency dependent on the particle speed and this mobility is converted to the zeta potential which can be expressed by the Henry or Smoluchowski equation:

$$U_E = 2 \epsilon z f(\kappa a) / 3 \eta \quad eq.II.2$$

where U_E = electrophoretic mobility, z = zeta potential, ϵ = dielectric constant, η = viscosity and $f(\kappa a)$ = Henry's function.

For particles at size higher than $0.2 \mu m$ dispersed in electrolyte at concentration higher than $10^{-3} M$ this equation is transformed to Smoluchowski approximation:

$$\zeta = \mu \eta / \epsilon \quad eq.II.3$$

Where ζ is zeta-potential, μ is the electrophoretic mobility, η - viscosity and ϵ - dielectric constant of the solvent.

- Experimental protocol

The zeta-potential of coated CaCO_3 particles was measured using a Malvern Zetasizer NanoZS. After polyelectrolyte deposition, the particles were washed with 0.01M NaCl (pH 6.5). All measurements were performed at 25°C, taking the average value of five measurements. A reference measurement using the Malvern ζ -potential standard was run prior to each sample analysis to check for correct instrument operation.

2.3.6. Size Exclusion Chromatography (SEC)

The molecular weight distribution and the weight average molecular weight of the HA samples were determined by size exclusion chromatography using a Waters GPCV Alliance 2000 chromatograph (USA) equipped with three on-line detectors: a differential refractometer, a viscometer and a light scattering detector (MALLS) from Wyatt (USA).

This technique provides information about the molecular weight, radius of gyration or intrinsic viscosity of the sample. The polymer fractions are separated according different hydrodynamic volumes of polymers. Experimental details are described in Chapter 3.

References :

- (1) Cho, J., Grant, J., Piquette-Miller, M., and Allen, C. *Biomacromolecules* **2006**, 7, 2845-2855.
- (2) Andrieux, K., Lesieur, P., Sylviane Lesieur, Ollivon, M., and Grabielle-Madelmont, C. *Analytical Chemistry* **2002**, 74, 5217-5226.
- (3) Armstrong, J. K.; Wenby, R. B.; Meiselman, H. J.; Fisher, T. C. *Biophysical Journal* **2004**, 87, 4259-4270.
- (4) Fowlkes, J. D., Hullander, E. D., Fletcher, B. L., Retterer, S. T., Melechko, A. V., Hensley, D. K., Simpson, M. L., and Doktycz, M.J. *Nanotechnology* **2006**, 17, 5659-5668.
- (5) Berth, G.; Voigt, A.; Dautzenberg, H.; Donath, E.; Moehwald, H. *Biomacromolecules* **2002**, 3, 579-590.
- (6) Nathan S. Claxton, T. J. F., and Michael W. Davidson. The Florida State University, Tallahassee, Florida, Department of Optical Microscopy and Digital Imaging.
- (7) www.perkinelmer.com.
- (8) Pierce, M. M., Raman, C.S. **1999**, 19, 213-221.
- (9) <http://www.microcal.com/>.
- (10) Irwin, E. F.; Ho, J. E.; Kane, S. R.; Healy, K. E. *Langmuir* **2005**, 21, 5529-5536.
- (11) Li, Q.; Quinn, J. F.; Wang, Y.; Caruso, F. *Chemistry of Materials* **2006**, 18, 5480-5485.
- (12) Tatsiana Shutava, M. P., Dinesh Kommireddy, and Yuri Lvov. *Macromolecules* **2005**, 38, 2850-2858.
- (13) C. Picart, P. L., P. Hubert, F. J. G. Cuisinier, G. Decher, P. Schaaf, and J.-C. Voege. *Langmuir* **2001**, 17, 7414-7424.
- (14) <http://www.q-sense.com/>.
- (15) Voinova, M. V. R., R.; Jonson, R.; Kasemo, B. *Physica Scripta* **1999**, 5.
- (16) Hunter, R. J. *Zeta potential in colloid science: principles and applications*; New York: Academic Press: London, 1981.
- (17) <http://www.malvern.co.uk/>.

CHAPTER 3

*Multilayer Assembly of Hyaluronic
Acid/Poly(allylamine): Control of the Buildup
for the Production of Hollow Capsules*

3.1. Résumé (fr)

Dans ce chapitre, nous démontrons la possibilité de préparer, à partir du HA et de la poly(allylamine) et dans des conditions douces, des capsules stables malgré l'absence de pontages covalents entre les couches. La stratégie de synthèse des capsules repose sur l'utilisation de microparticules de carbonate de calcium (diamètre moyen $\sim 3 \mu\text{m}$) comme supports sacrificiels. Ces particules présentent l'avantage d'être biocompatibles et de pouvoir être dissoutes dans des conditions douces par complexation avec un agent chélatant (acide citrique ou acide éthylènediaminetétraacétique). Néanmoins, la structure poreuse du cœur de carbonate entraîne la diffusion des polyélectrolytes, susceptible de fragiliser la paroi des capsules. Nous montrons que ce phénomène est limité par l'utilisation de lots de HA de masses molaires supérieures ou égales à 820000 g/mol. L'épaisseur des films apparaît dépendre de la concentration en HA utilisée lors du dépôt couche-par-couche. L'utilisation de solutions de $\text{HA} \geq 5 \text{ g/L}$ permet d'obtenir des capsules avec des parois plus épaisses, améliorant la cohésion du film multicouche. Ce dernier voit de plus ses propriétés mécaniques renforcées par sa réticulation chimique en présence d'un carbodiimide hydrosoluble, permettant la formation de liaisons amide entre les fonctions carboxylate et amine des polyélectrolytes partenaires.

3.2. Article

Langmuir 2008, 24, 9767–9774

9767

Multilayer Assembly of Hyaluronic Acid/Poly(allylamine): Control of the Buildup for the Production of Hollow CapsulesAnna Szarapak,^{†,‡} Isabelle Pignot-Paintrand,[†] Claire Nicolas,[§] Catherine Picart,[§] and Rachel Auzély-Velty^{*,†}

Centre de Recherches sur les Macromolécules Végétales (CERMAV-CNRS), BP53, 38041 Grenoble cedex 9, France, affiliated with Université Joseph Fourier, and member of the Institut de Chimie Moléculaire de Grenoble, Institute of Chemistry and Environmental Protection, Jan Dlugosz University of Czestochowa, Armii Krajowej Ave. 13/15, 42-200 Czestochowa, Poland, and DIMNP, Dynamique des Interactions Membranaires Normales et Pathologiques, CNRS, Université Montpellier II et I, cc 107, 34 095 Montpellier, France

Received April 23, 2008. In Final Form: June 14, 2008. Revised Manuscript Received June 13, 2008

The objective of this work was to investigate the formation of hollow microcapsules composed of hyaluronic acid (HA) and poly(allylamine) (PAH) by layer-by-layer adsorption on CaCO_3 microparticles and subsequent core removal by addition of chelating agents for calcium ions. We found that the molecular weight of HA as well as the HA solution concentration used during deposition are crucial parameters influencing the multilayer structure. Whereas the effect of molecular weight of HA was mainly attributed to the porous structure of the template which allows penetration of polyelectrolytes when their size is below the maximum pore size of the template (~ 60 nm), that of the concentration of the HA solution was related to the intrinsic properties of the polysaccharide. Indeed, as shown by quartz crystal microbalance with dissipation monitoring as well as electron microscopy techniques, the latter leads to dense structures for concentrations from five to ten times the critical overlap concentration during adsorption. Such conditions were found to be favorable for the formation of hollow shells. Regarding conditions for core dissolution, we demonstrated the possibility to use either ethylenediaminetetraacetic acid (EDTA) or citric acid as chelating agents. However, in some cases, it was necessary to chemically cross-link the shell to maintain its integrity.

Introduction

Administration of drugs is often limited by problems of insolubility, inefficient distribution, enzymatic hydrolysis, lack of selectivity, and side effects raising health concerns. During the past decades a large variety of micro- and nanocarriers have been developed in order to improve efficiency, availability, and toxicity profiles of drugs. Among the currently available carrier systems, hollow capsules prepared by the layer-by-layer (LbL) assembly of oppositely charged polyelectrolytes on a colloidal template, followed by its decomposition, have recently emerged as attractive vehicles in the field of drug delivery.^{1–5} These capsules possess a fascinating multicompartment structure, with the possibility to introduce a high degree of functionality at the nanometer scale within their shell.

To date, the most studied capsules are of poly(allylamine)/poly(styrenesulfonate) (PAH/PSS). Several properties including permeability^{6–9} and stability against environmental alterations such as pH and temperature^{10,11} of the capsules have been

investigated. Owing to the potential applications of capsules in the fields of biotechnology and drug delivery, the use of natural polysaccharides and derivatives, which have the advantages of biocompatibility, biodegradability, and, in some cases, bioactivity, has emerged to prepare LbL capsules. Examples of nanoshells made from chitosan (CHI), chitosan sulfate, dextran sulfate, sodium alginate, carboxymethyl cellulose,^{9,12–16} and, recently, hyaluronic acid,¹⁷ have thus been reported. Compared to the planar films made from natural polysaccharides, little is known about capsules with polysaccharide nanoshells. In particular, since films containing polysaccharides often exhibit exponential growth of their thickness with the number of deposited layers, they are more hydrated and mechanically softer than their synthetic counterparts.¹⁸ These assemblies are thus to be handled with more caution as their exposure to solvents, pH, and ionic strength can affect their structural integrity.¹⁹ Based on these considerations, the choice of a suitable colloidal template and the dissolution protocol are crucial in the formation of capsules from polysaccharides. The harsh conditions (0.1 N HCl, 1 M HF, THF) generally used for the preparation of synthetic polyelectrolyte capsules are not suitable in the case where oppositely charged polyelectrolytes which form the nanoshell are weak natural polymers such as polypeptides and polysaccharides.

* Corresponding author.

† CERMAV-CNRS.

‡ Jan Dlugosz University of Czestochowa.

§ DIMNP.

- (1) De Geest, B. G.; Sanders, N. N.; Sukhorukov, G. B.; Demeester, J.; De Smedt, S. C. *Chem. Soc. Rev.* **2007**, 36, 636.
- (2) Johnston, A. P. R.; Cortez, C.; Angelatos, A. S.; Caruso, F. *Curr. Opin. Colloid Interface Sci.* **2006**, 11, 203.
- (3) Kim, B.-S.; Choi, J.-W. *Biotechnol. Bioprocess Eng.* **2007**, 12, 323.
- (4) Peyratout, C. S.; Dähne, L. *Angew. Chem., Int. Ed.* **2004**, 43, 3762.
- (5) Wang, Y.; Angelatos, A. S.; Caruso, F. *Chem. Mater.* **2008**, 20, 848.
- (6) Antipov, A. A.; Sukhorukov, G. B.; Donath, E.; Möhwald, H. *J. Phys. Chem. B* **2001**, 105, 2281.
- (7) Caruso, F.; Yang, W.; Trau, D.; Renneberg, R. *Langmuir* **2000**, 16, 8932.
- (8) Donath, E.; Sukhorukov, G. B.; Caruso, F.; Davis, S. A.; Möhwald, H. *Angew. Chem., Int. Ed.* **1998**, 37, 2202.
- (9) Qiu, X.; Leporatti, S.; Donath, E.; Möhwald, H. *Langmuir* **2001**, 17, 5375.
- (10) Dejugnat, C.; Sukhorukov, G. B. *Langmuir* **2004**, 20, 7265.

- (11) Tong, W.; Gao, C.; Möhwald, H. *Chem. Mater.* **2005**, 17, 4610.
- (12) Berth, G.; Voigt, A.; Dautzenberg, H.; Donath, E.; Möhwald, H. *Biomacromolecules* **2002**, 3, 579.
- (13) Itoh, Y.; Matsusaki, M.; Kida, T.; Akashi, M. *Biomacromolecules* **2006**, 7, 2715.
- (14) Shutava, T. G.; Lvov, Y. M. *J. Nanosci. Nanotechnol.* **2006**, 6, 1655.
- (15) Zhang, Y.; Guan, Y.; Zhou, S. *Biomacromolecules* **2005**, 6, 2365.
- (16) Zhao, Q.; Mao, Z.; Gao, C.; Shen, J. *J. Biomater. Sci. Polym. Ed.* **2006**, 17, 997.
- (17) Lee, H.; Jeong, Y.; Park, T. G. *Biomacromolecules* **2007**, 8, 3705.
- (18) Picart, C. *Curr. Med. Chem.* **2008**, 15, 685.
- (19) Engler, A. J.; Richert, L.; Wong, J. Y.; Picart, C.; Discher, D. E. *Surf. Sci.* **2004**, 570, 142.

Furthermore, biocompatible cores would be preferable in the case of biological applications. Very few examples of capsules composed of natural polysaccharides and templated on biocompatible cores that can be removed under mild conditions have been reported so far. These capsules are made of either chitosan/alginate or poly(L-lysine) (PLL)/hyaluronic acid multilayers assembled on inorganic particles of CaCO_3 ¹⁶ or microgel beads,¹⁷ respectively. By using microgel beads, which can be dissolved out using reducing agents, the possibility of producing capsules containing HA, which is a highly hydrated and weak polyacid, was thus demonstrated. However, these capsules have a rather large diameter ($\sim 16 \mu\text{m}$) and may not be easily phagocytosed by macrophages and dendritic cells, compared to smaller size microcapsules in the $0.1\text{--}10 \mu\text{m}$ range.²⁰

Since microcapsules based on hyaluronic acid exhibiting excellent biocompatibility and biodegradability may have great potential for drug delivery applications,^{21,22} we aimed to design microcapsules from hyaluronic acid and poly(allylamine hydrochloride) using CaCO_3 microtemplates. PAH was selected as the polycation in this study, as much is known about its behavior in multilayer films with weak polyacids.^{23–27} In addition, biomaterial applications of multilayer films containing PAH have previously been proposed.²⁸ Furthermore, CaCO_3 particles were chosen as microtemplates, as they can be easily prepared with a narrow size distribution ranging from 4 to 6 μm , and they are nontoxic and can be easily dissolved by complexation with ethylenediaminetetraacetic acid (EDTA) or under slightly acidic conditions.²⁹ Another advantage of using such templates is that their porous interior can be exploited to encapsulate various low molecular weight and macromolecular materials, either by physical adsorption onto the preformed particles or by coprecipitation during their formation.^{30–32}

In this paper, we focus on conditions used for the layer-by-layer deposition of HA and PAH at the surface of CaCO_3 microparticles to produce microcapsules. Although the porous structure of such microparticles may be useful for encapsulation of various biologically active substances in the perspective of drug delivery applications as discussed above, this may also lead to diffusion of polyelectrolyte layers inside the core, which can influence not only the properties of the capsule wall but also the bioactivity of the encapsulated material.³¹ We thus demonstrate the possibility of controlling diffusion of polyelectrolytes forming the multilayer assembly by the appropriate choice of the molecular weight of HA. Moreover, the HA solution concentration used during adsorption is shown to also be a crucial parameter influencing the formation and surface morphology of the hollow capsules.

(20) De Koker, S.; De Geest, B. G.; Cuvelier, C.; Ferdinande, L.; Deckers, W.; Hennink, W. E.; De Smedt, S.; Mertens, N. *Adv. Funct. Mater.* **2007**, *17*, 3754.

(21) Larsen, N. E.; Balazs, E. A. *Adv. Drug Delivery Rev.* **1991**, *7*, 279.
(22) Yadav, A. K.; Mishra, P.; Agrawal, G. P. *J. Drug Targeting* **2008**, *16*, 91.

(23) Burke, S. E.; Barrett, C. J. *Langmuir* **2003**, *19*, 3297.

(24) Burke, S. E.; Barrett, C. J. *Biomacromolecules* **2005**, *6*, 1419.

(25) Kato, N.; Schuetz, P.; Fery, A.; Caruso, F. *Macromolecules* **2002**, *35*, 9780.

(26) Mauser, T.; Dejugnat, C.; Sukhorukov, G. B. *Macromol. Rapid Commun.* **2004**, *25*, 1781.

(27) Schuetz, P.; Caruso, F. *Adv. Funct. Mater.* **2003**, *13*, 929.

(28) Mendelsohn, J. D.; Yang, S. Y.; Hiller, J. A.; Hochbaum, A. I.; Rubner, M. F. *Biomacromolecules* **2003**, *4*, 96.

(29) Antipov, A. A.; Shchukin, D.; Fedutik, Y.; Petrov, A. I.; Sukhorukov, G. B.; Möhwald, H. *Colloids Surf., A* **2003**, *224*, 175.

(30) Petrov, A. I.; Volodkin, D. V.; Sukhorukov, G. B. *Biotechnol. Prog.* **2005**, *21*, 918.

(31) Volodkin, D. V.; Larionova, N. I.; Sukhorukov, G. B. *Biomacromolecules* **2004**, *5*, 1962.

(32) Volodkin, D. V.; Petrov, A. I.; Prevot, M.; Sukhorukov, G. B. *Langmuir* **2004**, *20*, 3398.

Experimental Section

Materials. The bacterial hyaluronic acid samples of different molecular weight under the sodium salt form were produced by ARD (Pomacle, France). Poly(allylamine hydrochloride) (PAH, Mw $\sim 70\,000$), FITC-labeled dextrans with molecular weight of 4×10^3 , 500×10^3 , and 2000×10^3 g/mol, fluorescein isothiocyanate (FITC), ethylenediaminetetraacetic acid (EDTA), calcium chloride (CaCl_2), sodium carbonate (Na_2CO_3), citric acid, *N*-hydroxysulfosuccinimide sodium salt (sulfo-NHS), and 1-ethyl-3-(3-dimethylaminopropyl)carbodiimide hydrochloride (EDC) were purchased from Sigma-Aldrich-Fluka. All chemicals were used without any further purification. FITC-labeled PAH was synthesized as described previously,³¹ by mixing FITC and PAH in 0.05 M borate buffer, followed by dialysis against pure water. FITC-labeled HA was prepared by the same procedure starting from HA modified by adipic dihydrazide groups (HA-ADH). The latter, having a degree of substitution of 0.08, was synthesized as reported in detail elsewhere.³³ The water used in all experiments was purified by a Millipore Milli-Q Plus purification system, with a resistivity of 18.2 M Ω cm.

Capsule Preparation. Microcapsules were prepared using calcium carbonate (CaCO_3) microparticles as a sacrificial template. CaCO_3 microparticles were synthesized from solutions of CaCl_2 and Na_2CO_3 as reported in the literature.^{29,32} The CaCO_3 microparticles were coated using the layer-by-layer technique, by incubating them at a concentration of 2% (w/v)³⁰ in a solution of HA (C_p at 1 or 5 g/L) and PAH (C_p at 2 g/L) containing 0.15 M NaCl (pH 6.5). After shaking for 10 min, the microparticles were collected by centrifugation and the residual nonadsorbed polyelectrolyte was removed by washing twice with 0.01 M NaCl (pH 6.5).

After the desired number of layers were deposited, the CaCO_3 core was removed by treatment with 0.1 M citric acid (pH 5.4). To avoid mechanical damage of “soft” polyelectrolyte shells, the dissolved ions resulting from the decomposition of CaCO_3 were removed by dialysis against pure water, using spectra Por dialysis bags with a molecular weight cutoff of 6–8 kDa.

Cross-Linking of the HA/PAH Multilayers. Chemical cross-linking of the multilayer shells was performed by activation of the carboxylic acid groups of HA using the water-soluble carbodiimide, 1-ethyl-3-(3-dimethylaminopropyl)carbodiimide hydrochloride (EDC), and *N*-hydroxysulfosuccinimide (NHS) at concentrations of 0.2 and 0.05 M, respectively, in 0.15 M NaCl.³⁴ The core-templated HA/PAH multilayers were incubated in the EDC/NHS solution (pH 6.5) overnight. The cores were dissolved by shaking the particle dispersion in 0.1 M EDTA (pH = 7.2).

Size Exclusion Chromatography (SEC). The molecular weight distribution and the weight-average molecular weight of the HA samples were determined by size exclusion chromatography using a Waters GPCV Alliance 2000 chromatograph (USA) equipped with three online detectors, a differential refractometer, a viscometer, and a light scattering detector (MALLS) from Wyatt (USA); the solutions were injected at a concentration of 5×10^{-4} g/mL in 0.1 M NaNO_3 . The weight average molecular weights (M_w) were determined to be 11×10^3 , 200×10^3 , 820×10^3 , and 1100×10^3 g/mol. The different HA samples are thus designated as HAx where x reflects the M_w value divided by 10^3 .

Zeta-Potential Measurements. PAH/HA multilayer growth on CaCO_3 particles was followed by measuring the electrophoretic mobility of the coated particles in pure water using a Malvern Zetasizer NanoZS. It was determined after rinsing particles coated by the desired number of layers in pure water (pH 6.5). All measurements were performed at 25 °C just after the washing steps (to avoid problems of reproducibility related to sedimentation), taking the average value of five measurements. The zeta-potential (ζ -potential) was calculated from the electrophoretic mobility (μ) using the Smoluchowski function $\zeta = \mu\eta/\epsilon$, where η and ϵ are the viscosity and permittivity of the solvent, respectively.

(33) Charlot, A.; Heyraud, A.; Guenet, P.; Rinaudo, M.; Auzely-Velty, R. *Biomacromolecules* **2006**, *7*, 907.

(34) Richert, L.; Boulmedais, F.; Laval, P.; Mutterer, J.; Ferreux, E.; Decher, G.; Schaaf, P.; Voegel, J.-C.; Picart, C. *Biomacromolecules* **2004**, *5*, 284.

Film Characterization by Quartz Crystal Microbalance with Dissipation Monitoring (QCM-D). The (PAH/HA)_i film buildup (where *i* denotes the number of layer pairs) was followed by *in situ* quartz crystal microbalance (QCM with dissipation monitoring, D300, Qsense, Sweden).³⁵ The quartz crystal was excited at its fundamental frequency (about 5 MHz, $\nu = 1$) as well as at the third, fifth, and seventh overtones ($\nu = 3, 5$, and 7 corresponding to 15, 25, and 35 MHz, respectively). Changes in the resonance frequencies Δf and in the relaxation of the vibration once the excitation is stopped were measured at the four frequencies. As the silica coated quartz crystal is negatively charged, depositions always started with the positively charged polyelectrolyte.

Confocal Laser Scanning Microscopy (CLSM). Capsule suspensions were observed with a Leica TCS SP2 AOBS (Acoustico Optical Bean Splitter) confocal laser scanning system and an inverted fluorescence microscope equipped with an oil immersion objective lens 63 \times . FITC-labeled PAH and HA were visualized by excitation of the fluorochrome with a 488 nm argon/krypton laser, and the emitted fluorescence was collected between 497 and 576 nm, precisely defined by the AOBS.

Scanning Electron Microscopy (SEM). Drops of capsule suspensions were deposited onto copper stubs and allowed to air dry. The samples were sputtered with Au/Pd and observed in secondary electron imaging mode with a Jeol JSM6100 microscope using an accelerating voltage of 8 kV. For high resolution SEM analysis, the specimens were coated by 2 nm of electron beam evaporation carbon and observed in secondary electron imaging mode with a Zeiss ultra 55 FEG-SEM (CMTC-INPG, Grenoble) at an accelerating voltage of 3 kV, using an in-lens detector.

Transmission Electron Microscopy. The samples were postfixed with 1% osmium tetroxide in water for 2 h at 4 °C, in order to enhance differential contrast among the resin, particles, and multilayers. After dehydration by incubation for 20 min in ethanol/water mixtures (7/3, 95/5) and finally twice in ethanol, the samples were infiltrated with ethanol/Lowicryl HM20 resin mixtures (2/3–1/3, 1/3–2/3), for 90 min each time. The resin was polymerized at 22 °C, allowing preservation of the morphology of particles and multilayered assembly, under indirect UV light for 72 h, using the Automatic Freeze-Substitution System (AFS Leica). Ultrathin sections (70 nm) were prepared with a diamond knife on an UC6 Leica ultramicrotome and collected on carbon-coated 200 μ m mesh copper grids. Ultrathin sections were viewed at 80 kV with a Philips CM200 transmission electron microscope. Osmium tetroxide was used to enhance differential contrast among the resin, particles, and multilayers. In order to avoid modification of the morphology of particles and multilayers, we used a resin for the preparation of ultramicrotomed sections which can be polymerized under mild conditions, i.e., at room temperature.

Incubation with FITC-Labeled Dextran. A phosphate buffer solution (0.3 mL, prepared from 0.1 M NaH₂PO₄ (50 mL) and 0.1 M NaOH (13.9 mL), pH 6.5) was added to a suspension of HA/PAH capsules (prepared from HA820) in water (0.3 mL) and left overnight at room temperature. FITC-labeled dextrans (25 μ L at 2 mg/mL in the phosphate buffer solution) were allowed to react with 25 μ L of the capsule suspension for 30 min before the samples were observed by CLSM.

Results and Discussion

PAH/HA Multilayer Formation on CaCO₃ Microparticles and Planar Surfaces: Effect of the Molecular Weight of HA. The CaCO₃ particles were prepared by colloidal crystallization after mixing of aqueous solution of calcium chloride and sodium carbonate, as reported in the literature.^{29,32} A scanning electron microscopy image of these microparticles, characterized by a spherical morphology and porous internal structure, is shown in Figure 1. These colloidal templates were obtained with a rather narrow size distribution ranging from 4 to 6 μ m. It has been

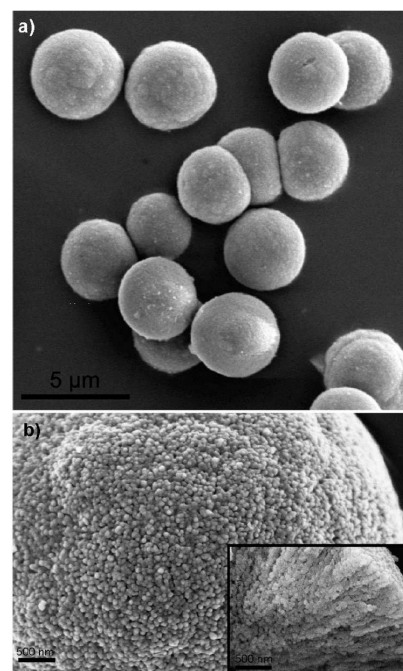


Figure 1. Scanning electron microscopy images showing spherical CaCO₃ microparticles (a) and the porous surface and internal structure (insert) of a microparticle (b) (FEG-SEM, in lens detector).

Table 1. Macromolecular Characteristics of the HA Used for Preparation of Planar Films and Capsules: Weight Average Molecular Weights (M_w), Polydispersity Indices (M_w/M_n), Intrinsic Viscosity ($[\eta]$), and Critical Overlapping Concentration (C^*) of HA Samples

	M_w (g/mol)	M_w/M_n	$[\eta]$ (mL/g) ^a	C^* (g/L) ^b
HA11	11 000	2.1	51	19.6
HA200	200 000	1.8	508	1.97
HA820	820 000	1.4	1550	0.65
HA1100	1.1×10^6	1.1	1955	0.51

^a The values of intrinsic viscosity, i.e., the reduced viscosity at infinite dilution, were derived from the relation³¹ $[\eta] = 0.0336 M_w^{0.79}$. ^b The values of C^* , the overlap concentration of the polymer chains, were deduced from the intrinsic viscosity assuming that $C^*[\eta]$ is about unity.⁵²

reported that, for particles with sizes in this range, the diameter of the pores is from 20 to 60 nm.³² Multilayer formation may be thus influenced by the molecular weight of the polyelectrolytes, as macromolecules with a size of several nanometers can penetrate inside the core during the polyelectrolyte adsorption process.³² Having HA samples with different molecular weights (i.e., HA11, HA200, HA820, and HA1100) whose characteristics are given in Table 1, we investigated the effect of the polysaccharide size on the formation of polyelectrolyte films on the CaCO₃ particles, always starting deposition with HA as the surface charge of the CaCO₃ particles is positive at physiological pH.³¹ The CaCO₃ microparticles were thus coated by sequential incubation for 10 min (to achieve equilibration from QCM-D experiments) in aqueous solutions of HA having different molecular weights ($C_p = 1$ g/L) and of PAH ($C_p = 2$ g/L) containing 0.15 M NaCl at pH 6.5. After each adsorption step, two washing steps were performed to remove the nonadsorbed polyelectrolyte. Film growth was confirmed by following (PAH/HA) film deposition on a planar solid substrate by QCM-D (Figure 2) and by following the reversal of ζ -potential during polyelectrolyte adsorption on the microparticles (Figure 3). Although QCM-D experiments are performed on a nonporous planar substrate that has a low

(35) Picart, C.; Laval, P.; Hubert, P.; Cuisinier, F. J. G.; Decher, G.; Schaaf, P.; Voegel, J. C. *Langmuir* **2001**, *17*, 7414.

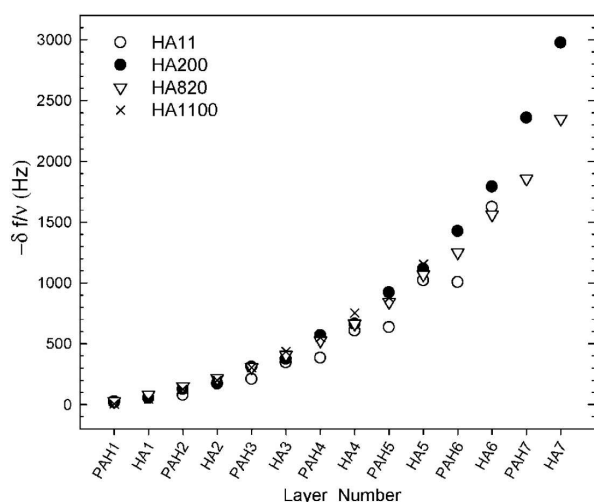


Figure 2. (PAH/HA) film growth in 0.15 M NaCl (pH 6.5) as measured by QCM-D on a SiO₂ coated crystal. Differences in the QCM frequency shifts measured at 15 MHz are plotted for each PAH and HA layer. Data are given at 15 MHz for the HA of different M_w : (○) HA11, (●) HA200, (▽) HA820, and (×) HA1100 (PAH at 2 g/L and HA at 1 g/L).

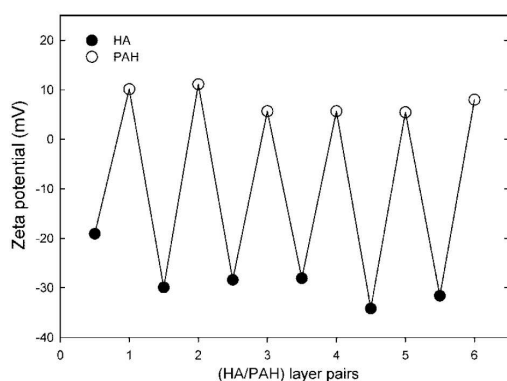


Figure 3. ζ -potential as a function of layer number during LbL coating of CaCO₃ particles with alternating HA/PAH bilayers. The odd-numbered layers correspond to PAH and the even-numbered layers to HA adsorption.

roughness (silica coated quartz crystal), it can give useful information on the film buildup *in situ*, which is not possible to get by microscopy (TEM and SEM) techniques. It thus allowed a direct comparison of film growth between HA of various M_w . As can be seen in Figure 2 for the QCM measurements, film growth is exponential in our working conditions (0.15 M NaCl at pH 6.5) and very similar for all the HA of different molecular weights (from HA11 to HA1100). Actually, HA/PAH films have already been described as exponentially growing films in a previous study performed at the same ionic strength for a HA sample of intermediate molecular weight (4×10^5 g/mol),³⁶ but linear growth was reported in low ionic strength conditions (0.01 M NaCl).²⁴ Exponential growth could be related here to the diffusion of PAH within the film architecture (*cf.* Supporting Information, Figure S1: CLSM images of a (PAH/HA200)₂₄-PAH^{FITC} film deposited on a glass slide), as previously observed for films containing HA in combination with other polysaccharides

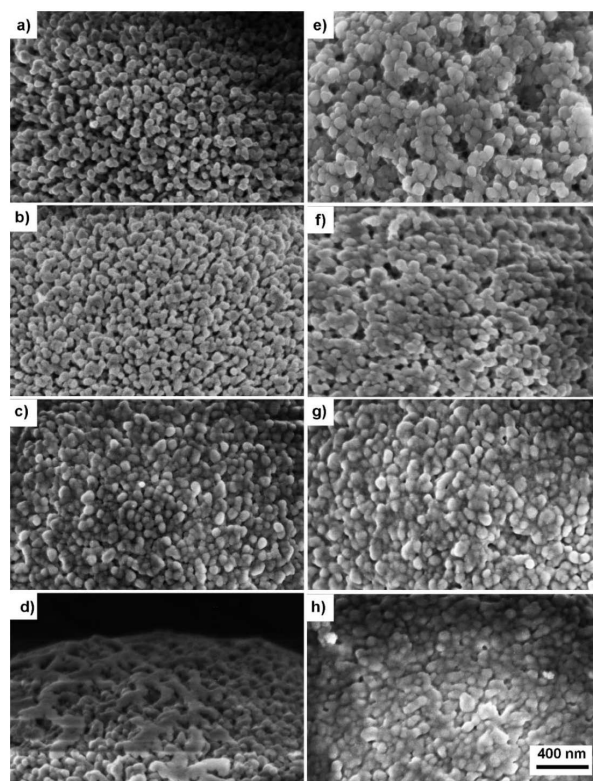


Figure 4. SEM and FEG-SEM images showing the surface of CaCO₃ particles after deposition of two HA/PAH bilayers (a–d) and six HA/PAH bilayers (e–h). The LbL assemblies were performed using HA11 (a,e), HA200 (b,f), HA820 (c,g), and HA1100 (d,h).

such as PLL³⁷ and CHI.³⁸ The fact that the type of growth depends on the ionic strength of the working solution and can be changed from linear to exponential with increasing ionic strength was indeed reported for other films such as chitosan/hyaluronic acid films.³⁸ Concerning the ζ -potential values of the layers of HA and PAH obtained in our work, it can be noted that they are in the same order of magnitude as those reported by Lee et al.¹⁷ (from -10 to -30 mV) and Volodkin et al.³² (from $+5$ to 10 mV) during the fabrication of HA/PLL and PSS/PAH capsules, respectively.

In contrast to films prepared on a nonporous solid surface, HA/PAH film growth on porous CaCO₃ microparticles was found to be influenced by the molecular weight of HA. We first observed the surface of the film coated CaCO₃ microtemplates by SEM (Figure 4). We noticed that the particles coated with two or six layer pairs of HA11/PAH and HA200/PAH exhibit surfaces with rather large pores, similar to those of the initial CaCO₃ particles (Figure 4a,b,e,f). On the other hand, the particles treated with HA820/PAH and HA1100/PAH solutions show surfaces with much smaller pore sizes (Figure 4c,d and g,h). We also performed TEM experiments (Figure 5), suggesting the formation of a polyelectrolyte film on the surface of particles coated with two layer pairs of HA1100/PAH (Figure 5d) contrary to the other ones treated with HA samples of lower M_w (Figure 5a–c). In the case of particles coated with six layer pairs, the formation of polyelectrolyte films could be distinguished for the higher M_w HA (Figure 5g,h).

(37) Picart, C.; Mutterer, J.; Richert, L.; Luo, Y.; Prestwich, G. D.; Schaaf, P.; Voegel, J. C.; Lavalle, P. *Proc. Natl. Acad. Sci. U.S.A.* **2002**, *99*, 12531.

(38) Richert, L.; Lavalle, P.; Payan, E.; Shu Xiao, Z.; Prestwich Glenn, D.; Stoltz, J.-F.; Schaaf, P.; Voegel, J.-C.; Picart, C. *Langmuir* **2004**, *20*, 448.

(36) Ball, V.; Huebsch, E.; Schweiss, R.; Voegel, J.-C.; Schaaf, P.; Knoll, W. *Langmuir* **2005**, *21*, 8526.

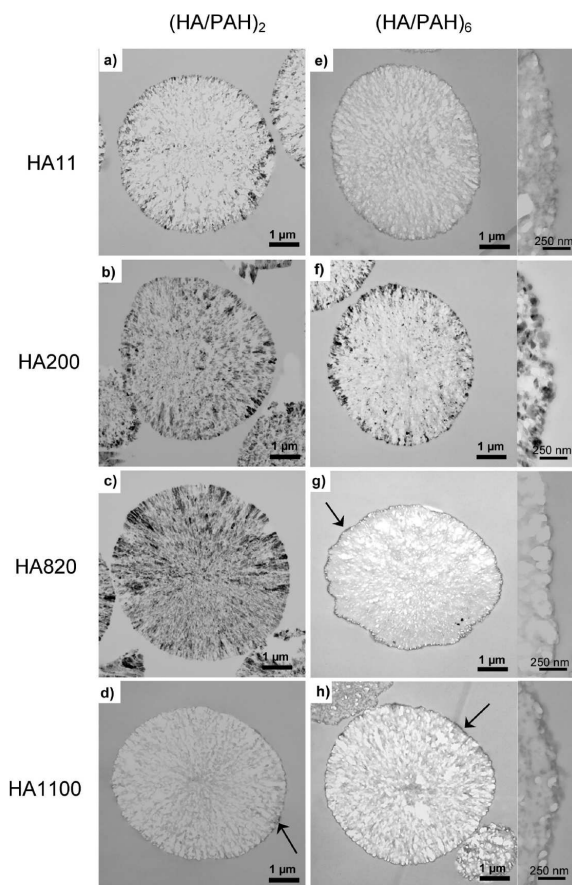


Figure 5. TEM images of sections of CaCO_3 particles after deposition of two HA/PAH bilayers (a–d) and six HA/PAH bilayers (e–h). The LbL assemblies were performed using HA11 (a,e), HA200 (b,f), HA820 (c,g), and HA1100 (d,h). The arrows indicate the presence of polyelectrolyte layers on the surface of particles.

All these observations suggest the formation of a more dense film for the high M_w HA820 and HA1100, which could be related to their large size with respect to the pore size of the CaCO_3 particles. Indeed, a previous study on the infiltration of poly(acrylic acid) (PAA) in nanoporous silica particles revealed that the extent of polymer infiltration strongly depends upon the relative sizes of the nanopores and the PAA macromolecules.³⁹ Comparison of the pore size distribution of CaCO_3 microparticles³¹ with the hydrodynamic diameter distribution of HA samples derived from size exclusion chromatography analysis and from the molecular weight dependence of the hydrodynamic radius for HA chains⁴⁰ provided evidence of the crucial role played by the macromolecular size in infiltration. As can be seen from Figure 6, the high hydrodynamic diameter values of the HA1100 chains totally prevent their penetration into the CaCO_3 microparticles, while HA820 might only partially diffuse inside the core. On the other hand, the sizes of the HA11 and HA200 chains are lower than or in the same range as those of the template pores, which can explain diffusion observed experimentally for these samples.

(39) Wang, Y.; Angelatos, A. S.; Dunstan, D. E.; Caruso, F. *Macromolecules* **2007**, *40*, 7594.

(40) Takahashi, R.; Kubota, K.; Kawada, M.; Okamoto, A. *Biopolymers* **1999**, *50*, 87.

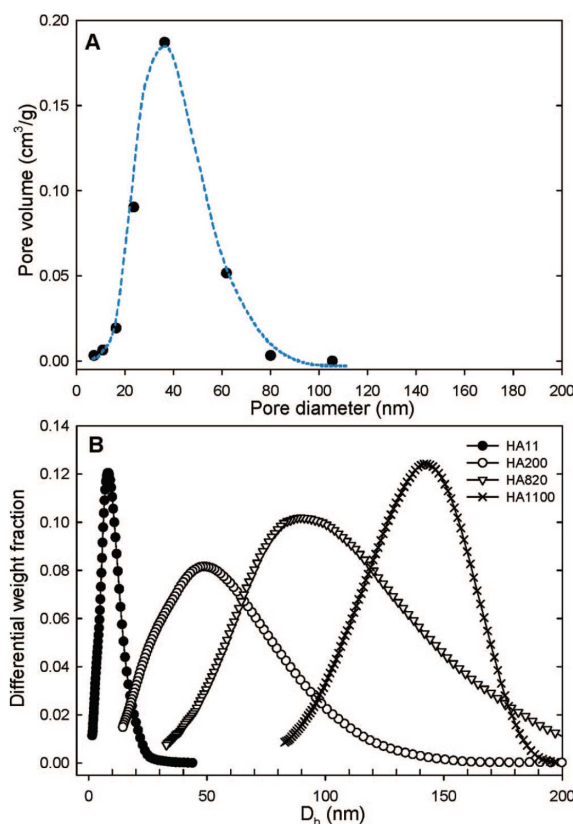


Figure 6. Size distribution of (A) pores of CaCO_3 microparticles³¹ and (B) of hyaluronic acid chains for HA11, HA200, HA820, and HA1100 samples. The values of the hydrodynamic diameters were derived from size exclusion chromatography analysis of the different samples of HA and from the molecular weight dependence of the hydrodynamic radius for HA chains.⁴⁰

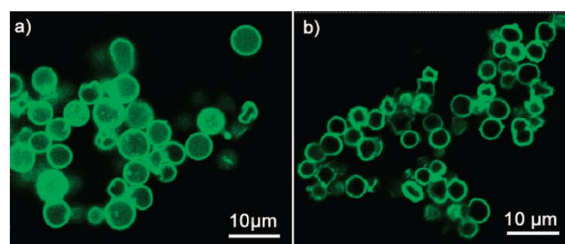


Figure 7. CLSM images of hollow $\text{HA}^{\text{FITC}}/\text{PAH}$ (a) capsules and $\text{HA}/\text{PAH}^{\text{FITC}}$ (b) capsules obtained after treatment by citric acid. The LbL assembly (4 bilayers) was performed using HA820.

PAH/HA Microcapsules: Conditions for Core Dissolution, Effect of Polyelectrolyte Concentration, and Shell Wall Permeability. *Conditions for Core Dissolution.* After the adsorption of the desired number of layer pairs was achieved, the calcium carbonate core was subjected to decomposition. The first method for CaCO_3 core dissolution that consists of lowering the pH of the solution ($\text{pH} \sim 2$) could not be applied here due to the perturbation of the HA/PAH assembly. Moreover, the treatment of the coated carbonate particles under neutral conditions (EDTA solutions at $\text{pH} 7.2$) generally used for capsule preparation leads to the destruction of the multilayer assembly. Such capsule dissolution might be the result of the

stronger complexation between EDTA and PAH than that between HA and PAH, with the EDTA/PAH complex being indeed soluble.

However, we found that core dissolution with EDTA in neutral conditions was possible once the capsules have been cross-linked with a water soluble carbodiimide (data not shown). For this, we followed the procedure already developed for HA-based polyelectrolyte multilayers on planar surfaces³⁴ and cross-linked the HA/PAH assembly by an amine–acid coupling reaction performed at pH 6.5 using the water soluble carbodiimide, 1-ethyl-3-(3-dimethylaminopropyl)carbodiimide hydrochloride (EDC), in combination with *N*-hydroxysulfosuccinimide (NHS). Cross-linking of the (HA/PAH) films was checked by Fourier transform infrared spectroscopy (*cf.* Supporting Information Figure S2), which is now an established technique to characterize film cross-linking.^{34,41,42} The percentage of cross-linking was estimated at 32%. Hollow capsules were thus obtained with no apparent defects in the shell.

We also tested an alternative route for core dissolution without the requirement for cross-linking. In this protocol, 0.1 M citric acid at pH 5.4 was employed to dissolve the CaCO_3 support, citric acid being a good chelating agent for calcium ions.^{43,44} As EDTA, citric acid binds calcium ions in a 1:1 ratio though with a lower binding constant ($K_{\text{a}}(\text{EDTA}/\text{CaCl}_2) \sim 2 \times 10^8 \text{ M}^{-1}$ and $K_{\text{a}}(\text{citric acid}/\text{CaCl}_2) \sim 10^{3.5} \text{ M}^{-1}$ at pH 7).⁴³ Also, the PAH/citric acid complex is insoluble, which should not cause the multilayer dissolution. In our case, the HA/PAH multilayer structure was preserved and we verified that the multilayer wall effectively contained HA and PAH. This was achieved by confocal laser scanning microscopy using fluorescently labeled polyelectrolytes (HA^{FITC} and PAH^{FITC}) (Figure 7). It can be noted that comparison of the fluorescence intensities in the capsule wall and in the aqueous core indicates that some HA is still inside the capsule. There is about 2.5 times more HA at the wall than in the core. This might be related to the partial diffusion of HA820 during the first adsorption step as suggested by the profile of the hydrodynamic diameters obtained for this sample (see Figure 6).

Effect of HA Concentration. In the next step, we explored more deeply the formation of capsules by varying concentration of HA11 from 2 to 14.25 g/L in 0.15 M NaCl. As can be seen from Figure 8, capsules prepared with a low HA concentration (2 g/L, Figure 8a) exhibit a “grainy” surface in contrast to those obtained from higher HA concentrations ($C_{\text{p}} \geq 5 \text{ g/L}$), which show smooth surfaces (Figure 8b–d). Such grains look like those observed during the formation of hyaluronic acid containing films at the initial stages of the buildup, when a continuous film is not totally formed.³⁵

The method of deposition of HA/PAH layer thus depends not only on the molecular weight of HA, but also on its concentration used during multilayer formation. This was supported by TEM images of films deposited on CaCO_3 particles using two different concentrations of HA11 (Figure 9). The film appears to be thicker when the HA concentration in 0.15 M NaCl (pH 6.5) is increased from 5 (Figure 9a) to 14.25 g/L (Figure 9b).

The effect of HA concentration was then examined for all the HA samples. Figure 10 compares SEM images of $(\text{HA/PAH})_4$ capsules prepared from all the different HA, using HA

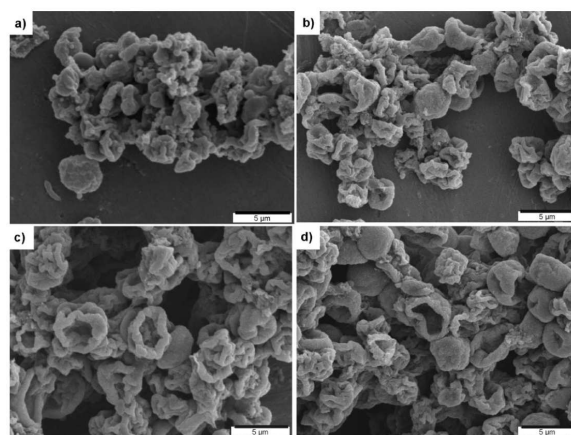


Figure 8. SEM images of capsules prepared using different HA (HA11) concentration during deposition: 2 g/L (a), 5 g/L (b), 10 g/L (c), and 14.25 g/L (d).

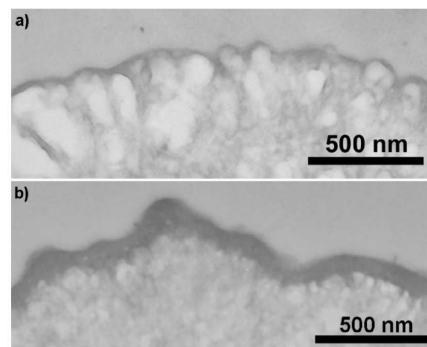


Figure 9. TEM images of sections of CaCO_3 particles after deposition of six HA/PAH bilayers using two different concentrations of HA11: 5 g/L (a) and 14.25 g/L (b) in 0.15 M NaCl.

concentrations of 1 and 5 g/L. These images provide evidence of the crucial role played by HA concentration in the formation of hollow capsules. HA/PAH microcapsules can thus be obtained with good reproducibility if HA is used at a minimum concentration of 5 g/L in 0.15 M NaCl during its deposition on carbonate particles. Indeed, the growth of HA/PAH films on a solid substrate followed by QCM-D also exhibited a strong dependence on HA concentration (Figure 11). In this figure, the increment in frequency measured for each deposited HA layer (at 15 MHz) is plotted as a function of the HA layer number, for HA11 and HA200 at 1 and 5 g/L. The frequency increment is much higher when HA is deposited from a solution at 5 g/L than from a solution at 1 g/L, with, again, a similar behavior observed for two different molecular weights HA.

All these results show that for both solid substrates and CaCO_3 porous microparticles, film growth depends on the HA concentration. Increasing the concentration of HA from 1 to 5 g/L may promote the formation of entanglements between the HA chains ($5 \text{ g/L} > C^*$ for HA200, HA820, and HA1100; from Table 1) resulting in a higher density of the deposited film. This is indeed suggested by the QCM-D measurements of the viscous dissipations during film buildup, which show that the dissipation is systematically higher for films built with HA at 5 g/L as compared to those built with HA at 1 g/L (*cf.* Supporting Information Figure S3).

(41) Kozlovskaya, V.; Kharlampieva, E.; Mansfield, M. L.; Sukhishvili, S. A. *Chem. Mater.* **2006**, *18*, 328.

(42) Schneider, A.; Francius, G.; Obeid, R.; Schwint, P.; Hemmerle, J.; Frisch, B.; Schaaf, P.; Voegel, J.-C.; Senger, B.; Picart, C. *Langmuir* **2006**, *22*, 1193–1200.

(43) Keowmaneechai, E.; McClements, D. J. *J. Agric. Food Chem.* **2002**, *50*, 7145.

(44) Poncelet, D.; Babak, V.; Dulieu, C.; Picot, A. *Colloids Surf., A* **1999**, *155*, 171.

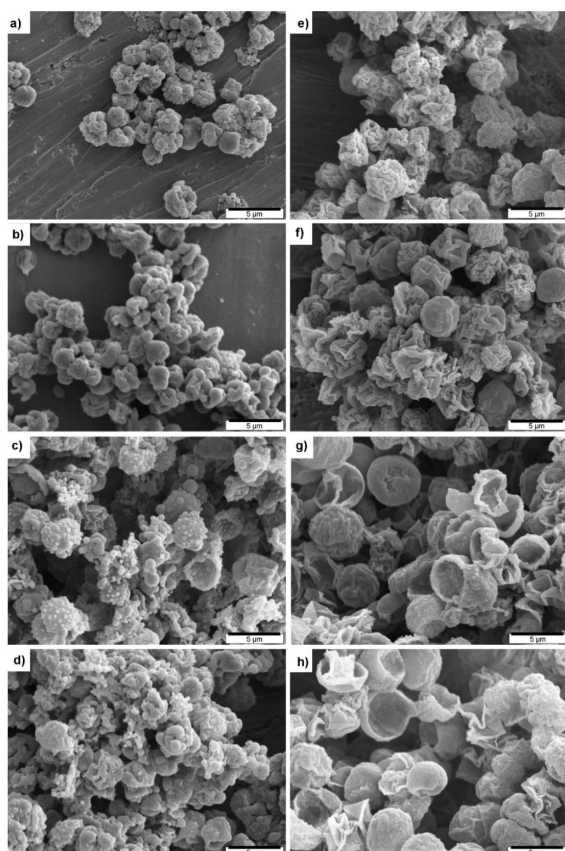


Figure 10. SEM images of capsules prepared with four HA/PAH bilayers using different HA samples: HA11 (a,e), HA200 (b,f), HA820 (c,g), and HA1100 (d,h), at two concentration 1 g/L (left) and 5 g/L (right).

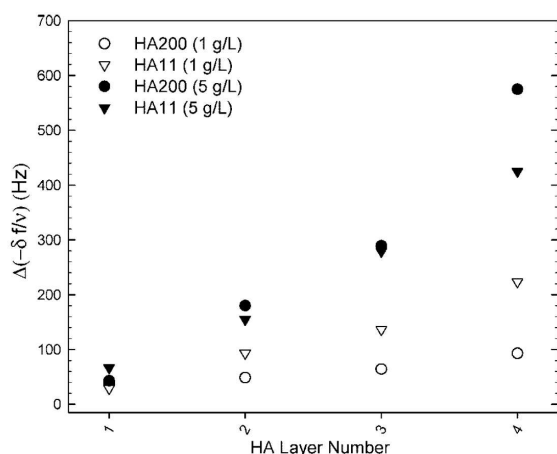


Figure 11. Increment in the QCM frequency shift ($\Delta(-\delta f/v)$) in Hz measured at 15 MHz during the deposition of HA layers plotted as a function of the HA layer number. Two different HA are compared: HA200 and HA11 at two HA concentrations of 1 g/L and 5 g/L. PAH concentration was kept constant at 2 g/L.

Shell Wall Permeability. In the perspective of using such capsules as drug vehicles, we were interested in evaluating the permeability of the shell walls to molecules of various sizes, the

Table 2. Qualitative Analysis of the Shell Wall Permeability for (HA/PAH)₄ Capsules in a Phosphate Buffer Solution without Added Salt (pH 6.5) by CLSM Using Dextran-FITC Samples with Different Molecular Weights (M_w)^a

M_w of dextran-FITC (g/mol)	presence of dextran-FITC inside the core of capsules	
	HA/PAH capsules	cross-linked HA/PAH capsules
4×10^3	±	±
500×10^3	—	—
2000×10^3	—	—

^a Dextran was either totally rejected (—) or was mainly rejected (±).

latter being able to be encapsulated by adsorption on the porous carbonate particles, as discussed above. As a first approach to this study, we thus examined diffusion by CLSM of various molecular weight FITC-labeled dextrans (dextran^{FITC}-4, -500 and -2000 with $M_w = 4 \times 10^3$, 500×10^3 , and 2000×10^3 g/mol, respectively), as models of biologically active substances of different sizes (in the range from 3.8 to 53.8 nm from the hydrodynamic diameter values reported for different samples of dextran).^{45,46} Capsules were prepared by LbL deposition of four HA/PAH bilayers on CaCO_3 particles using conditions allowing good reproducibility and low diffusion of polyelectrolytes inside the core. From the results described above, we thus selected HA820 ($C_p = 5$ g/L in 0.15 M NaCl during deposition). The permeability was studied on cross-linked as well as un-cross-linked shells.

Observation of capsules 30 min after the addition of dextran^{FITC} in a phosphate buffer solution without added salt (pH 6.5) revealed some differences as a function of the molecular weight of dextran. Both types of capsule were partially permeable to dextran^{FITC}-4, whereas dextran^{FITC}-500 and dextran^{FITC}-2000 were totally rejected from the shell wall (see Table 2 and cf. Supporting Information Figure S4). A similar behavior was observed for chitosan/chitosan sulfate capsules in water (pH ~ 6), which were found to be impermeable for dextran^{FITC} with M_w above 200 000 g/mol.¹² One can notice that the cross-linked HA/PAH capsules prepared under our cross-linking conditions and the non-cross-linked ones exhibit comparable permeability. These results thus demonstrate the possibility to obtain hollow HA/PAH shells having semipermeable properties without multilayer chemical cross-linking. According to previous results performed on planar multilayers made of PLL/HA^{42,47} as well as on hydrogel capsules composed of poly(methacrylic acid) layers covalently linked by ethylenediamine,⁴¹ we can assume to control the degree of cross-linking of the shell wall either by varying the amount of the amide coupling agent (EDC) or the cross-linking time. Such an approach might thus be advantageously exploited not only to tune the stability of capsules as a function of the environment conditions, but also to study the effect of cross-linking density on the permeability of the capsules.

Conclusion

In conclusion, this study establishes the feasibility of obtaining hollow microcapsules based on the multilayer assembly of hyaluronic acid and poly(allylamine). Due to the sensitivity of HA/PAH assembly, in particular, to low and high pH values, we used CaCO_3 microtemplates which have the advantage of being dissolved under mild conditions. However, in contrast to previous

(45) Armstrong, J. K.; Wenby, R. B.; Meiselman, H. J.; Fisher, T. C. *Biophys. J.* **2004**, *87*, 4259.

(46) Koehler, K.; Sukhorukov, G. B. *Adv. Funct. Mater.* **2007**, *17*, 2053.

(47) Ren, K.; Crouzier, T.; Roy, C.; Picart, C. *Adv. Funct. Mater.* **2008**, *18*, 1378.

results showing the possibility of producing hollow capsules made of synthetic, even weak, polyelectrolytes after dissolution of CaCO_3 particles by treatment with EDTA, the use of this chelating agent leads to the destruction of the multilayer assembly in our case. The problem of core decomposition could be overcome either by chemically cross-linking the shell before treatment with EDTA or by the use of citric acid as a chelating agent of Ca^{2+} ions.

Moreover, this work clearly demonstrates the strong influence of the molecular weight of HA on the surface morphology of the capsules. This was mainly attributed to the porous structure of the template which allows penetration of polyelectrolytes when their size is below the maximum pore size of the carbonate template (~ 60 nm). We thus found that diffusion of the initial layers in the carbonate core becomes limited by using an HA sample having weight-average molecular weight equal to or higher than 820 000 g/mol. Besides the macromolecular size, concentration of the HA solution during adsorption also appeared to be a crucial parameter influencing the multilayer structure, with higher HA concentrations leading to a more dense and entangled structure.

In addition, we verified that these HA containing microcapsules are biocompatible and not cytotoxic by introducing a high concentration of capsules in a myoblast culture (*cf.* Supporting Information Figure S5). These capsules hold promise in the controlled delivery of drugs due to their reservoir properties as well as to the large number of possible chemical modifications on HA for specific purposes such as cross-linking,⁴⁸ grafting of drugs,⁴⁹ or cage molecules.³³ They may also be designed for

specific cell targeting, as HA has an important role in the early recognition events of a cell in its microenvironment due to its presence in the pericellular coat of many cell types.⁵⁰

Acknowledgment. We gratefully acknowledge Frédéric Charlot at CMTIC-INPG, Grenoble, for his help with SEM observations using the Zeiss ultra 55 FEG-SEM. A.S. was a recipient of a Marie Curie Fellowship of the European Community's Sixth Framework Programme under contract number MEST-CT-2004-503322. This research project was partly supported by a "Association Recherche contre le Cancer grant" (ARC, n° 7918) and by a "Fondation Recherche Médicale" grant (FRM, n° INE20061108297) to C.P. CP is a Junior Member of the "Institut Universitaire de France" whose support is gratefully acknowledged. We wish to thank the support from the ANR PNANO 2007.

Supporting Information Available: CLSM images of a (PAH/HA200)₂₄-PAH^{FITC} film deposited on a glass slide, FTIR-ATR spectra before and after the addition of EDC/NHS solution for a (HA820/PAH)₄ film, dissipation changes for the third overtone measured by QCM-D during the (HA/PAH) film deposition on a SiO_2 crystal for HA11 and HA200 at two different concentrations, CLSM images of cross-linked and non cross-linked HA820/PAH capsules incubated in solutions of FITC-labeled dextran-4, dextran-500 and, dextran-2000, transmission images of cross-linked (HA820/PAH)₄ microcapsules added in a myoblast culture. This material is available free of charge via the Internet at <http://pubs.acs.org>.

LA801274Z

(48) Segura, T.; Anderson, B. C.; Chung, P. H.; Webber, R. E.; Shull, K. R.; Shea, L. D. *Biomaterials* **2005**, 26, 359.

(49) Thierry, B.; Kujawa, P.; Tkaczyk, C.; Winnik, F. M.; Bilodeau, L.; Tabrizian, M. *J. Am. Chem. Soc.* **2005**, 127, 1626.

(50) Cohen, M.; Joester, D.; Sabanay, I.; Addadi, L.; Geiger, B. *Soft Matter* **2007**, 3, 327.

(51) Milas, M.; Rinaudo, M.; Roure, I.; Al-Assaf, S.; Phillips, G. O.; Williams, P. A. *Biopolymers* **2001**, 59, 191.

(52) Auzely-Velty, R.; Rinaudo, M. *Macromolecules* **2002**, 35, 7955.

3.3. Supporting information

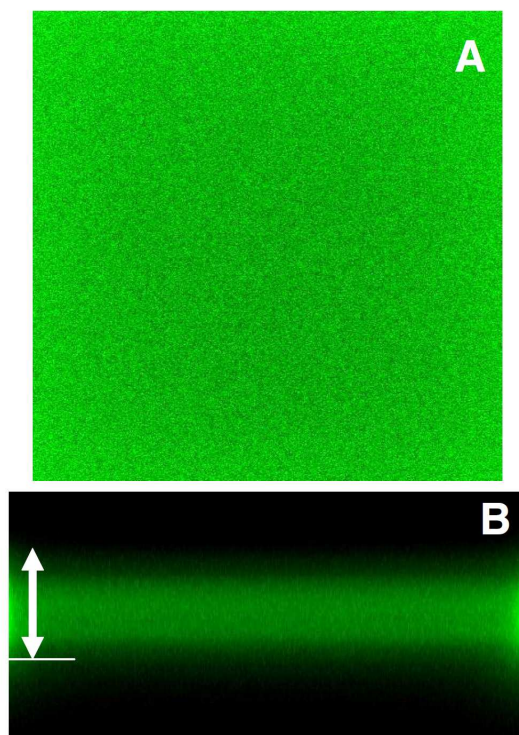


Figure S1 : CLSM images of a $(\text{PAH/HA200})_{24}\text{-PAH}^{\text{FITC}}$ film deposited on a glass slide : (A) top-view image of the film ($142.9 \times 142.9 \mu\text{m}$); (B) vertical section of the same film (image size is $35.7 \mu\text{m}$ (width) \times $14.1 \mu\text{m}$). Film thickness is about $6.5 \mu\text{m}$ (white line).

Fourier Transform Infrared Spectroscopy in Attenuated Total Reflection.

Film buildup and subsequent crosslinking of a (HA/PAH)₄ film deposited on a ZnSe crystal (pre-coated with a polyethyleneimine precursor layer) were investigated by *in situ* Fourier transform infrared (FTIR) spectroscopy in attenuated total reflection (ATR) mode with a Vertex 70 spectrophotometer (Bruker Optic GmbH, Ettlingen, Germany). All the experimental details have been given previously.^{S1} The experiments were performed in a deuterated 0.15 M NaCl solution at pD 6.5. D₂O is used as the solvent instead of water because the amide and carboxylic band of HA are affected by the strong water band absorption around 1643 cm⁻¹ (O-H bending), whereas the corresponding vibration in D₂O is found around 1209 cm⁻¹. During the buildup, the film was continuously in contact with the 0.15 M NaCl solution and was never dried. After each polyelectrolyte deposition (4 mL for each layer were flushed in the measuring cell), rinsing step, and the final contact with the EDC/NHS solution, single-channel spectra from 32 interferograms were recorded between 400 and 4000 cm⁻¹ with a 2 cm⁻¹ resolution, using Blackman-Harris three-term apodization and the standard Bruker OPUS/IR software (version 6.5). The spectrum from the bare ZnSe crystal in contact with the 0.15 M NaCl solution (pH 6.5) was taken as reference. During the contact of the film with the EDC/NHS solution (0.2 M and 0.05 M final concentrations respectively), single-channel spectra from 32 interferograms were recorded every 20 min. Spectra were acquired before, during, and after cross-linking. Band decomposition in the 1540-1740 cm⁻¹ region was achieved by means of the OPUS software after baseline correction, peak position determination and fitting of the peaks assuming a Gaussian shape for all of them.

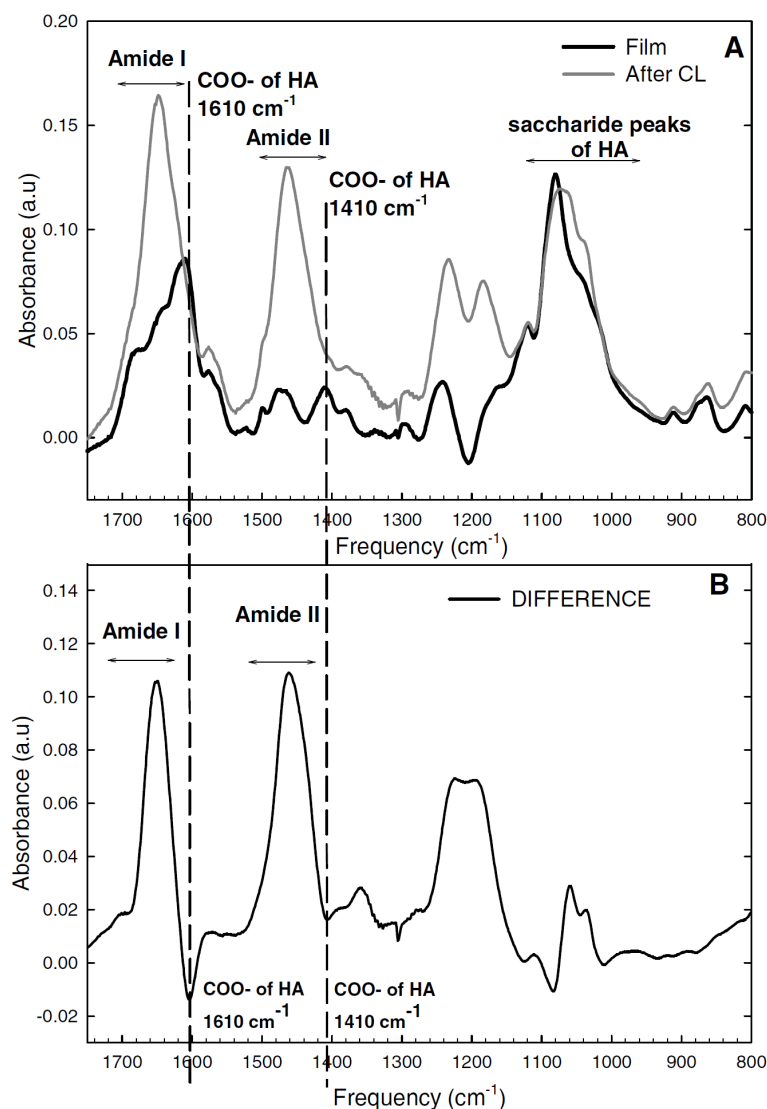


Figure S2 : (A) FTIR-ATR spectra before (black line) and after the addition of EDC/NHS solution (gray line) for $(\text{HA/PAH})_4$ film. (PAH at 2 g/L, HA820 at 5 g/L). (B) The difference between the two spectra (before and after cross-linking) is represented. Noticeably, the carboxylic peaks of HA have decreased whereas the amine I and amine II bands have increased, proving the effective formation of covalent amide bonds within the film. The intensity of the 1610 cm^{-1} carboxylic peak was obtained after a spectral decomposition. Its decrease from 0.075 before cross-linking to 0.051 after cross-linking gives an estimate of the cross-linking rate (32%).

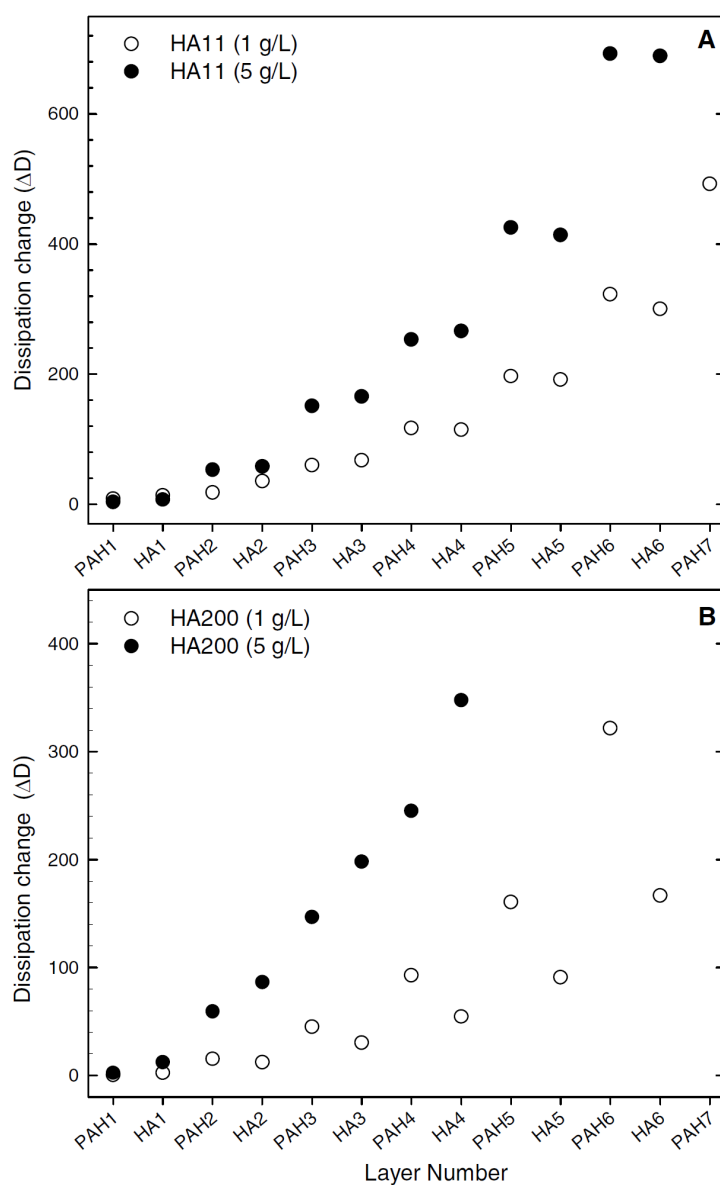


Figure S3 : Dissipations changes for the third overtone measured by QCM-D during the (HA/PAH) film deposition on a SiO_2 crystal, for HA at two different concentrations: 1 g/L (\circ) and 5 g/L (\bullet) and for two different molecular weights : (A) HA11 and (B) HA200.

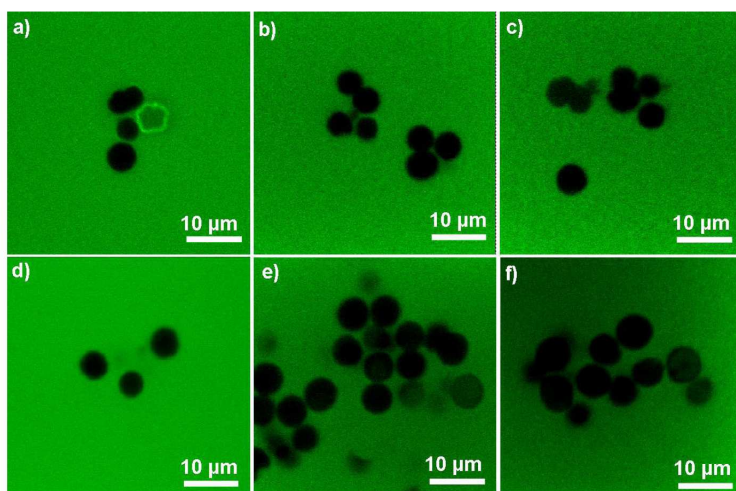


Figure S4 : CLSM images of non cross-linked (top) and cross-linked (bottom) HA/PAH capsules incubated in solutions of FITC-labeled dextran-4 (a,d), dextran-500 (b,e) and, dextran-2000 (c,f).

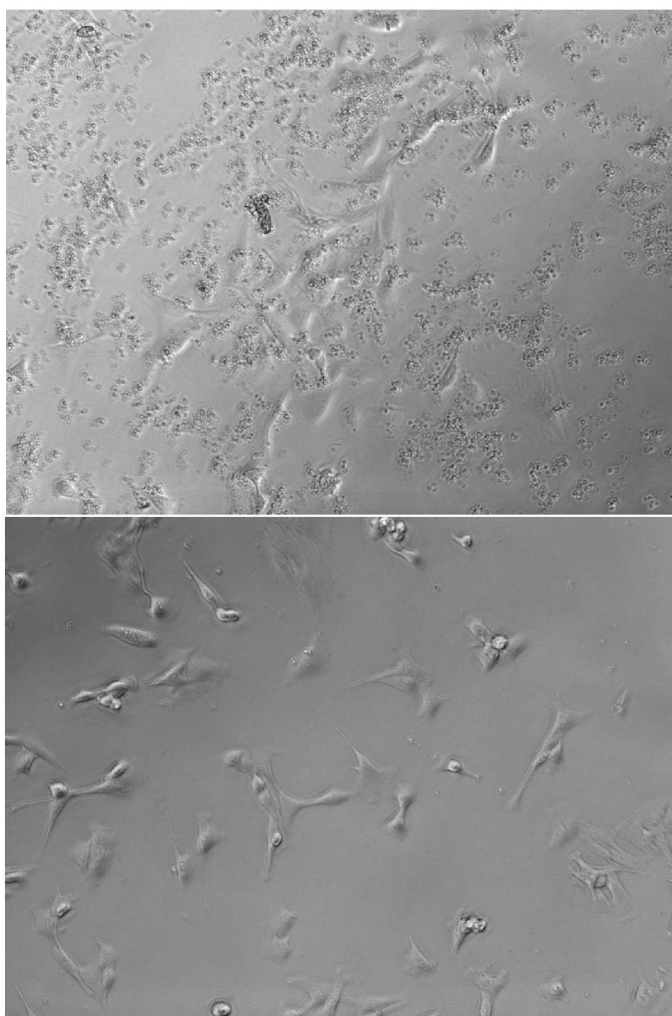


Figure S5. Transmission images of cross-linked (HA/PAH)₄ microcapsules added in a myoblast culture (C2C12 cells)² four hours after cell plating (2.5×10^4 cells/cm²) and observed after 18 H of contact with the cells (upper image). The cell aspect was similar to that of cells cultured without capsules in their medium (lower image).

References

- S1. Schwinte, P.; Voegel, J. C.; Picart, C.; Haikel, Y.; Schaaf, P.; Szalontai, B. *J. Phys. Chem. B* **2001**, *105*, 11906-11916.
- S2. Ren, K.; Crouzier, T.; Roy, C.; Picart, C. *Adv. Funct. Mater.* **2008**, *18*, 1378-1389.

3.4. Complementary results

3.4.1. Use of HA at low concentration during the HA/PAH multilayer build-up.

Different concentration regimes can be distinguished for hyaluronic acid in aqueous solution :

- (i) the dilute regime $C < C^*$, where C^* is the critical overlap concentration which depends on the M_w of HA, solvent and temperature.
- (ii) The semi-dilute disentangled regime $C^* < C < C_e$, where C_e is the concentration at which entanglements become elastically effective. In this regime, the viscoelastic properties of the solution are controlled by the Rouse dynamics¹.
- (iii) The semi-dilute entangled regime with $C_e < C < C^{**}$, where C^{**} corresponds to the transition to the concentrated domain. In this concentration domain, the viscoelasticity of the solution is described by the reptation model².

Bases on these considerations, in the first part of our study, we examined the formation of HA/PAH capsules using HA samples with different M_w at concentrations 25% below C^* .

Table CR 3.1. gives the C^* values of the different HA samples used in this study. These values were derived from the intrinsic viscosity, assuming that $C^*[\eta]$ is about unity³.

$$C^*[\eta] \approx 1 \quad \text{eq.III.1}$$

Table CR 3.1. C^* values of HA at various M_w .

HA sample	η [mL/g] ^a	C^* [g/L]	Concentration of HA used (25% below C^*): [g/L]
HA11	51.4	19.4	14.25
HA200	517.7	1.9	1.42
HA820	1578.4	0.6	0.45
HA1100	1990.8	0.5	0.37

^aMeasured in PBS at 25 °C

From the observation of the SEM images in **Figure CR 3.1**, it can be concluded that diluted solutions of HA are not suitable for capsule formation, whatever the M_w of HA. One can assume that below C^* , HA cannot fully cover the CaCO_3 particles. Moreover, as detailed in this chapter, low M_w HA chains diffuse into the pores of carbonate particles. This however can be limited by the use of a solution of HA at high concentration (14g/L), which enables formation of a HA/PAH film (see **Figure CR 3.1.a**).

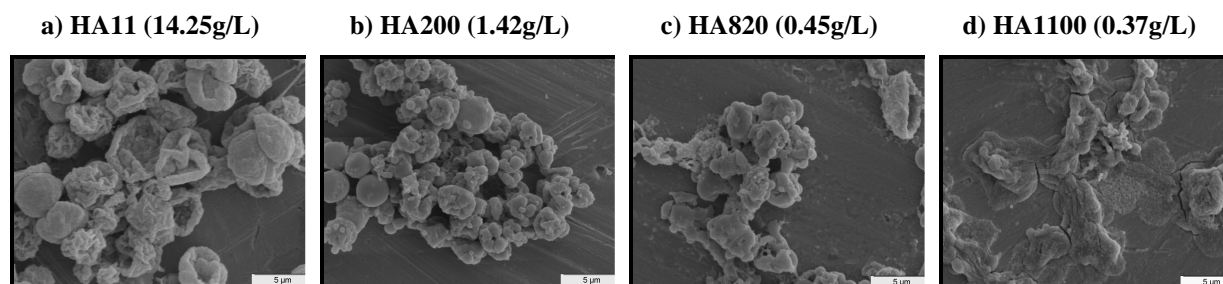


Figure CR 3.1. HA/PAH capsule formation from different M_w of HA and concentrations below C^* and PAH of 2g/L. Polyelectrolytes were dissolved in 0.15M NaCl (pH 6.5). Citric acid (0.1M, pH 5.4) was used for core dissolution.

3.4.2. Effect of the chelating agent on the polyelectrolyte assemblies

EDTA, which was successfully used for the dissolution of CaCO_3 for the synthesis of PSS/PAH capsules⁴ caused multilayer dissolution when HA at low M_w was used.

From this result, citric acid was selected for core dissolution instead of EDTA, resulting in hollow capsules for all HA samples tested (HA11, HA200, HA820 and HA1100), as described previously.

As soon as we established the optimal conditions for the fabrication of HA/PAH capsules (HA820 at a concentration of 5g/L), EDTA could be successfully used to dissolve carbonate particles. The resulting capsules are shown in **Figure CR 3.2** and compared with the HA820/PAH capsules obtained after core decomposition with citric acid.

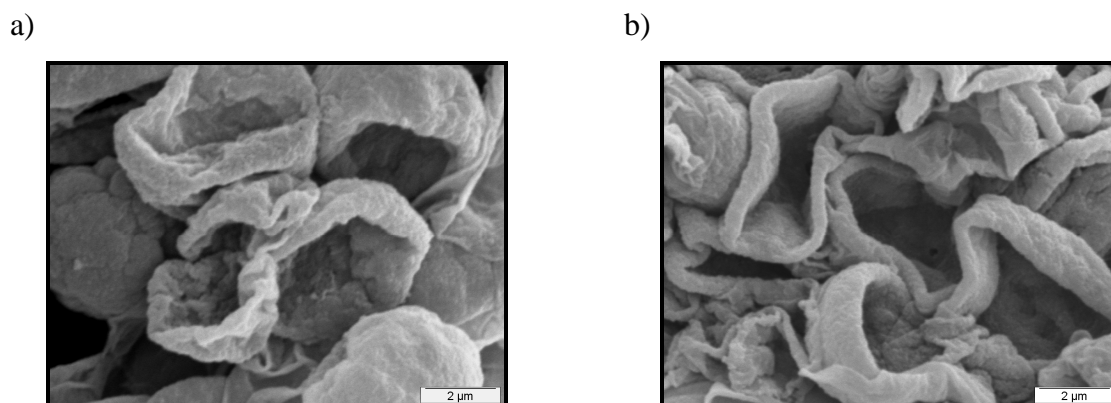


Figure CR 3.2. HA820/PAH capsules (HA of 5g/L) after core removal using citric acid (a), EDTA (b).

The morphologies of the hollow capsules look similar. In order to provide explanation for the disruption of the HA11/PAH multilayers and not HA820/PAH ones by EDTA, we examined the effect of adding EDTA to complexes formed in the bulk, by precipitation of the PE in the bulk. It was found, that the non-soluble HA11/PAH complex in the bulk can be rapidly dissolved after treatment with EDTA (0.1M, pH 7.2), while the HA820/PAH precipitate remains stable under the same conditions. Further additions of EDTA lead to the formation of transparent gel-like aggregates which could be dissolved completely only after high EDTA excess. These observations thus indicate that the HA11/PAH multilayers are more sensitive to the presence of EDTA than the multilayers based on entangled chains of high M_w HA820.

3.4.3. Dialysis process

The use of gentle dialysis instead of centrifugation during the core dissolution and washing steps with water allowed us to improve the morphology of capsules. As shown by **Figure CR 3.3** the “soft” capsules were not deformed when dialysis process was used.

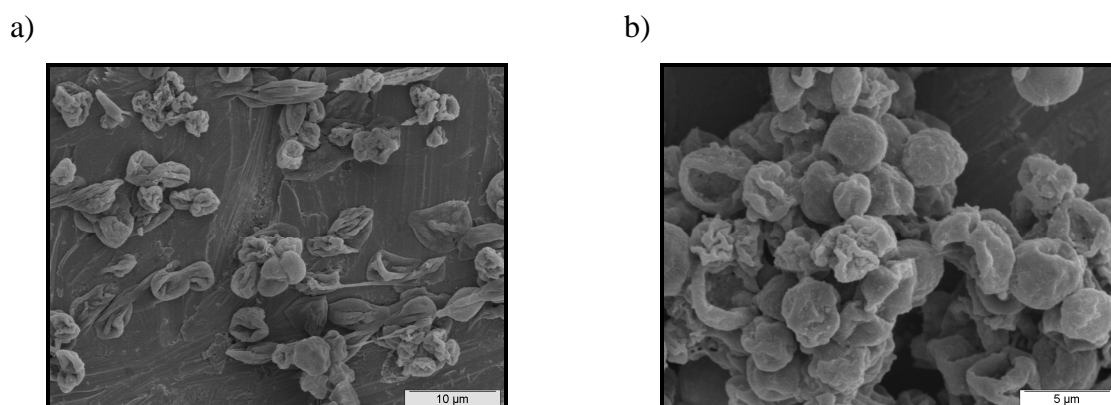


Figure CR 3.3. HA200/PAH capsules after core removal using centrifugation a) and dialysis process b). Scale bars 10μm a) and 5μm b).

References :

- (1) Rouse, P. E. J. *J. Chem. Phys.* **1953**, 21, 1272.
- (2) DeGennes, P. G., Ed. *Scaling Concepts in Polymer Physics*: Thaca, New York, 1979.
- (3) Macosko, C. W. G., Ed. *Rheology: Principles, Measurements and Applications*, 1994.
- (4) Alexei A. Antipov, D. S., Yuri Fedutik, Alexander I. Petrov, Gleb B. Sukhorukov, Helmuth Mohwald. *Colloids and Surfaces A: Physicochemical and Engineering Aspects* **2003**, 224, 175-183.

CHAPTER 4

*Effect of Polycationic Partner of HA
on Capsule Morphology Characterization and
Preliminary Release Assessment*

4.1. Résumé (fr)

Ce chapitre est consacré à la sythèse et caractérisation de capsules à base d'acide hyaluronique et de polycations biocompatibles. Ces capsules étant destinées à être utilisées comme transporteurs de principes actifs, nous avons cherché à remplacer la poly(allylamine)(utilisée dans le chapitre 3) par un polypeptide, la poly(L-lysine) (PLL), et un polysaccharide, un dérivé quaternisé du chitosane (QCH).

Les capsules à base de HA/QCH s'avèrent être stables malgré l'absence de pontages chimiques entre les couches contrairement aux capsules préparées à partir de la PLL. L'obtention de capsules à partir de ce polypeptide et de HA a nécessité une étape de réticulation chimique du film de HA/PLL par couplage amine-acide en présence d'un carbodiimide hydrosoluble. Ces résultats s'expliquent par des propriétés de complexation différentes de la PLL et du dérivé QCH vis-à-vis du HA.

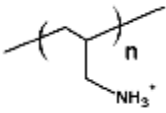
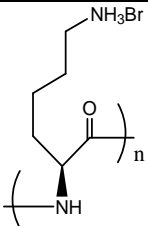
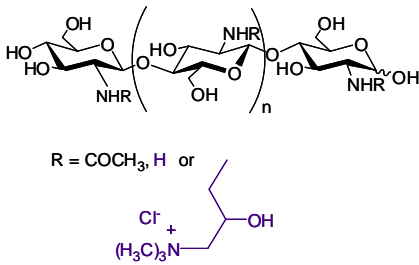
Afin d'évaluer les applications potentielles de ces capsules pour la libération de médicaments, nous avons comparé les propriétés de perméabilité et de dégradation enzymatique de ces différents types de capsules. Les résultats obtenus au cours de cette étude indiquent la possibilité de moduler la perméabilité des capsules en fonction du degré de réticulation et de la présence d'enzyme hydrolysant le HA, dans le milieu environnant.

4.2. Introduction

The study presented in chapter 3, dealing with the fabrication of capsules made from HA and the synthetic polyelectrolyte PAH, showed that the formation of hollow capsules made from sensitive, highly hydrated hyaluronic acid requires suitable mild experimental conditions. In particular, the molecular weight of hyaluronic acid and its concentration play important role in the formation of the multilayer assembly, which should remain stable after core dissolution. We first selected a synthetic polyelectrolyte - poly (allylamine) PAH as the polycationic partner of HA since much is known about its behaviour in the case of LbL capsules made from synthetic polymers. However, for controlled drug delivery, it would be preferable that LbL capsules are composed of fully biocompatible, biodegradable, nontoxic components.

In the next step of this work, we thus replaced PAH by biocompatible positively charged polymers: a polypeptide, i.e. poly(L-lysine) (PLL)), and a polysaccharide, i.e. a chitosan derivative (QCH) (**Table 4.1**).

Table 4.1. Molecular structures of polycations used as partners of HA for the synthesis of microcapsules.

Cationic polyelectrolyte	Molecular structure	M_w (g/mol)	pKa
Poly(allylamine) chloride PAH		70×10^3	$\sim 8.5^1$
Poly (L-lysine) bromide PLL		$15 \times 10^3 - 30 \times 10^3$	$\sim 9.0^2$
Quaternized chitosan QCH		$180 \times 10^3^*$	$\sim 8.5^3$

*-value of initial CH

PLL was selected, since it is biocompatible, non toxic, non antigenic⁴, but also can be easily modified with bioactive molecules⁵. This polymer is also widely used for the promotion of cell adhesion on solid substrates⁶.

The second polycation selected as a partner of HA for LbL capsule formation is chitosan, the main derivative of chitin. CH is used for different biomedical and pharmaceutical applications in wound healing, drug delivery, rheumatology, taking advantage of its biodegradability, biocompatibility, bioadhesivity, antifungal, antibacterial and immunoadjuvant properties⁷. Since chitosan is soluble in water only under acidic conditions, which are not suitable for our conditions of capsule preparation, a CH derivative soluble in water at neutral pH was required. For this aim, a selectively quaternized derivative of chitosan (QCH) was synthesized³, following a literature method⁸.

In order to evaluate the potential use of capsules as drug carriers, we first investigated their morphology and stability properties under physiological conditions using several complementary techniques (ITC, QCM-D, ζ -potential measurements, microscopy techniques,). These properties were compared in the first section of the chapter.

Since disruption of the multilayer was observed for some capsules, we investigated routes to improve the stability of the shell, based on its chemical cross-linking. These chemical modifications are described in the second section of this chapter.

Finally, having the established feasibility to obtain stable capsules from different polycationic partners, we report in the two last sections the permeability and enzymatic degradation properties of the nanoshells.

4.3. Results and discussion

4.3.1. Synthesis of capsules based on HA, role of the polycationic partner on the morphology and stability properties

4.3.1.1. Analysis of HA/PAH, HA/PLL and HA/QCH complexation in the bulk and on planar surface

- **Isothermal Titration Calorimetry (ITC)**

Isothermal titration microcalorimetry experiments were performed on HA/PAH, HA/PLL and HA/CH systems. From this technique, correlation between the film build-up and the complexation heat was found⁹. Indeed, it has been reported that in the case of multilayer film build-up, strong interactions between polyelectrolytes lead to linear growth of the film with the number of deposited layers whereas weak interactions make exponentially growing films. Spontaneous complexation between two oppositely charged polyelectrolytes such as PSS/PAH is accompanied by negative value of Gibbs free energy change (ΔG). ΔG change is related to the enthalpy change (ΔH), entropy change (ΔS), and temperature (T), according to:

$$\Delta G = \Delta H - T\Delta S \quad \text{eq. IV.1}$$

ΔG is negative for any interaction for which ΔH is negative and ΔS is positive. Since the polyanion/polycation interactions are usually accompanied by an entropy increase, only enthalpy changes are considered. When the polyanion/polycation complexation process is exothermic (negative ΔH), the complex is expected to be “strong” with a tendency to form linearly growing LbL film. On the other hand, when the polyanion/ polycation complexation process is endothermic (positive ΔH), the complex should be much weaker. This is expected in the case of exponentially growing films⁹.

In our studies we performed isothermal titration calorimetry experiments on different systems:

- HA having two different M_w (HA820 and HA200) and PAH
- HA820/PLL and HA820/QCH

Since the ionic strength can influence the complexation process, the experiment for each system was carried out in 1) 10mM TRIS buffer and 2) 10mM TRIS + 0.15 M NaCl. An example of experimental data is given in **Figure 4.1**.

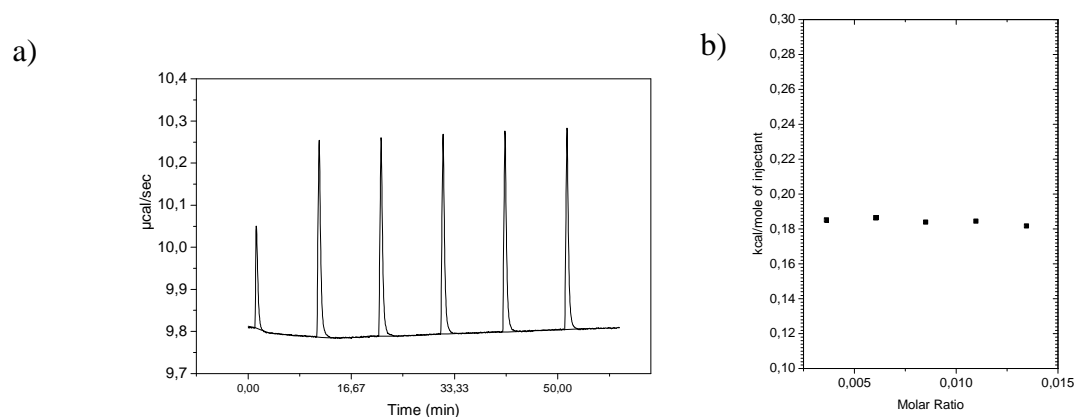


Figure 4.1. Calorimetric titration of a PAH solution ($C_p=2\text{g/L}$ or 21.3 mM) in TRIS buffer (pH 7.4) containing 0.15M NaCl at 25°C . Raw ITC data (a) and integrated values of the enthalpy changes following injection of HA ($C_p=3\text{g/L}$ or 7.4 mM) (b).

Each peak represents a heat change resulting from the injection of a small volume of HA solution ($10\mu\text{L}$) into the ITC reaction cell containing the PAH solution. The amount of heat absorbed or released is in direct proportion to the amount of binding. The plot of the heat from each injection against the ratio of introduced HA solution can be obtained. In our case the amount of added polyanion is low (the molar ratio of added polyanion over the available polycation is ~ 0.03 after 5 injections) which ensures a large excess of polycation and free charged units to interact with them upon further polyanion injection. This allows us to make the assumption that all the HA chains have reacted with the amino groups of PAH (PLL or QCH). For precision data, we took into account the heat of dilution. The values for each system are given in **Table 4.2**.

Table 4.2. Values of enthalpy changes for polyanion/polycation complexation measured by ITC. Concentrations: HA200=3g/L (7.4mM), HA820=3g/L (7.4mM) ; PAH=2g/L (21.3mM), PLL=2g/L (10mM), QCH=5 g/L (23mM) dissolved in TRIS or TRIS + NaCl.

Polyelectrolyte combination	Conditions	Global enthalpy (kJ/mol)	Dilution enthalpy (kJ/mol)	Complexation enthalpy (kJ/mol)
HA820-PAH	25°C, TRIS 10mM, pH=7,4	2.292	-0.22	2.512
HA820-PAH	25°C, NaCl 150mM, pH=7,4	0.827	-0.21	1,037
HA820-PLL	25°C, TRIS 10mM, pH=7,4	2.76	-0.22	2.98
HA820-PLL	25°C, NaCl 150mM, pH=7,4	1.306	-0.21	1.516
HA820-CHI	25°C, TRIS 10mM, pH=7,4	1.565	-0.22	1.785
HA820-CHI	25°C, NaCl 150mM, pH=7,4	0.816	-0.21	1.026
HA200-PAH	25°C, TRIS 10mM, pH=7,4	2.503	-0.23	2.733
HA200-PAH	25°C, NaCl 150mM, pH=7,4	1.957	-0.003	1.96

As illustrated by **Figure 4.2** the positive values of ΔH obtained from complexation between HA and the polycations confirm weak interactions between the polyelectrolytes.

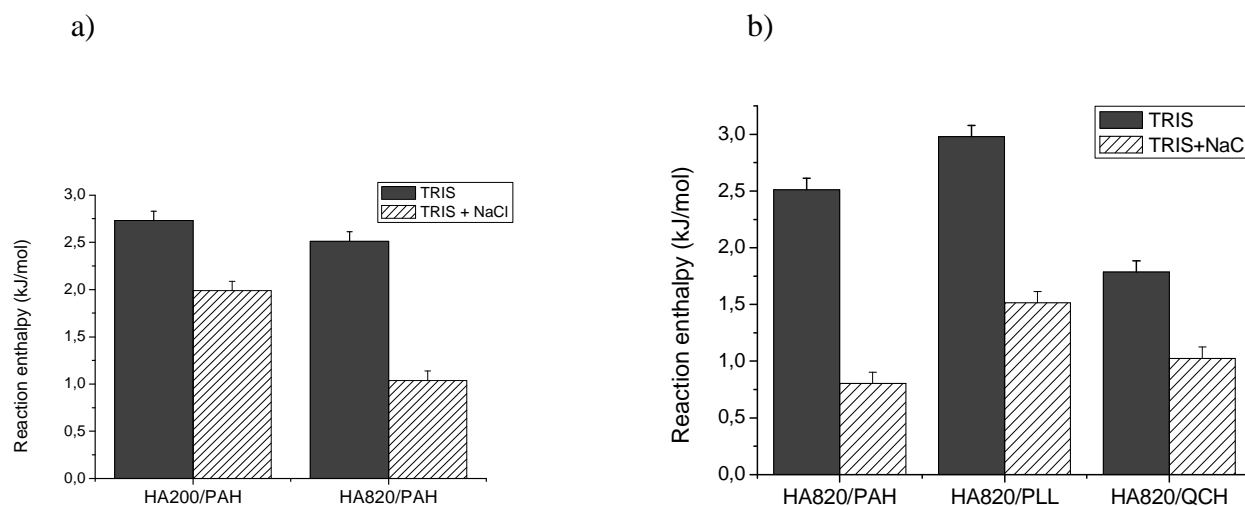


Figure 4.2. Values of complexation enthalpy for HA200/PAH and HA820/PAH (a) and, HA820/PAH; HA820/PLL and HA820/CH (b) in TRIS buffer (grey columns)) and TRIS + 0.15M NaCl (white patterned columns). The error of subsequent measurements for one sample was in the range of 6 %.

In comparison, the literature data of the PSS/PAH heat complexation show an exothermic process suggesting strong electrostatic interactions⁹. However, we can observe some differences in enthalpy changes between the studied systems.

First, we can notice some discrepancies between the enthalpy changes, depending on the Mw of HA (**Figure 4.2.a**). With HA820, we obtained lower and energetically more favourable values than with HA200. This difference is much higher for the reaction performed in aqueous 0.15 M NaCl. **Figure 4.2.b** compares the enthalpy variation values for the different HA/polycation systems. In TRIS buffer, the lowest energy of complexation process was observed for HA/QCH complexation, whereas the highest for HA/PLL combination (HA/QCH < HA/PAH < HA/PLL). In the presence of salt, the HA/PLL appears to be the weakest complex with respect to HA/PAH and HA/QCH, which show similar values.

- **Quartz Crystal Microbalance with Dissipation monitoring (QCM-D)**

As ITC indicated weak interactions between polyelectrolyte partners, QCM-D experiments were performed to check the multilayer assembly formation.

Following the optimal conditions described in Chapter 3, the polyanion (HA820) and polycation (PAH, PLL or QCH) were alternatively deposited at concentrations of 5 and 2g/L, respectively.

Figure 4.3 displays the evolution of the frequency shift $\Delta f/\nu$ during the film build-up. Different harmonics 5, 15, 25, and 35 MHz (fundamental and three overtones) corresponding to ν equal to 1, 3, 5, and 7, respectively, were recorded. Deposition of the subsequent layers on the gold electrodes results in the decrease of the $\Delta f/\nu$ for all investigated harmonics. These variations are denoted as $-\Delta f/\nu$ and for third, fifth and seventh harmonics presented below.

The frequency changes ($-\Delta f$) decrease with each polycation or HA injection, indicating that adsorption of additional mass occurred. When rinsing with buffer, the observed small variation of Δf toward higher negative values could be attributed to additional complexation of residual HA staying in the tube. The high concentration of HA leading to a viscous solution causes adhesion onto the tube wall and hinders the free flow. The early portion of rinsing buffer contains the remaining HA.

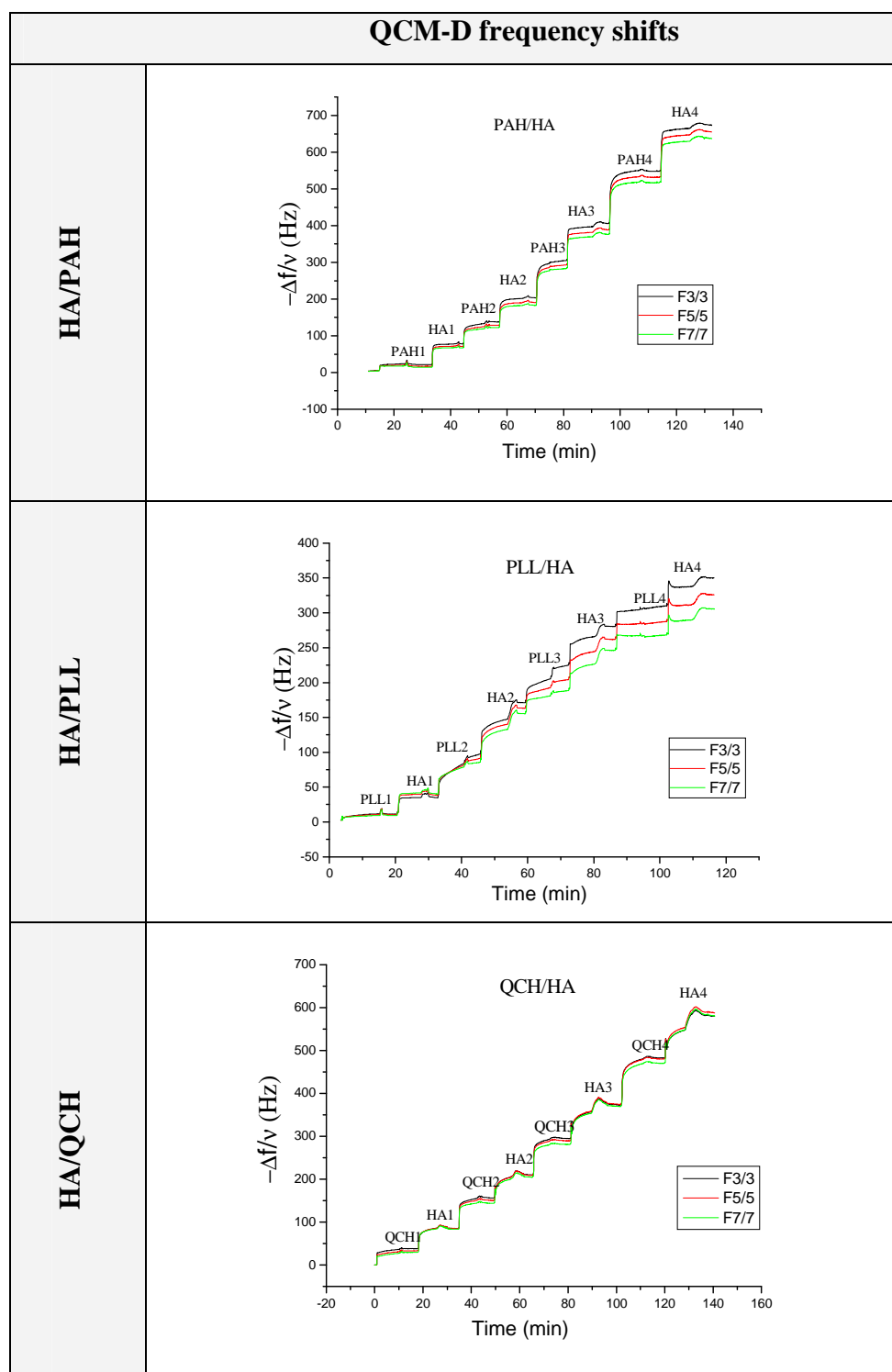


Figure 4.3. QCM-D frequency shifts $-\Delta f/\nu$ during the alternate deposition PAH/HA, PLL/HA and QCH/HA multilayers obtained at harmonics 15 MHz (black line) , 25 MHz (red line) and 35 MHz (green line) as a function of time. HA820 at concentration 5g/L and polycations at concentration 2g/L were used for solution preparation.

The changes of the $-\Delta f/\nu$ as a function of time, for the HA/PAH, HA/PLL and HA/QCH films build-up from 4 bilayers, exhibited different features. To have clear illustration of the film

growth as a function of deposited layers, we show the points of QCM frequency shifts $-\Delta f/\nu$ after polymer deposition and rinsing step (**Figure 4.4**).

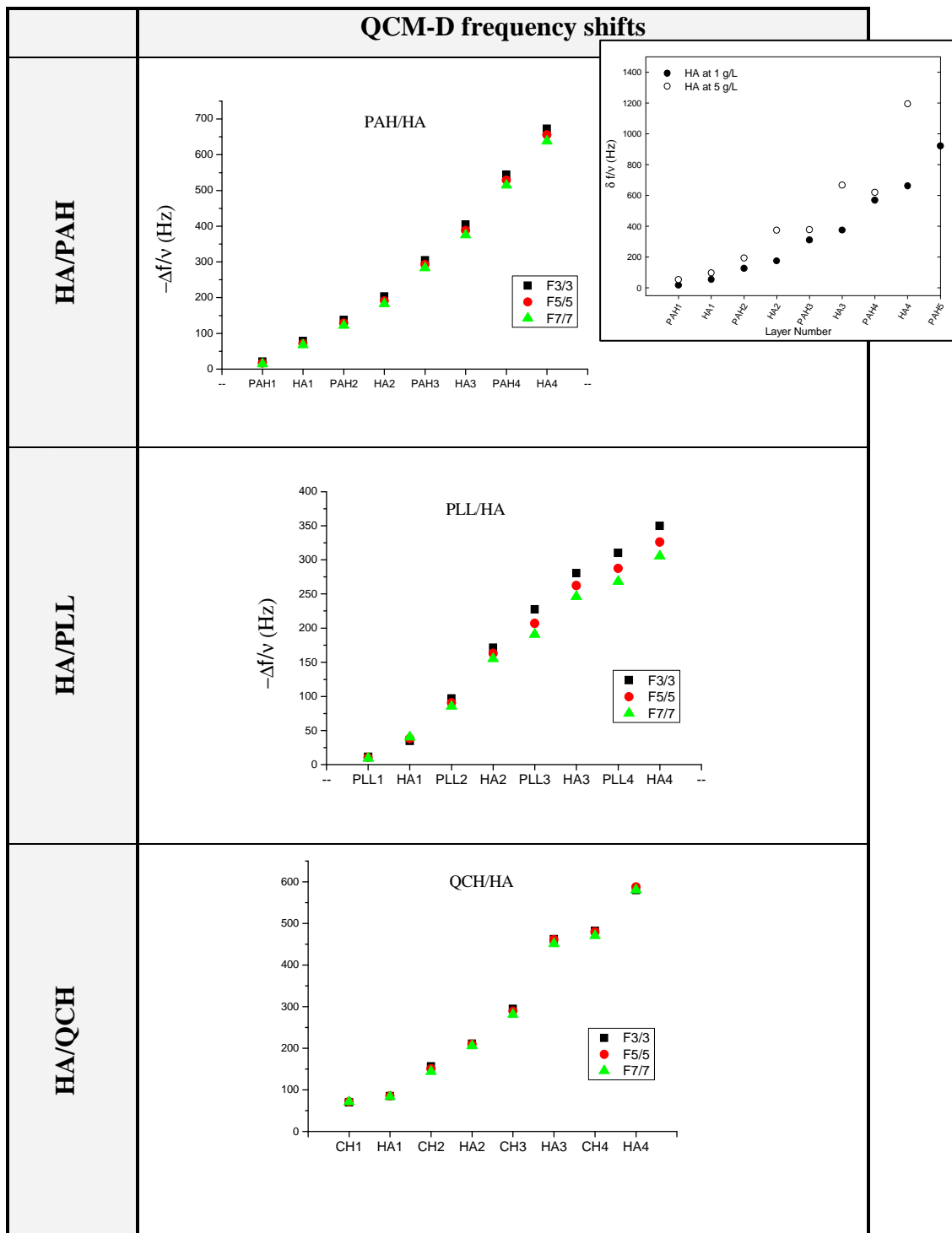


Figure 4.4. QCM-D frequency shift $-\Delta f/\nu$ during the alternate deposition of PAH/HA, PLL/HA and QCH/HA obtained at harmonics 15 MHz (black squares), 25 MHz (red circles) and 35 MHz (green triangles) as a function of deposited layer, the points demonstrate the polyelectrolyte deposition after rinsing step. HA820 and the polycation were used at a concentration of 5g/L and 2g/L, respectively. Inset compares the PAH/HA film growth using HA200 at 1 g/L or 5 g/L.

An exponential growth of HA/PAH film can be reasonably assumed, whereas the HA/PLL and HA/QCH systems behave differently. The alternative adsorption of HA and PLL layers shows irregular growth, with lower growth starting from 3rd bilayer. Such behaviour of HA/PLL film build-up was already reported¹⁰. In the case of the HA/QCH system, the assembly seems to grow rather linearly with the number of layers. These results could also be illustrated by **Figure 4.5** showing the film thickness as the function of the number of layers. The 4 bilayers of HA/PAH lead to a thickness of ~140nm, similarly to HA/QCH (~ 130nm). On the other hand, the HA/PLL assembly is characterized by lower thickness (~100 nm).

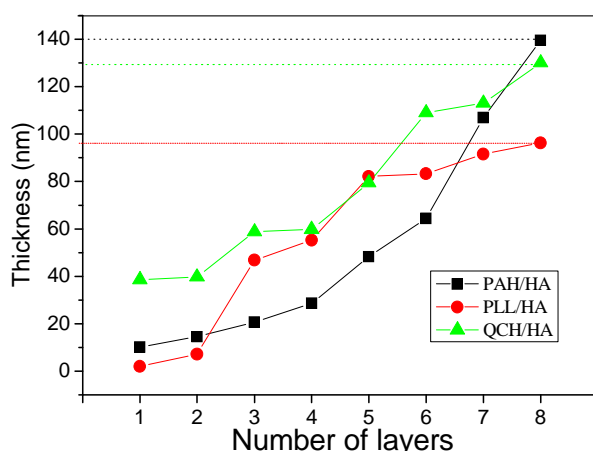


Figure 4.5. Film thickness as a function of the number of layers estimated by QCM-D. Deposition of layers are represented by symbols: PAH/HA (black squares), PLL/HA (red circles), and QCH/HA (green triangles).

The differences between our results and thickness values reported in the literature for (HA/PAH)_{4.5} (~45nm¹⁰), (HA/PLL)₅ (from 20 to 40nm¹⁰⁻¹²) or (HA/CH)₈ (150-200nm¹³) can be attributed to different conditions for the preparation of capsules. The authors usually use lower concentrations of HA (below 2g/L). As described in Chapter 3, the polysaccharide concentration has a large impact on the film formation. For a HA concentration of 5g/L, the film growth was more rapid than that for a HA concentration of 1g/L (**Figure 4.4**, inset).

In conclusion, QCM-D analysis allowed us to observe the multilayer build-up from HA820 with the three different PAH, PLL, QCH polycations. Rapid growth of film thickness due to the high HA concentration was observed in all studied films. However the film growth process was found to depend closely on the nature of polycation.

4.3.1.2. Synthesis of HA/PAH, HA/PLL and HA/QCH hollow capsules and their characterization

a) Build-up of multilayer assembly on CaCO_3 core

For the construction of the multilayer assembly from HA and the different polycations on calcium carbonate template, we used the optimized conditions established for the synthesis of HA/PAH capsules.

Figure 4.6 illustrates the changes of the ζ -potential values of the particle suspensions during the alternative adsorption of HA and polycations.

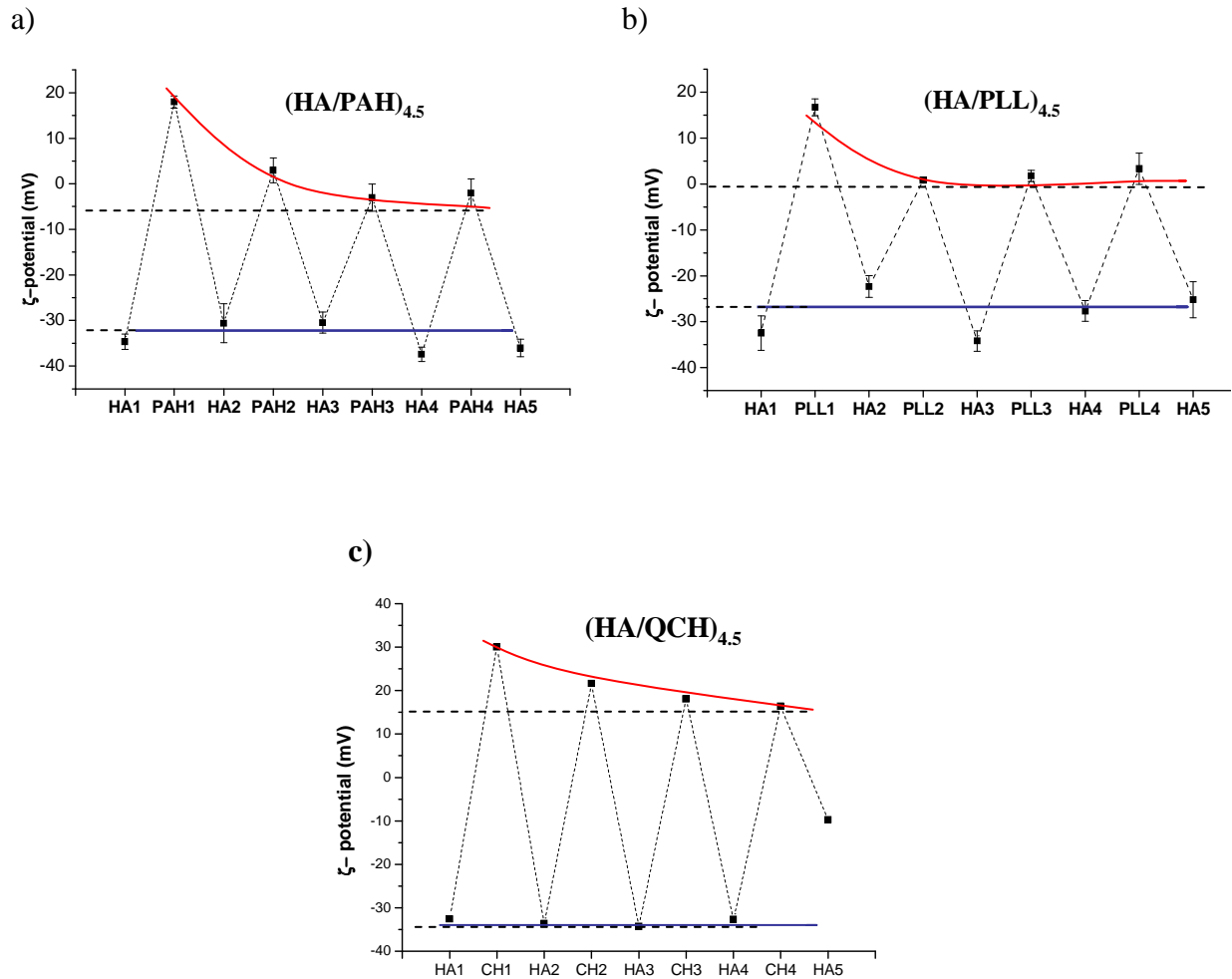


Figure 4.6. Variation of the ζ -potential value as a function of layer number during LbL coating of CaCO_3 particles: a) HA/PAH, b) HA/PLL and c) HA/QCH bilayers.

The first deposited HA polyelectrolyte layer is characterized by a low (~ -30 mV) potential. The adsorption of polycations turns the potential sign to +20 for PAH and PLL, and +30 mV for QCH. Deposition of the next HA layer results in a zeta potential value again around -30mV in all three cases. However, the subsequent adsorption of the polycations shows that the value increases but not so strongly as initially (the values are slightly positive or close to zero). PAH, PLL or QCH exceed the minimum amount needed to neutralize the charges of HA islets which are formed at early stage of the LbL film formation. These individual islands interconnect and provide an increased surface area that may facilitate polycation diffusion into the whole film¹⁴. Polycation chains together with their counterions travel in and out of the multilayer without forming complex bearing the negative charge of Cl^- . In consequence, the zeta potential value of covered particle is low.

The constant positive value of QCH-coated particles near to 20 mV suggests a different behaviour of QCH chains compared to PAH and PLL. QCH is a semi-rigid polymer with a high M_w 180×10^3 g/mol compared to PLL and PAH (15×10^3 - 30×10^3 and 70×10^3 g/mol, respectively). These macromolecular features may limit diffusion of the cationic polysaccharide within the multilayer assembly.

The changes of zeta potential of coated HA200/PAH particles demonstrated in Chapter 3 also show strong negative and slightly positive values for HA and PAH deposited layers respectively.

In **Figure 4.7**, a model of chain behaviour in the multilayer film is presented.

The penetration of the flexible low M_w PAH or PLL into the HA layer is relatively easy, the contrary is observed for the high M_w and semi-rigid QCH.

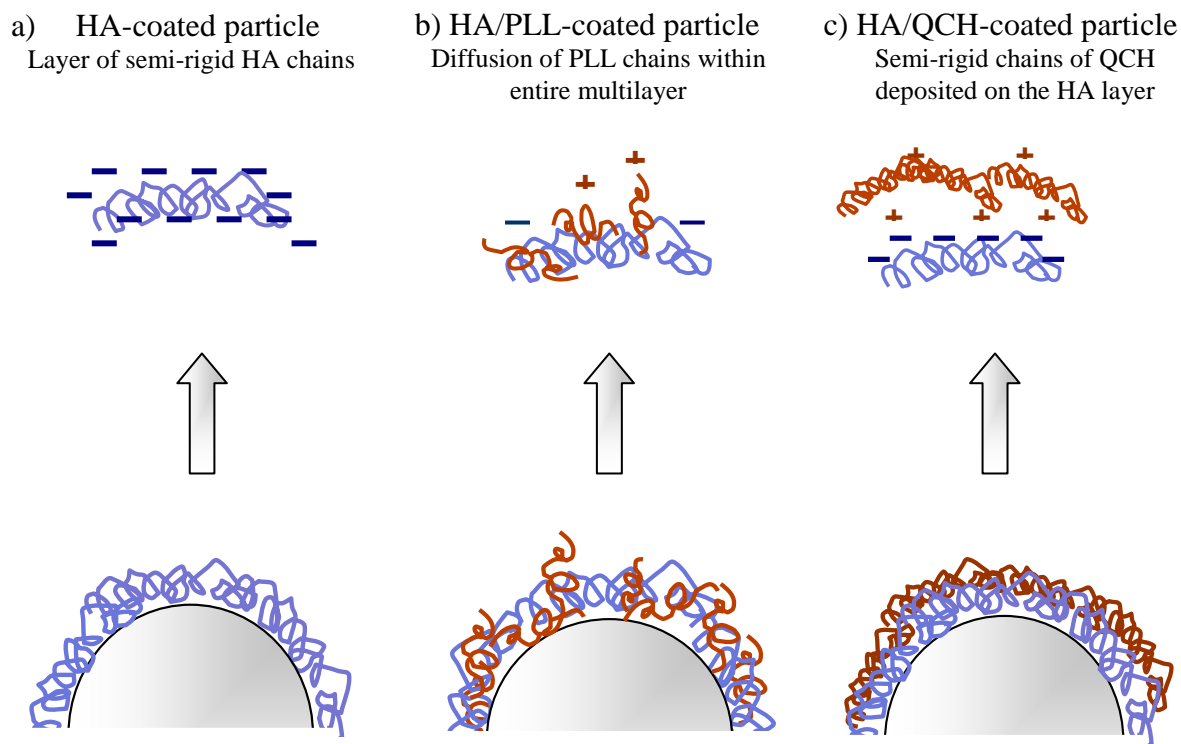


Figure 4.7. Schematic representation of multilayer build-up using HA as a polyanion. (a) The semi-rigid character and entangled chains of HA ($M_w = 820 \times 10^3 \text{ g/mol}$) promote the formation of a thick and cohesive layer; (b) flexible small synthetic polyelectrolytes (PAH and PLL) can diffuse easily into the porous layer of HA; (c) semi-rigid high Mw QCH chains ($M_w = 180 \times 10^3 \text{ g/mol}$) can not penetrate into the HA layer.

The CaCO_3 particles coated by HA/PAH, HA/PLL and HA/QCH films composed of 2.5, 4.5, 6.5 bilayers together with the native CaCO_3 particles are presented below (**Figure 4.8**).

Comparison of the surface of the native CaCO_3 particles with that of the particles coated by HA/PAH, HA/PLL or HA/QCH multilayers demonstrates good coating of the porous carbonate core in all cases, starting from 2.5 bilayers.

Films made from HA820 at a concentration of 5g/L successfully covers the pores whatever the polycation used.

Both above techniques (ζ -potential measurements and high resolution-SEM) provided evidence of film build-up on the carbonate surface.

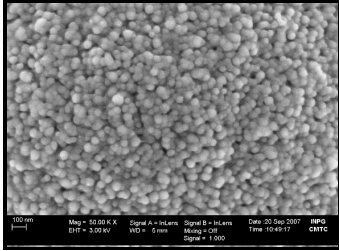
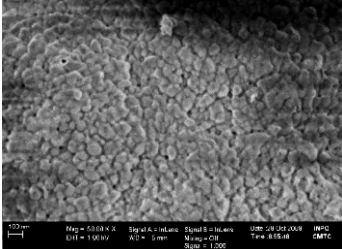
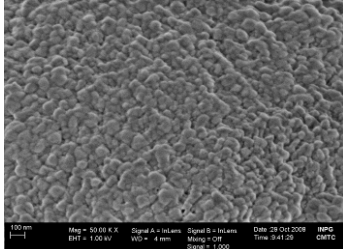
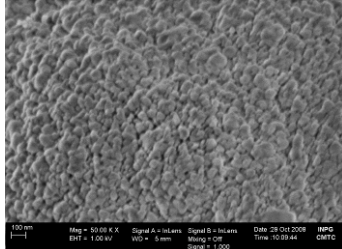
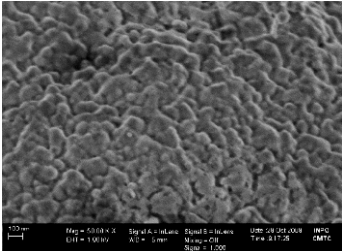
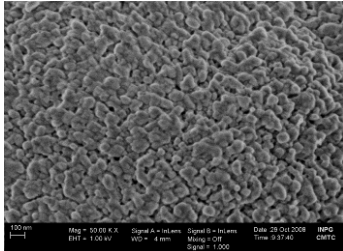
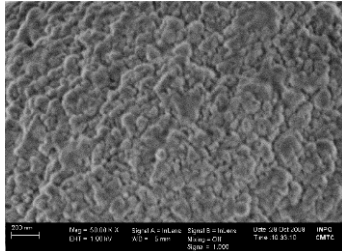
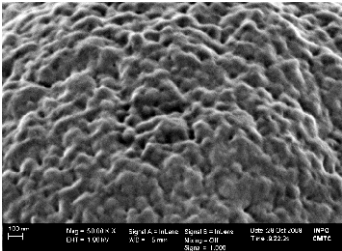
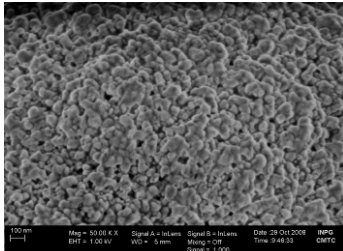
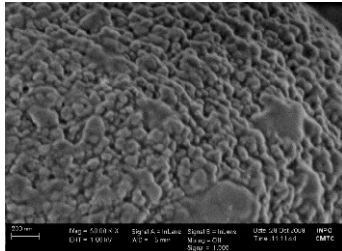
Number of bilayers	CaCO ₃ particle surface		
0	 100nm		
	HA/PAH	HA/PLL	HA/QCH
2.5	 100 nm	 100 nm	 100 nm
4.5	 100 nm	 100 nm	 200 nm
6.5	 100 nm	 100 nm	 200 nm

Figure 4.8. CaCO₃ particles alone and with n deposited layers of HA820 ($c = 5\text{g/L}$) and different polycations: PAH ($M_w = 70 \times 10^3 \text{ g/mol}$), PLL ($M_w = 15 \times 10^3 - 30 \times 10^3 \text{ g/mol}$), QCH ($M_w = 180 \times 10^3 \text{ g/mol}$) at a concentration = 2g/L each. The first and outermost deposited layer is HA.

b) Characterization of hollow capsules

- **Structural characterization by Fourier Transform Infrared Spectroscopy with Attenuated Total Reflectance (FTIR-ATR)**

As described in Chapter 3 in the complementary results, EDTA (0.1M, pH 7.4) was used to remove the core from the HA/PLL and HA/CH coating under mild conditions.

The composition of the hollow capsules was analysed by FTIR-ATR spectroscopy after direct deposition of freeze-dried capsules on a diamond crystal. **Figure 4.9** compares the spectra of HA/PAH, HA/PLL and HA/QCH capsules with those of initial polymer alone.

In the spectra of hollow HA/PAH, HA/PLL and HA/CH capsules, three main regions can be distinguished: the peak between 950 and 1200 cm^{-1} corresponding to the skeletal vibration of the saccharide units^{15,16}, the intense peak at 1550 - 1680 cm^{-1} which corresponds to the amide I and amide II bands of HA together with those of QCH¹⁵ or PLL¹⁷.

The symmetric stretch of -COO^- at 1400 cm^{-1} belonging to HA can be clearly identified in all the spectra confirming the successful formation of shells based on HA/polycation complexation.

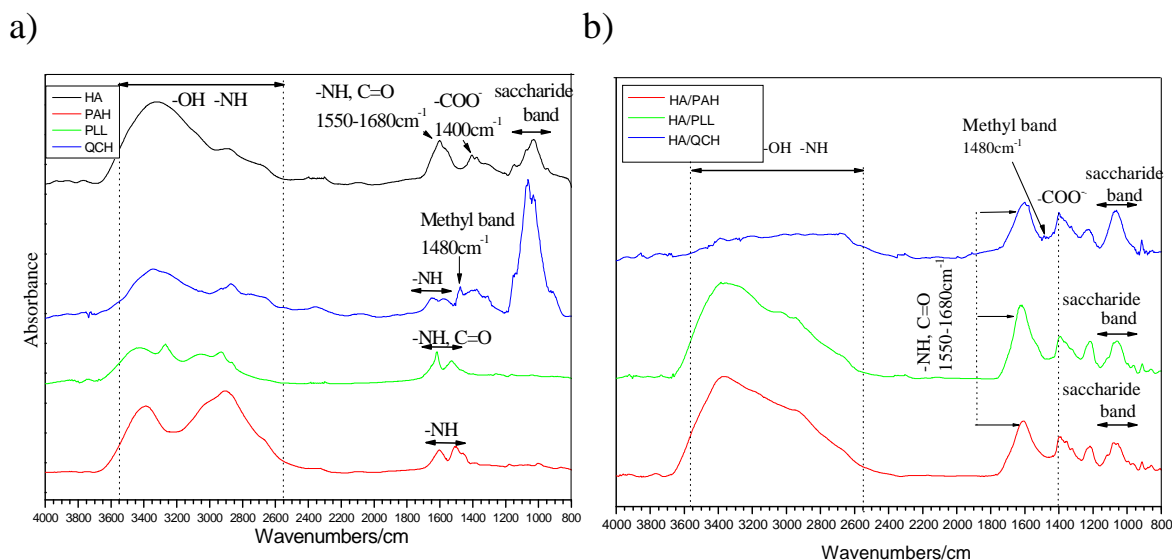


Figure 4.9. FTIR-ATR spectra of individual polymers: HA (black), PAH (red), PLL (green), QCH (blue) (a), and HA/PAH (red), HA/PLL (green) and HA/QCH (blue) capsules (b).

• **Morphology of hollow capsules**

Morphology of capsules was observed by SEM (**Figure 4.10**) and CLSM (**Figure 4.11**) techniques in the dried state and in aqueous solution, respectively.

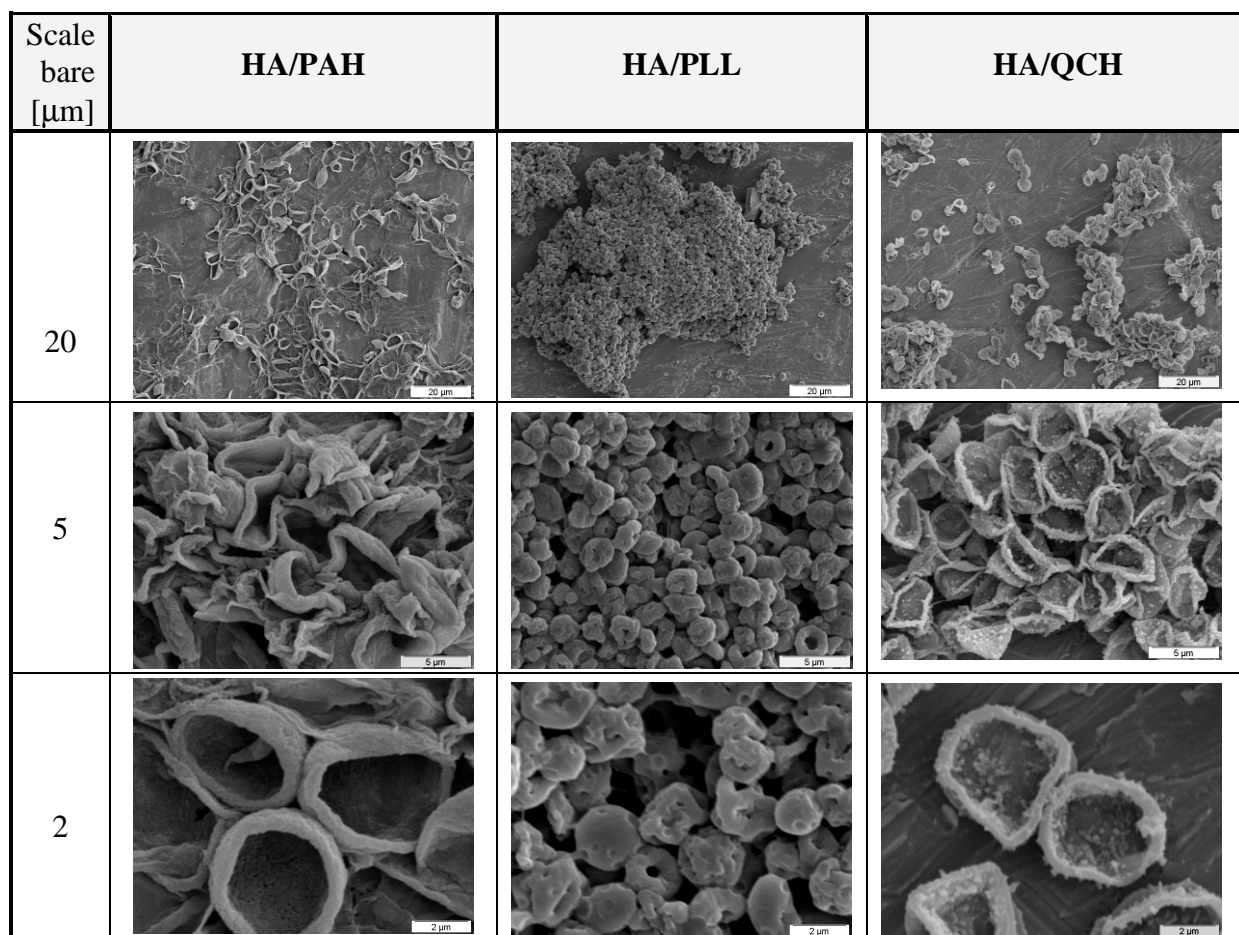


Figure 4.10. SEM images of dried HA/PAH, HA/PLL and HA/QCH capsules. All multilayers were composed of 4.5 bilayers (HA occurred as the first and the last deposited layer). Scale bar: 20, 5 and 2 μm , respectively.

As already discussed in Chapter 3, HA/PAH capsules are collapsed after drying. The diameter is about 5 μm which corresponds to the core size. The same conclusion can be drawn for the HA/QCH capsules although some irregularities (grains) on the shell surface can be observed. Such small grains were already observed on the wall surfaces of (PSS/PDADMAC)₅¹⁸, attributed to local reorganization of chains as a result of water evaporation. In contrast, the HA/PLL capsules appear to be much smaller (~2.5 μm), which can be explained by the shrinkage of the capsules as suggested by the CLSM image (**Figure 4.11**). All capsules

prepared in this work showed a tendency to aggregate. This was more pronounced in the case of HA/PLL shells (**Figure 4.10**).

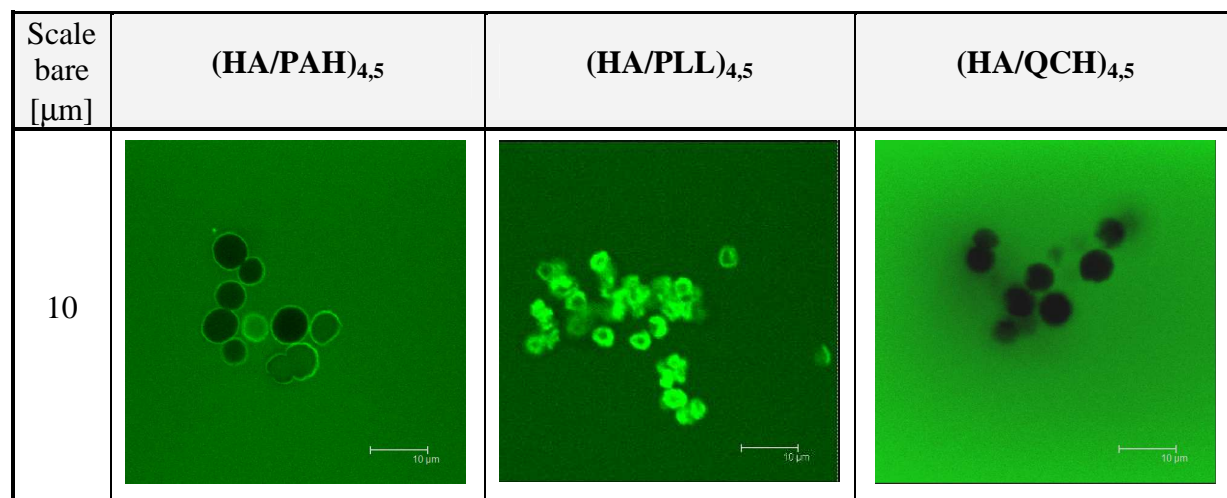


Figure 4.11. CLSM images of HA/PAH, HA/PLL and HA/QCH capsules as an aqueous suspension. The high intensity of green colour is the effect of fluorescent properties of dextran^{FTIC} ($M_w = 4 \times 10^3 \text{ g/mol}$) solution. FITC labelled dextran is adsorbed within the shells at high concentration allowing visualisation of capsules.

In order to get additional information about the multilayer shells, AFM experiments on dried capsules were performed. The folded flat topography induced by the collapse of the capsules during the drying process allows the measurements of the wall thickness. From its profile, the difference between the background and the lowest region of the shells gives the wall thickness (**Figure 4.12**).

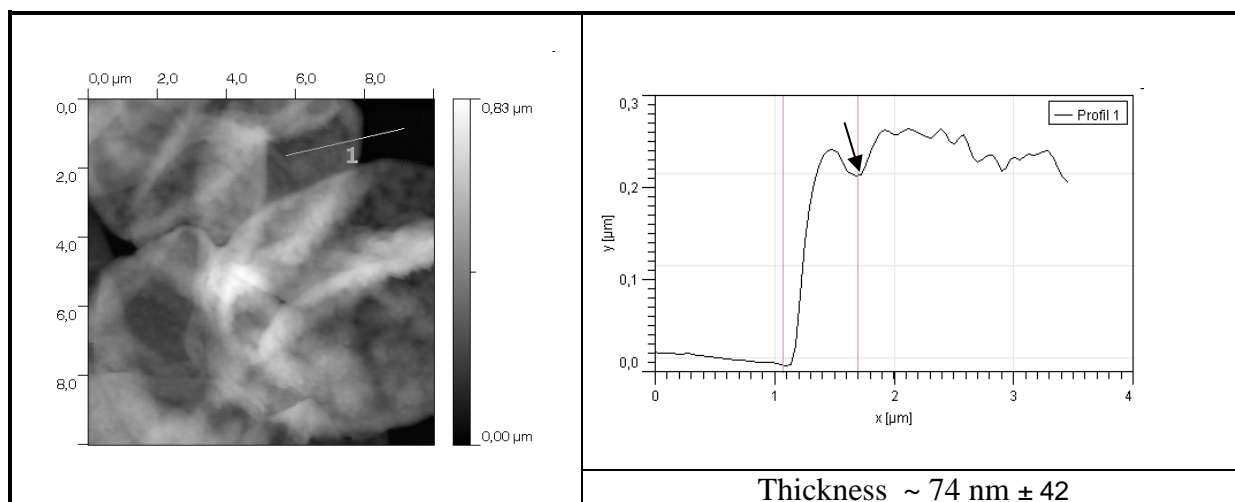


Figure 4.12. AFM image of a dried HA/PAH capsules with corresponding profile.

The values of the wall thickness for all capsules are given in **Table 4.3**. For comparison, the corresponding thicknesses derived from the QCM-D studies are presented.

Table 4.3. Values of the wall thickness of dried capsules determined by AFM and planar film thickness derived from QCM-D analysis. Capsules contain 9 layers and the planar films 8 layers.

Multilayer	Diameter	Thickness	
		AFM	QCM-D
HA/PAH	~5 μm	74 nm \pm 42	140 nm
HA/PLL	~2.5 μm	Not measured	100 nm
HA/QCH	~4 μm	160nm \pm 40	130 nm

The AFM image measurements were performed in the dried state, whereas QCM-D studies provided values of film thickness in the swollen state.

While the HA/PAH and HA/QCH planar films have almost the same thickness (~140 and 130nm), the HA/PLL assembly is characterized by a lower value (~100 nm). In the dried state, the HA/PAH capsules show thinner shells (~74 nm) than HA/QCH (~160 nm). The drying can induce strong interactions between HA and PAH via hydrogen bonding, resulting in a thin film. Such an effect may be limited for the HA/QCH capsules which are made of two semi-rigid polymers. As mentioned above, it was not possible to measure the HA/PLL shell thickness due to the shrunken structure of the capsules and the lack of collapsed flat domains (minimums) necessary for thickness estimation. The shrinkage reflects poor mechanical properties of the HA/PLL shell, which may be a consequence of the weak complex formed between HA and PLL. In such conditions, it can be assumed that EDTA can behave as a competitive agent of HA and act as a “plasticizer” between polymer chains.

The high values of HA/PAH and HA/QCH capsule thickness obtained by AFM after drying may be surprising but it can be partially explained by the porous structure of the CaCO_3 surface. The thickness of the film on porous surfaces should be higher than on the smooth surface of the QCM crystal as illustrated by **Figure 4.13**. Pores favour the adsorption of large amounts of polymer, higher than on a smooth surface¹⁹.

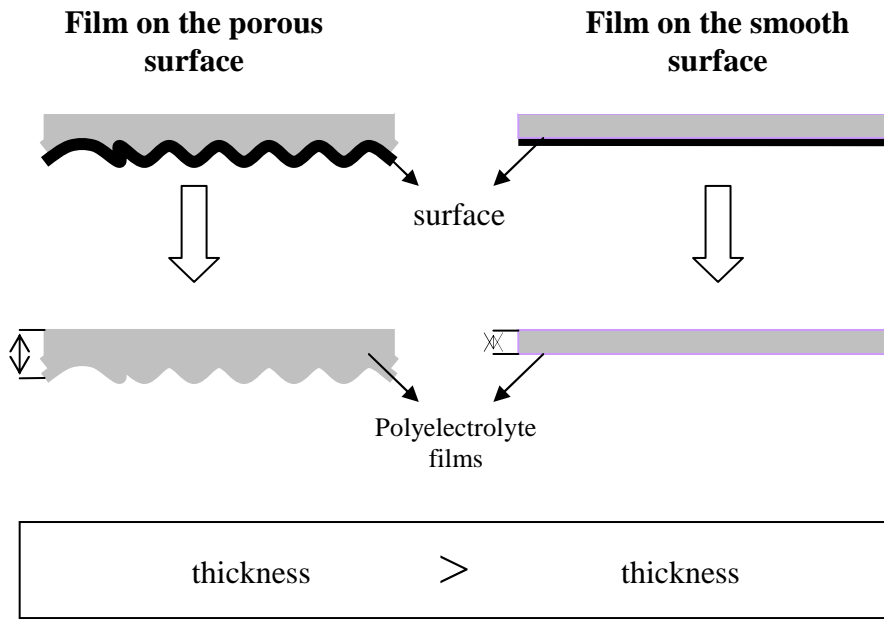


Figure 4.13. Formation of the polyelectrolyte film on porous (a) and smooth (b) surface.

The thickness of synthetic (PAH/PSS)₄ multilayers deposited on MnCO₃, CdCO₃ and CaCO₃ particles is equal to 15, 14 and 30nm, respectively¹⁹. Capsules prepared on smoother surface (MnCO₃ or CdCO₃) have thinner walls than those fabricated on very porous CaCO₃ particles, where layers are formed not only on the top of the particle, but also in the pores and inner cavities. High discrepancy in thickness between PAH/PSS shells¹⁹ and HA/polycation shells¹⁹ fabricated in our work can arise from several parameters such as: the semi-rigid nature of polysaccharides, their highly hydrated state and the specific conditions used for shell formation (high Mw and high concentration of HA).

Regarding the thickness values of multilayer films made of polysaccharides reported in the literature, they appear to be in the range of 40-200nm, depending on the polyelectrolytes used, number of layers and conditions of multilayer formation, see **Table 4.4**.

In conclusion, the hollow HA/PAH and HA/QCH capsules show a round shape, with a diameter of ~5μm and a wall thickness of 74 and 160nm, respectively. HA/PLL shells shrink, leading to a diameter of ~2.5 μm. The disrupted structure of the HA/PLL wall may be due to EDTA interference into the multilayer structure during core dissolution. The HA/PAH and HA/QCH complexes are strong enough to keep their integrity. HA/PAH walls exhibit a relatively smooth surface contrary to HA/QCH coated by grains. In order to overcome these problems, shell cross-linking was then investigated.

Table 4.4. Literature data of the film thicknesses made from polysaccharides deposited on planar surface except (CH/Dext)₂₀ deposited on the ibuprofen particles.

Multilayer	Method	Thickness
(HA/PAH) ₅	Ellipsometry Silicon wafers	~ 40nm ²⁰
(PLL/ALG) ₂	Ellipsometry Silicon wafers	~80 nm ²¹
(CH/Dext) ₂₀	Single particle Light Scattering Ibuprofen crystals	~40nm ²²
(HA/PAH) ₄	QCM-D	~40nm ¹⁰
(HA/PLL) ₄	QCM-D Elipsometry	~40nm ¹² , ~20nm ^{10,12}
(HA/CH) ₈	QCM-D	150-200nm ¹³

4.3.2. Cross-linking of the microcapsule shells: improvement of morphology and stability

a) Conditions of cross-linking and FTIR-ATR analysis of modified shells

The capsule shells were cross-linked using the amino-acid coupling reported in Chapter 3. The carboxylate groups of HA are converted into activated esters by reaction with EDC diimide group, which can then be reacted with the amine groups of the polycation to form amide bonds. This method of cross-linking for HA/PLL, HA/QCH, and HA/amine-modified HA multilayers on planar surface has been studied in detail^{10,11,15,17,23-27}. Herein, the elasticity, biodegradability, cell adhesive properties, stability of cross-linked planar films compared to non cross-linked films were analyzed. For capsules, EDC was applied to cross-link PAH/PAA shells²⁸.

In this study, we investigated the effect of cross-linking on the HA/PAH, HA/PLL and HA/QCH capsule morphology.

Reactions were performed on HA/polycation multilayer deposited on CaCO₃ particles in aqueous conditions at pH 6.5. This pH is favourable to keep complex integrity, especially in the early reaction step when the electrostatic interactions still play an important role on the multilayer integrity. The particles with deposited multilayers were incubated in freshly prepared EDC/NHS solutions overnight at room temperature followed by core dissolution (3

× 2h EDTA 0,1M) and washing with water. Considering that concentration of the coupling agent can influence the degree of cross-linking and hence, the mechanical properties of the film^{15,25}, different concentrations of EDC (50, 200 and 400mM) were tested from HA/PAH capsules. Structural and morphological changes after cross-linking were analysed by means of FTIR-ATR spectroscopy and SEM, respectively.

Figure 4.14 compares the FTIR-ATR spectra of the cross-linked and non cross-linked HA/PAH capsules, after treatment with EDC at different concentrations.

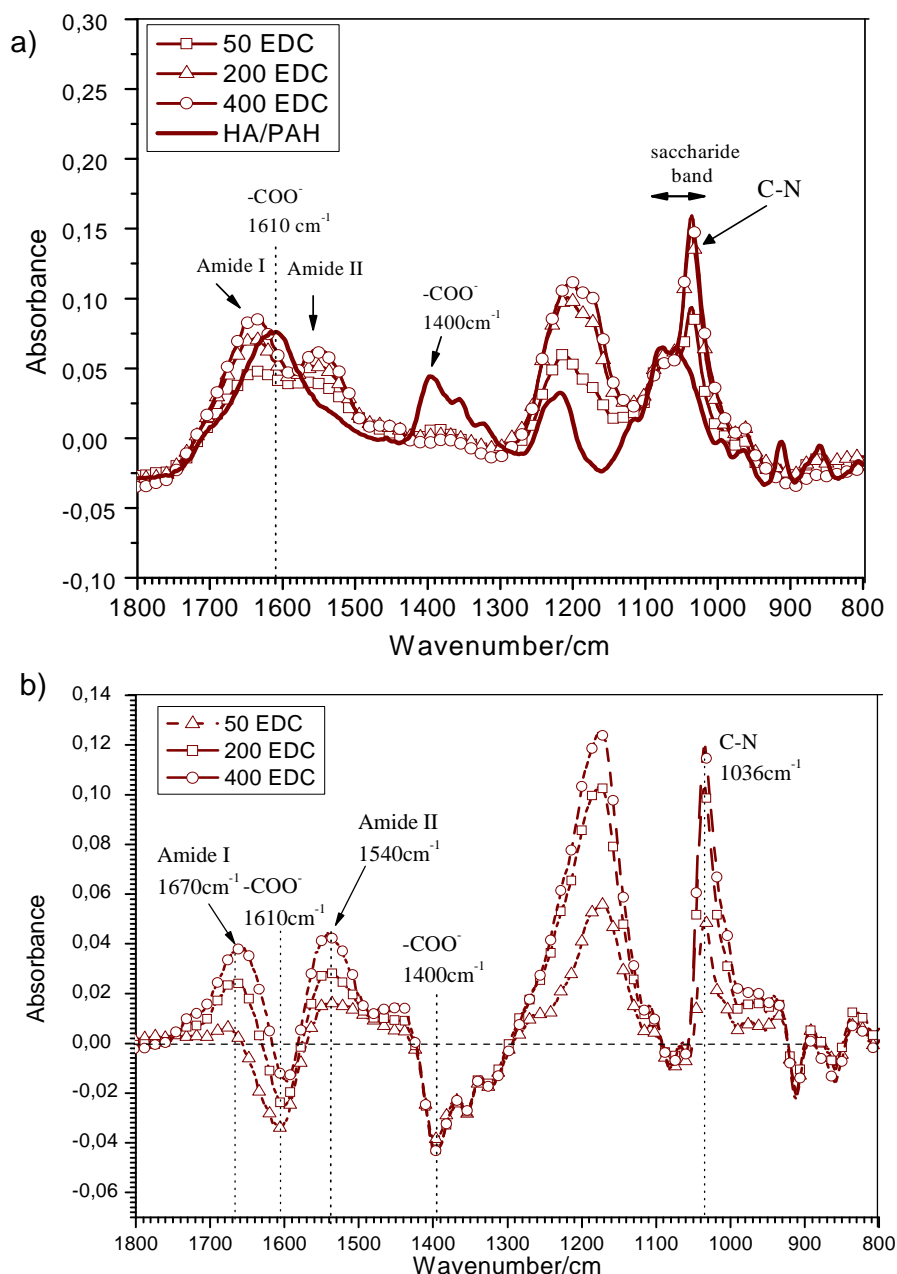


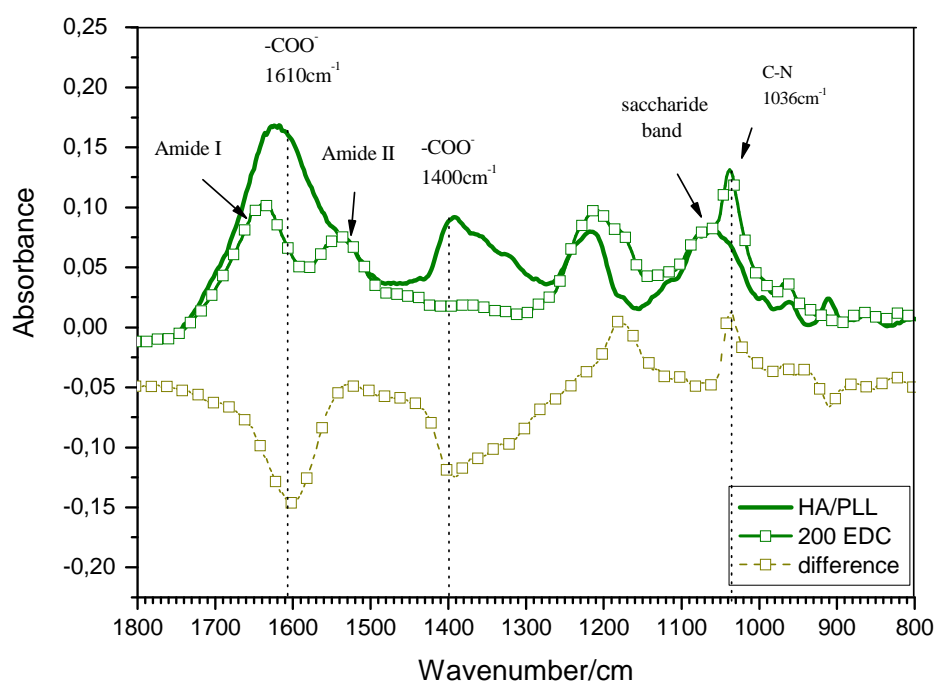
Figure 4.14. FTIR-ATR spectra of a) (HA/PAH)_{4,5} hollow dried capsules without cross-linking (red line) and cross-linked with 50mM EDC (triangles), 200mM EDC (squares), 400mM EDC (circles). The difference between the two spectra (before and after cross-linking) is represented b).

Compared to HA/PAH non cross-linked capsules, the intensity of the peaks attributed to COO^- symmetric ($\sim 1400\text{ cm}^{-1}$) and COO^- asymmetric stretch of HA ($\sim 1610\text{ cm}^{-1}$) significantly decreased after cross-linking (in all cases when cross-linking agent was used). The amide I and amide II bands at 1670 cm^{-1} and 1540 cm^{-1} respectively, emerged after covalent amide bond formation. It can be noticed, that these two peaks are better resolved when higher concentrations used, 200 and 400mM. The sharp peak at wavenumber 1036 cm^{-1} , attributed to C-N vibration¹⁶, increased also. The intensity of this band was found to be similar for the two higher EDC concentrations (200 and 400 mM) and approximately two times lower for the 50mM concentration.

Based on the assumption that the degree of cross-linking is nearly maximum for EDC concentration of 200mM, the HA/PLL and HA/QCH shells were cross-linked under these conditions.

Figure 4.15 compares the FTIR-ATR spectra of the HA/PLL and HA/CH cross-linked and non-cross-linked capsules.

a)



b)

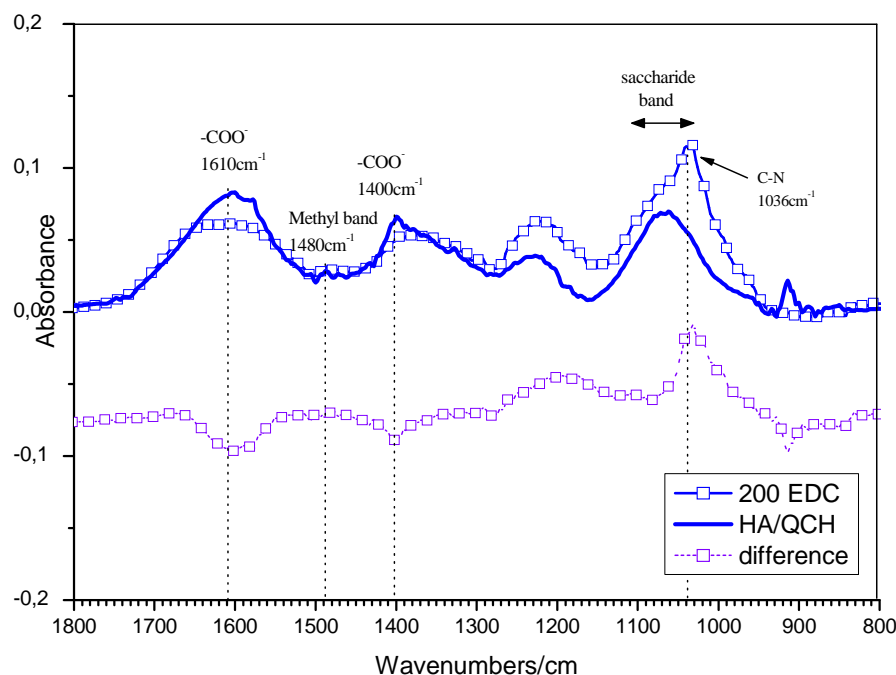


Figure 4.15. FTIR-ATR spectra of (HA/PLL)_{4,5} hollow dried capsules without cross-linking (thick line) and cross-linked with 200mM EDC (squares) (a), and (HA/QCH)_{4,5} hollow dried capsules without cross-linking (thick line) and cross-linked with 200mM EDC (squares) (b). Below, the differences between the two spectra (before and after cross-linking) are represented (dotted lines).

Several modifications of the FTIR-ATR spectrum of HA/PLL capsules after cross-linking could be observed. The peak of HA carboxylate decreased while the amide I and amide II bands emerged. These changes are less pronounced in the case of the HA/QCH capsules. Since the spectrum is the result of the association of two polysaccharides, some overlapping makes the identification of amide bands difficult. The differences between the spectra before and after cross-linking may be related to a low degree of cross-linking caused by quaternization of chitosan (DS=0.31). Additionally, as discussed above, the semi-rigid character and high Mw of QCH may hinder diffusion of the chains within the HA layer, which implies that some acid and amine groups may be not available for amide bond formation (**Figure 4.16**). However, in any case, the C-N band at 1036cm^{-1} can be seen, providing evidence of cross-linking.

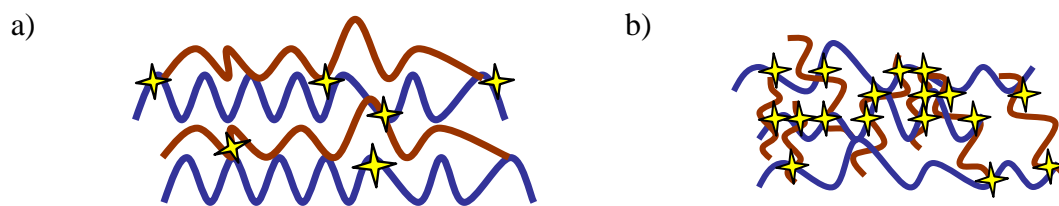


Figure 4.16. Structure of HA/QCH (a) and HA/PLL (b) multilayers with amide covalent bonds. Blue chains are from HA while the red ones are from polycations (QCH or PLL). Stars indicate the sites of amide bond formation.

b) Effect of cross-linking on the morphology of HA/PAH, HA/PLL and HA/QCH capsules

After cross-linking of the multilayers and core dissolution, the surface of the dried capsules was observed by SEM. Capsules were also observed in aqueous solution containing FITC labelled dextran as a fluorescent agent. **Figures 4.17** and **4.18** compare SEM and CLSM images of non cross-linked and cross-linked HA/PAH, HA/PLL and HA/QCH capsules. The SEM images show that cross-linked HA/PAH and HA/PLL capsules have smooth surface and a compact thin wall. Cross-linking process limits the swelling of the capsule shells. However, under such cross-linking conditions the “grains” observed on non cross-linked HA/QCH walls remained without changes.

All the cross-linked capsules presented in aqueous solution exhibit well formed spherical shapes with a size of $\sim 5\mu\text{m}$. Thus, the shrinkage of HA/PLL capsules could be prevented by cross-linking the multilayer assembly. One can also notice that cross-linked capsules have lower tendency to agglomerate than non cross-linked. The diffusion of fluorescent dye into cross-linked and non cross-linked capsules will be detailed in the next paragraph.

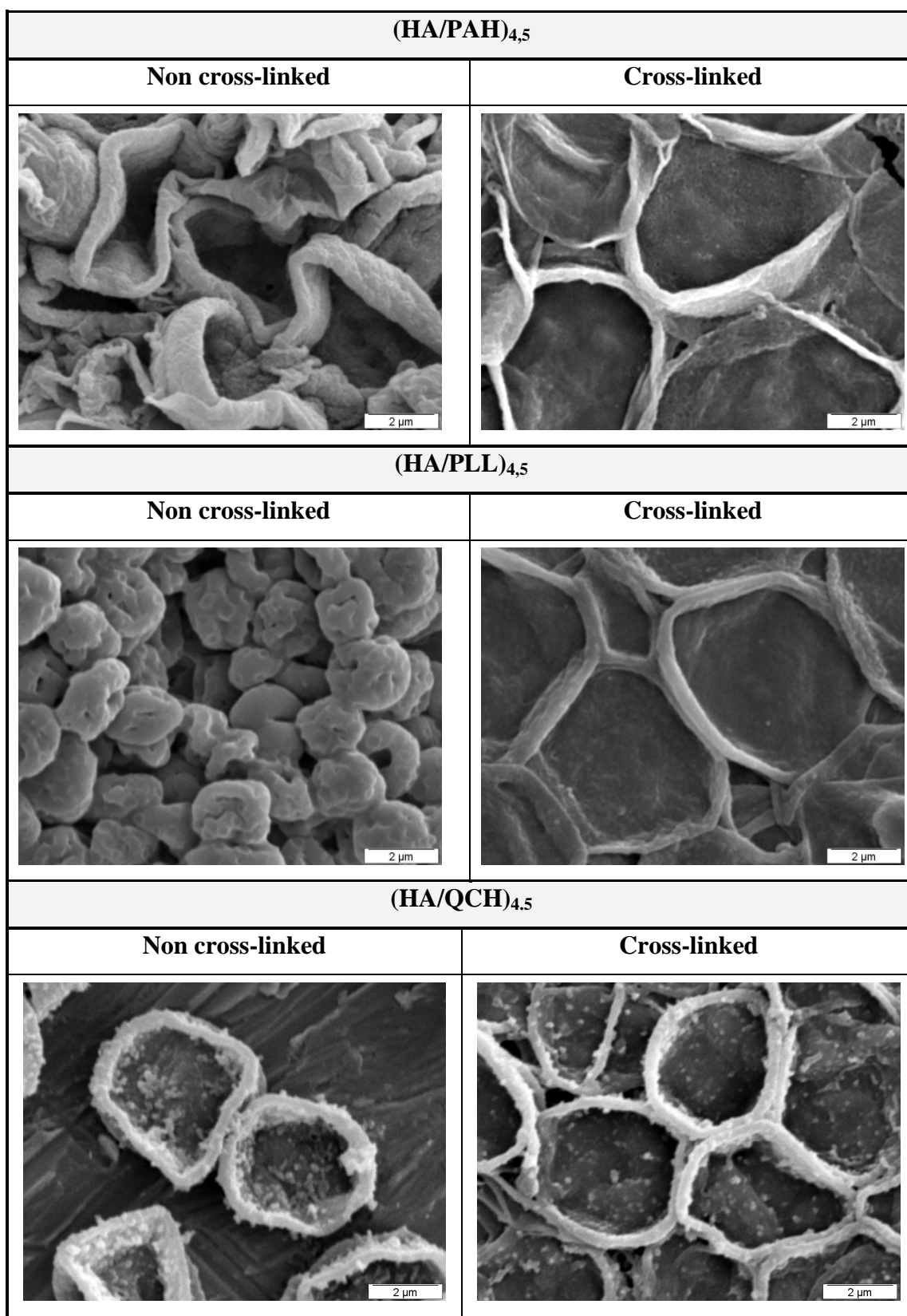


Figure 4.17. SEM images of $(\text{HA}/\text{PAH})_{4,5}$, $(\text{HA}/\text{PLL})_{4,5}$, and HA/QCH non cross-linked (left) and cross-linked (right) hollow capsules.

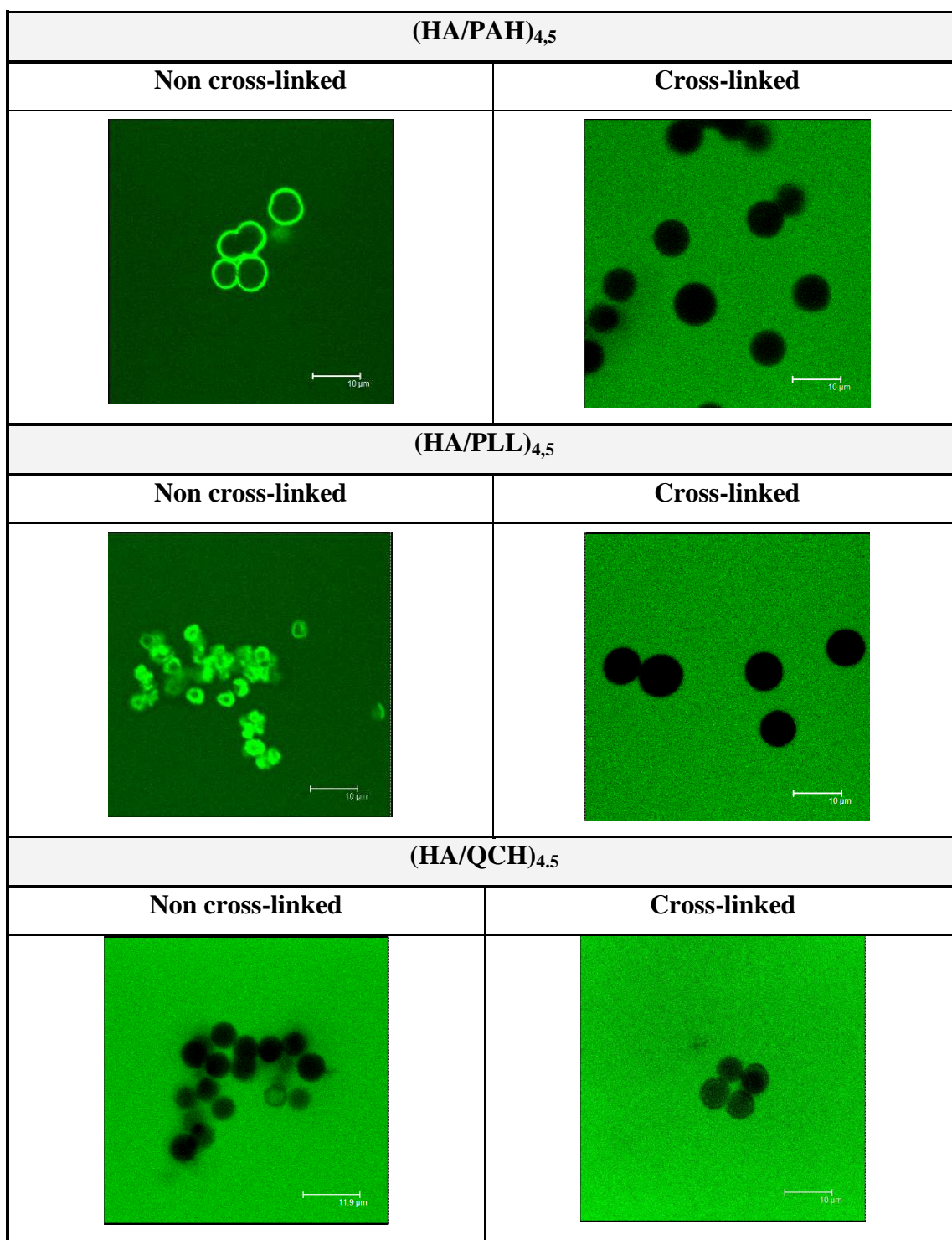


Figure 4.18. CLSM images of (HA/PAH)_{4,5}, (HA/PLL)_{4,5}, and (HA/QCH)_{4,5} non cross-linked (left) and cross-linked (EDC 200mM) (right) hollow capsules incubated in fluorescent dextran-4 solution. dextran-4 dissolved in MES at pH 6.5.

Regarding the influence of the degree of cross-linking (controlled by the amount of EDC added) on the capsule morphology, no clear difference could be observed by SEM images (Figure 4.19).

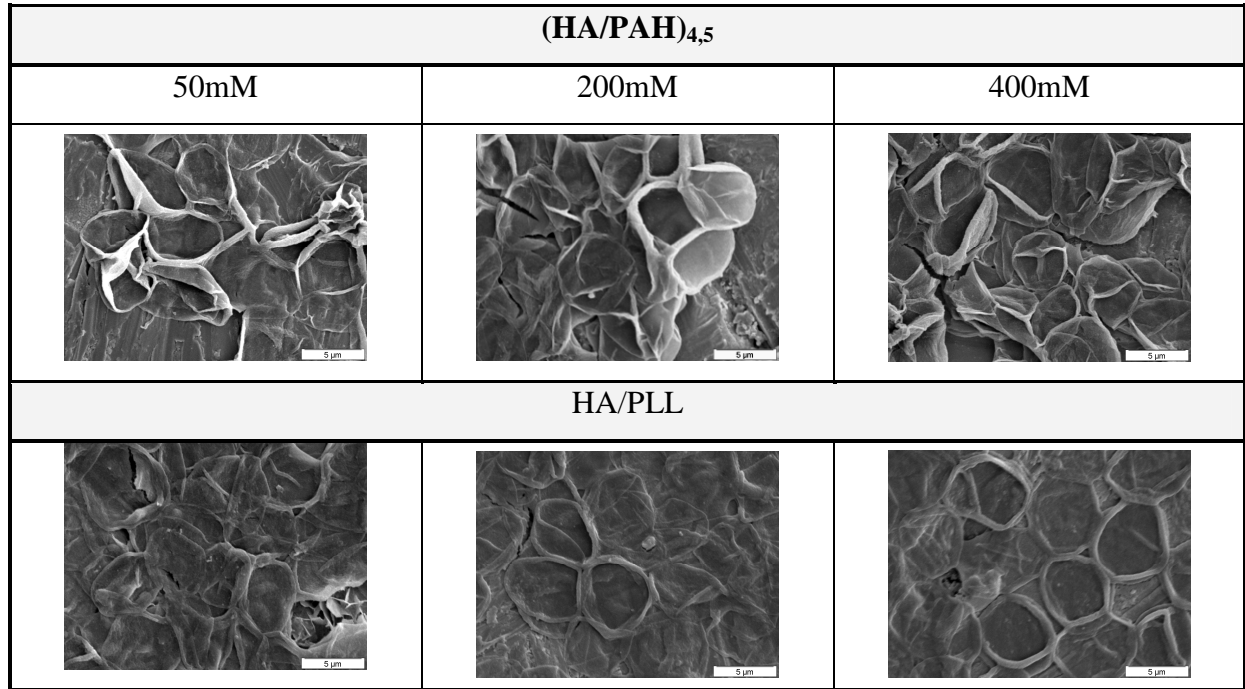


Figure 4.19. HA/PAH and HA/PLL capsules cross-linked by means of 50, 200 and 400mM EDC. Scale bar =5μm.

A small concentration of cross-linked agent (50mM) was enough to introduce morphological changes onto the capsule walls compared to the non cross-linked ones. Capsules are characterized by smooth thin walls in all cases. Finally, it can be noted that the HA/PLL capsules are more collapsed than the HA/PAH ones. This might be related to the lower thickness of the HA/PLL capsules as suggested by AFM data given in **Figure 4.19**. It was found to be three times lower than that of HA/PAH capsules.

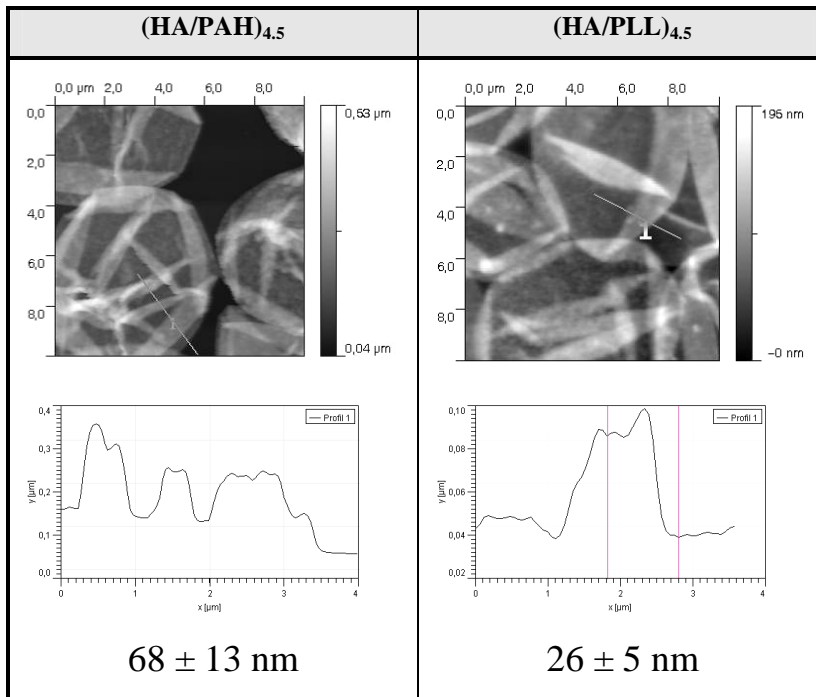


Figure 4.20. AFM images of air-dried (HA/PAH)_{4,5} (up) and (HA/PLL)_{4,5} (down) cross-linked (EDC 200mM) capsules and corresponding to them thickness profiles.

4.3.3. Shell permeability of cross-linked and non cross-linked capsules

Permeability of the LbL shells is one of the key properties of polyelectrolyte capsules. As discussed in the first chapter, permeability can depend on several parameters such as the layer thickness, used polyelectrolytes, external conditions such as pH, temperature, ionic strength, presence of organic solvent. The permeability also varies as a function of the nature, charge and size of the probe molecules^{22,29-34}.

Preliminary permeability studies of HA/PAH capsules are reported in Chapter 3. In this chapter we compare the permeability of all types of capsules. Cross-linked and non cross-linked capsules were investigated. Diffusion of dextran^{FITC} samples from outside into the interior of hollow capsules was first investigated as a function of the Mw of dextran (4×10^3 , 500×10^3 , $2\,000 \times 10^3$ g/mol) and the ionic strength of aqueous solution.

Following this, we examined the encapsulation of dextran as a model of drug.

a) Permeability in aqueous solution without salt

The permeabilities of non cross-linked and cross-linked capsules were evaluated from the ratio of fluorescence intensities between the capsule interior (I_{int}) and surrounding solution (I_{ext}).

In the case of non cross-linked HA/PAH capsules, the CLSM images show different permeability properties for a given sample (Figure 4.21). Whatever the M_w of dextran^{FITC}, about 30% of the capsules exhibit strong permeability toward the probe (>90% of probe penetration in the aqueous conditions).

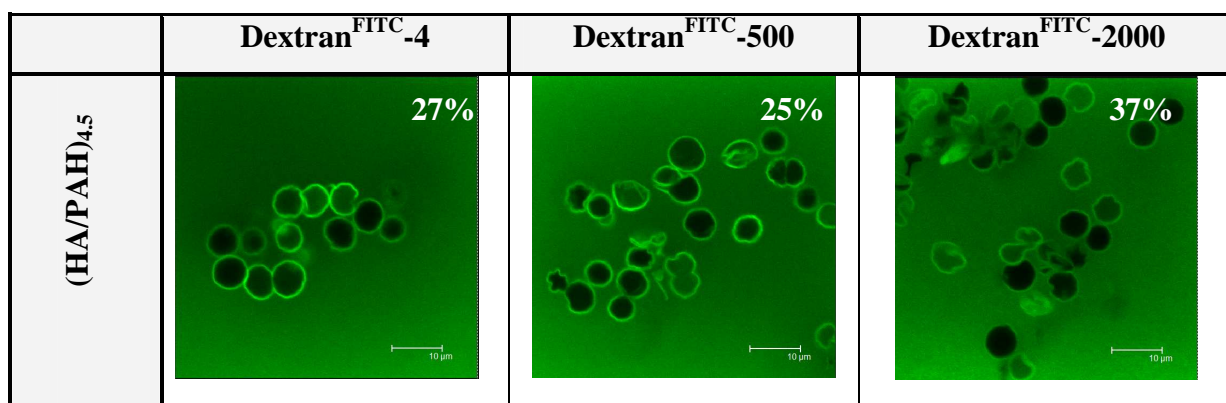


Figure 4.21. CLSM images of non cross-linked HA/PAH capsules incubated in dextran^{FITC}-4, -500 and -2000 solutions, respectively.

The difference between permeability of the shells disappeared after cross-linking. This result might suggest that cross-linking protects from disruption of the multilayer integrity during core dissolution. Indeed, this process allows the stabilisation of capsules by avoiding the diffusion of polyelectrolytes.

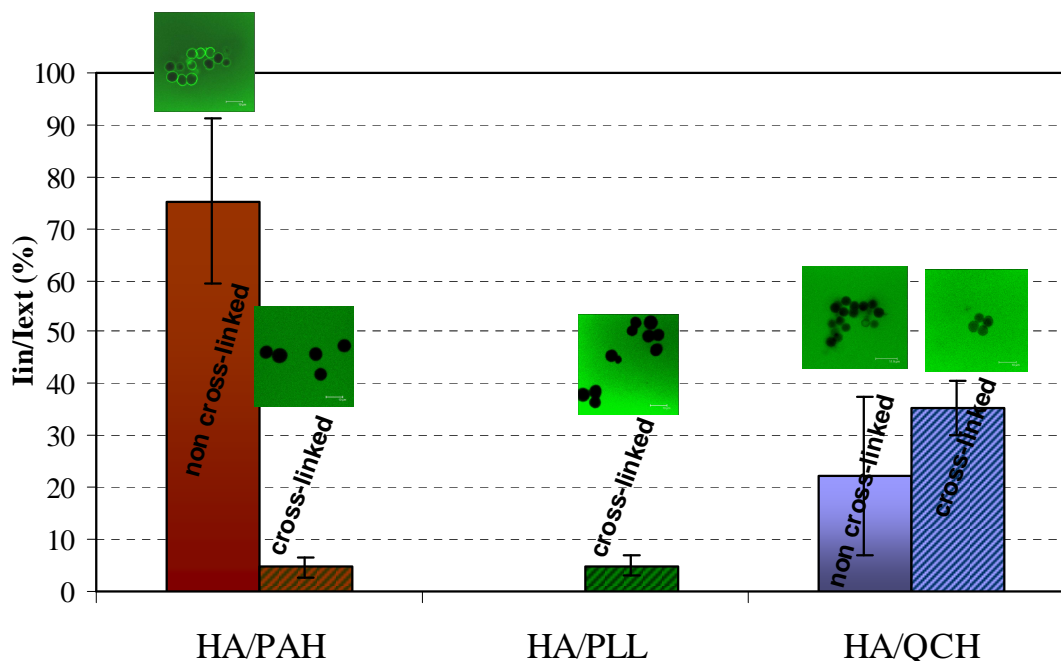


Figure 4.22. Permeability of non cross-linked and cross-linked capsules. Permeability is expressed as the ratio of intensities by capsules interiors (I_{int}) and surrounding solution (I_{ext}) 20 min after mixing capsules and solutions of dextran^{FITC}-4. For HA/PLL the permeability was estimated only for cross-linked capsules. Cross-linking was performed using EDC at a concentration of 200mM. The average value was taken from 7-10 capsules.

Compared to non cross-linked capsules of HA/PAH ($I_{int}/I_{ext} \sim 75\%$), those made of HA/QCH show lower permeability ($I_{int}/I_{ext} \sim 20\%$) (**Figure 4.22**). These capsules however become more

permeable than the HA/PAH ones after cross-linking. HA/PLL non cross-linked capsules were not analysed due to their shrunken structure. It can be noted that the permeability of HA/QCH capsules after cross-linking did not change significantly. As discussed previously, the cross-linking density may not be high enough to influence the permeability of the HA/QCH system. The lowest diffusion for cross-linked capsules was obtained for HA/PAH and HA/PLL capsules.

In the next step, in order to investigate the effect of cross-linking density on the permeability, we used HA/PAH and HA/PLL capsules treated with different amount of EDC (50, 200 and 400mM). **Figure 4.23** compares the permeability of HA/PAH and HA/PLL capsules as a function of EDC concentration and Mw of dextran (FITC, Dext^{FITC}-4, -500, -2000).

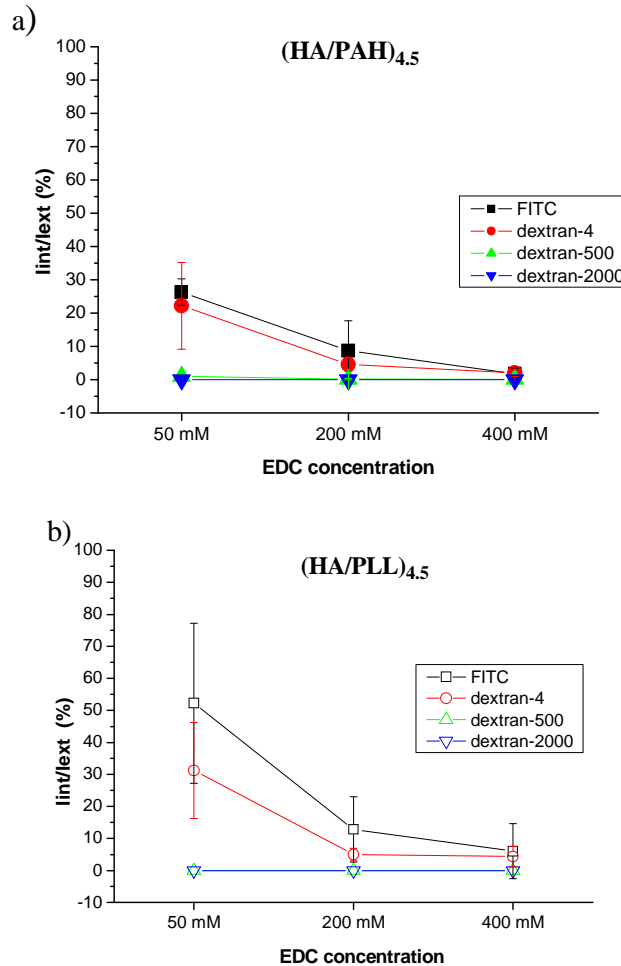


Figure 4.23. Ratio of fluorescence intensities capsules interiors (I_{int}) and surrounding solution (I_{ext}) 20min after mixing capsules and solutions of FITC (squares) and dextran^{FITC} molecules of different M_w (4×10^3 (rhomboids), 500×10^3 g/mol (triangles) and 2000×10^3 g/mol (turned triangles)) for HA/PAH (a) and HA/PLL cross-linked capsules (b). The covered points indicate the same permeability ratio.

The permeability of HA/PAH and HA/PLL cross-linked capsules for dextran^{FITC}-500 and dextran^{FITC}-2000 remains very low (equal or near to zero) for all cross-linked capsules. FITC and dextran^{FITC}-4 partially diffused into the interior of capsules, with permeability values depending on the amount of EDC used. Capsules showed relatively high permeability, when a low concentration of EDC was used, while permeability decreased significantly when EDC was used at concentrations of 200mM and 400mM. At a low concentration of coupling agent (50mM), the diffusion of FITC and dextran^{FITC}-4 molecules was higher in the case of HA/PLL (55 and 32%, respectively) than HA/PAH capsules (~ 25% for both). When EDC of 200mM used, permeability decreased down to ~ 10%. One can thus conclude that when an EDC concentration of 200mM is used, the permeability becomes relatively low.

Comparison with literature data supports our conclusions suggesting the possibility to tune the modulate permeability of capsules by cross-linking. The reduction of permeability in the shells after cross-linking was observed for the (PAH/PSS)₅ capsules which in the native form were permeable for dextran at Mw 460×10³g/mol and became impermeable after treatment with glutaraldehyde as a cross-linking agent³⁵. Cross-linking of ALG in the (ALG/CH)₅ capsule shells with calcium ions decreased the insulin release rate³⁶.

b) Permeability in salt

As described in Chapter 1, the permeability of capsules increases at higher ionic strength due to a weakening of the electrostatic binding between the oppositely charged polyelectrolytes^{22,32,34,37}.

In this study, NaCl was added into the aqueous suspension of capsules in order to increase the ionic strength (NaCl salt was added into MES to obtain a final concentration equal to 0.15M). As illustrated by **Figure 4.24** the permeability of HA/QCH non cross-linked capsules increased dramatically, contrary to HA/PAH ones, which maintained a similar level. This can be related to the different structure of HA/QCH multilayers as described in **paragraph 4.3.1.2**. The high molecular weight and semi-rigid conformation of QCH and HA hinder interpenetration of the chain and facilitates their repulsion in the presence of salt ions.

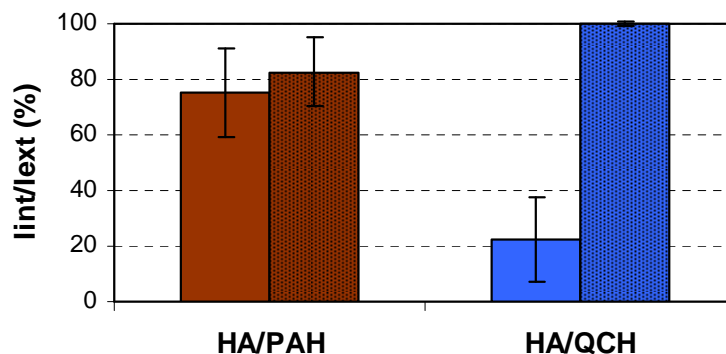
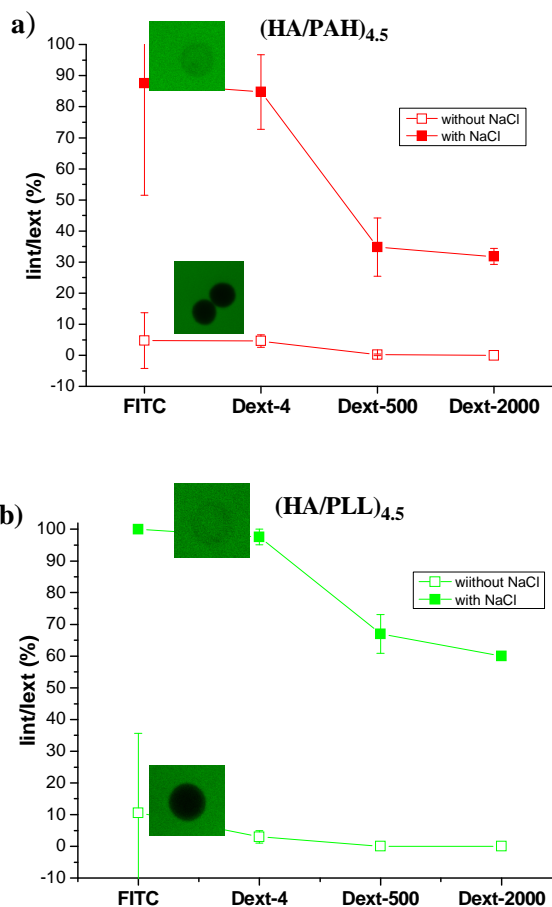


Figure 4.24. Permeability of non cross-linked HA/PAH (red) HA/QCH (blue) capsules without salt (uniform columns) and with presence of salt (0.15M) (spotted columns). Dextran^{FITC}-4 was used for diffusion.

In the case of cross-linked capsules (**Figure 4.25**), a high increase in diffusion, especially for small molecules such as FITC or Dext-4, was observed. In 0.02M MES buffer, the cross-linked capsules contain closed pores while in NaCl solution open pores which enable diffusion.



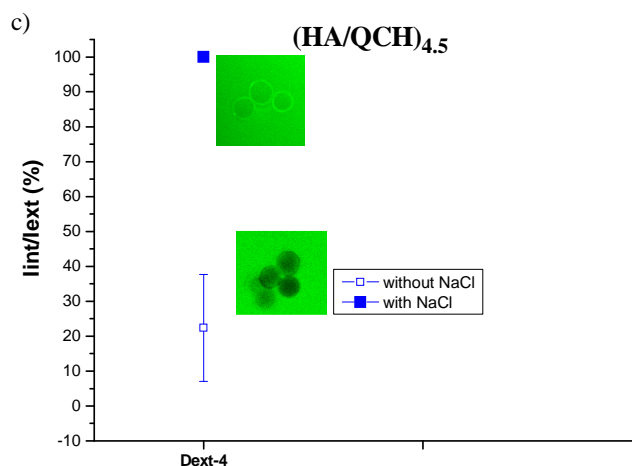
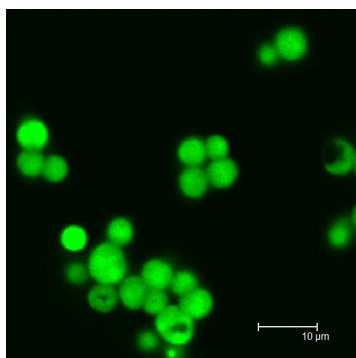


Figure 4.25. Permeability of cross-linked HA/PAH (a), HA/PLL (b) and HA/QCH (c) capsules in the absence (open squares) and in the presence (filled squares) of salt. Dextran^{FITC}-4, dextran^{FITC}-500, dextran^{FITC}-2000 were used for diffusion throw HA/PAH and HA/PLL shells, while only dextran^{FITC}-4 molecules for HA/QCH shells.

c) Encapsulation of fluorescent molecules as model drugs

The next step of the study considered the encapsulation of dextran-4, as a model drug, inside the capsule cores. High surface area and the presence of nanometer-sized pores and channels in CaCO_3 particles enable the adsorption/diffusion of macromolecules inside the core with very high loading³⁸. As reported in the literature³⁹, dextran-4 ($R_h = 2\text{nm}$) can diffuse into the interior of porous structure of CaCO_3 while dextran-2000 ($R_h = 26\text{nm}$) is retained on the surface due to its large size. Taking advantage of this, dextran-4 was encapsulated inside the core in order to be coated by the HA/polycation film.

a)



b)

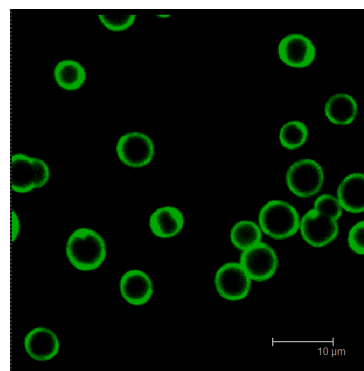


Figure 4.26. CaCO_3 particles with adsorbed Dextr-4 (a) and Dextr-2000 (b).

After adsorption of dextran-4 onto CaCO_3 particles, deposition of layers was performed up to 4.5 bilayers. For some capsules, the core was removed directly after multilayer deposition, while other coated particles were treated with EDC before template dissolution.

As illustrated by **Figure 4.27**, a large part of encapsulated Dext-4 diffused out of the non cross-linked capsules, while it remained entrapped in the case of cross-linked ones.

The measurements of the fluorescence intensity outside the cross-linked capsules incubated in MES or in MES with salt (after 4 hours) over fluorescence emitted by encapsulated dextran^{FITC} show very small amounts of released dextran (<5%). As can be seen from **Figure 4.28**, the release of dextran increased in the presence of salt, but only slightly. This result is different from that obtained from the experiments based on the diffusion of dextran from outside into the interior of capsules. Under these conditions, permeability dramatically increased in the presence of salt.

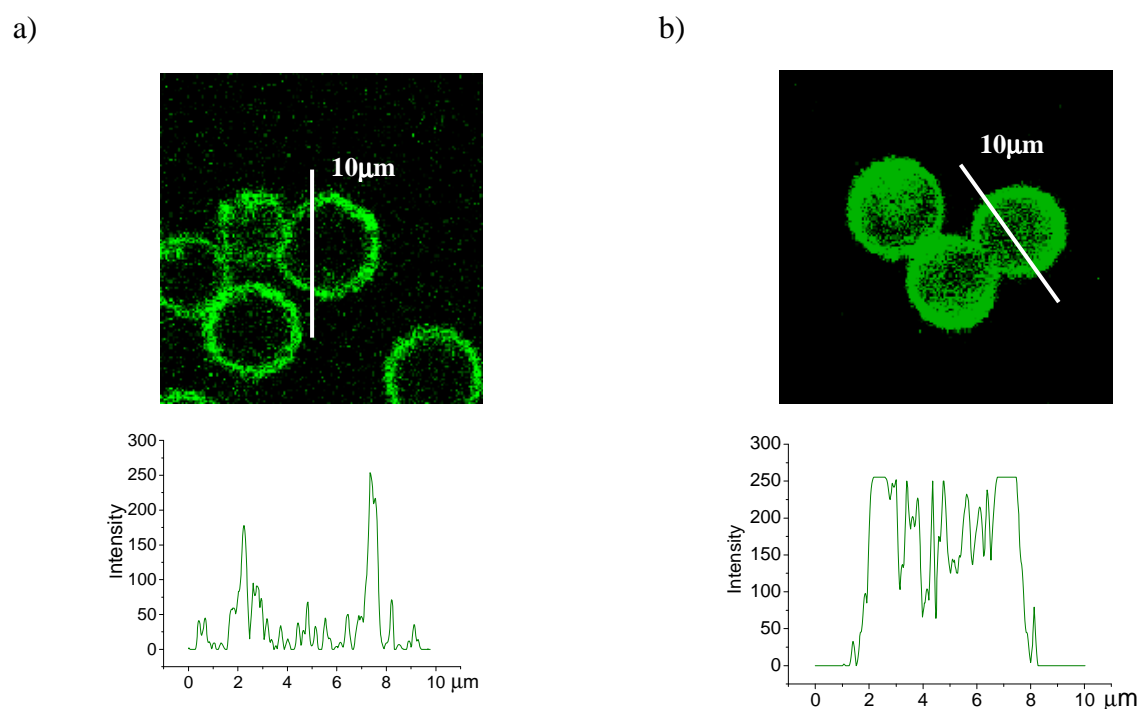


Figure 4.27. CLSM images of non cross-linked (a) and cross-linked (b) $(\text{HA/PAH})_{4.5}$ microcapsules with encapsulated dextran-4 (top) supported with the fluorescent profile (bottom).

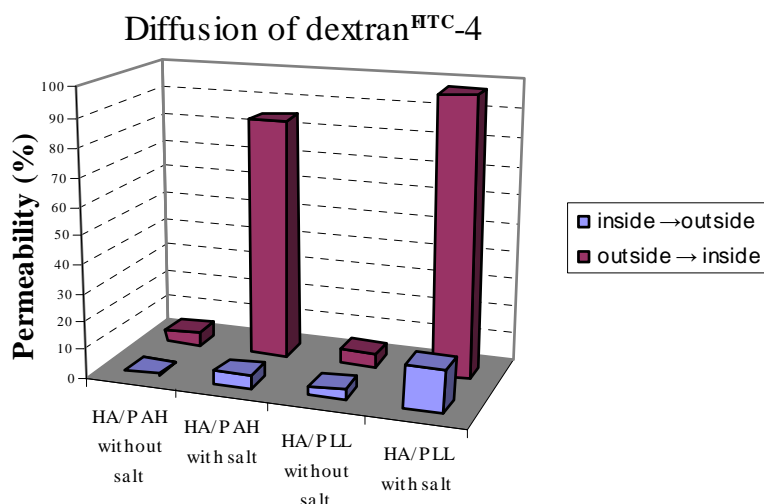


Figure 4.28. Permeability of the cross-linked HA/PAH and HA/PLL capsules without and in the presence of salt. Permeability was measured in two directions: diffusion of dextran-4 from external environment into interior of capsules (red columns), and liberation of encapsulated dextran-4 outside (blue columns).

This study thus established the possibility to load HA/PAH and HA/PLL cross-linked capsules with small molecules of dextran-4. Only a slight release was observed after 4 hours. Macromolecules encapsulated inside PSS/PAH capsules showed similar slight release. This was attributed to the formation of an internal network of complexed polyelectrolytes, due to the diffusion of the synthetic polymers in the carbonate core. In our case, we used high M_w HA to prevent diffusion. However, as mentioned in chapter 3, we could detect small amounts of HA in the interior of capsules. This may form a gel-like complex with other macromolecules, therefore limiting their leakage.

4.3.4. Enzymatic degradation

Degradation of native and chemically cross-linked HA by tissue enzyme such as hyaluronidase has been extensively studied⁴⁰⁻⁴⁵.

Hyaluronidase (Hase) is an enzyme which degrades hyaluronic acid (HA) by randomly cleaving β -*N*-acetyl-hexosamine - (1→4) glycosidic bonds, forming oligosaccharides, mainly tetrasaccharides as the smallest fragments with *N*-acetylglucosamine at the reducing end. Generally, the enzyme is extracted from bovine and sheep testes or from bacteria for

commercial aims. In the human body, it is found in organs (testes, spleen, skin, eye, liver, kidney, uterus and placenta) and body fluids (tear liquid, blood and sperma)⁴⁶⁻⁴⁹.

Enzyme concentration in human serum is 2.6 U/ml and is active at 37°C⁵⁰. Previous studies demonstrated that HA/QCH and HA/PLL planar films could be degraded by Hase at high concentrations (500 and 1000 U/ml, respectively)^{11,15}. Such concentrations are in the same range of magnitude of those used for degradation of HA-based chemical gels^{44,50}. In the case of gels, high Hase concentration is required for HA digestion which has been attributed to the formation of compact networks with a lower permeability to enzymes.

Owing to the potential applications of HA capsules as drug delivery systems, we investigated their enzymatic degradation using concentration in the range of 10-500U/mL. Incubation of capsules with Hase (from bovine testes) was performed at 37°C in MES buffer. In order to exclude the assumption that eventual changes in the capsules are due to the increase of temperature, we studied the behaviour of capsules at 37°C without enzyme.

The contact with Hase at concentrations of 10 and 50U/ml did not lead to noticeable changes of HA capsules. As can be seen from **Figure 4.29**, in the presence of 500U/mL Hase, only the HA/PLL capsules with initial shrunken morphology lose their structural stability.

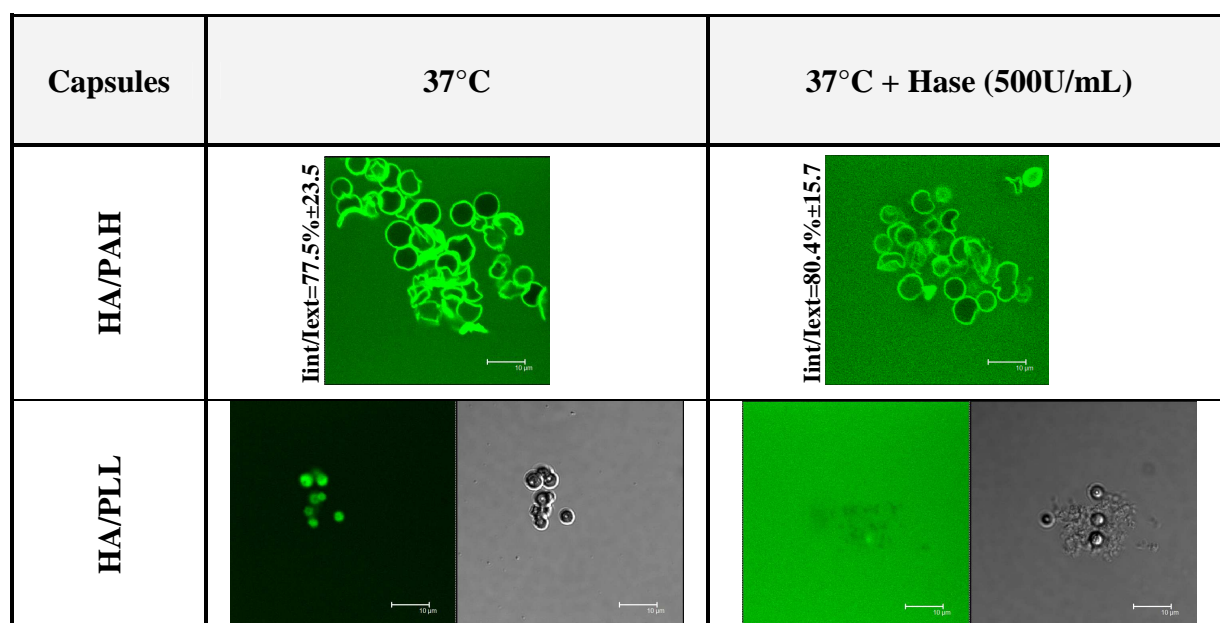


Figure 4.29. Confocal and their transmission equivalent images of HA/PAH and HA/PLL non cross-linked capsules at 37°C solution and at 37°C in contact with hyaluronidase of 500 U/mL. Enzyme was dissolved in 0.02M MES solution at pH 6.5. The capsules were mixed with dextran^{FITC}-4 20min before observation.

The higher sensitivity of the HA/PLL capsules may be due to weaker interactions between the polyelectrolytes compared to the HA/PAH or HA/QCH systems, as described above. This may facilitate the accessibility of the enzyme to glycosidic bonds of HA, resulting in a higher degradation of the multilayer. Moreover, it can be noted that the concentration used for HA/PLL degradation is close to that required for the degradation of films and gels.

Degradation of cross-linked capsules demonstrated in **Figure 4.30** shows that permeability of HA/PAH shells does not change after contact with enzyme contrary to the HA/PLL capsules of which permeability increased ~10 folds. However, the capsules did not change their spherical shape. These results may suggest only partial degradation of the shells due to the presence of covalent bonds between polyelectrolyte partners.

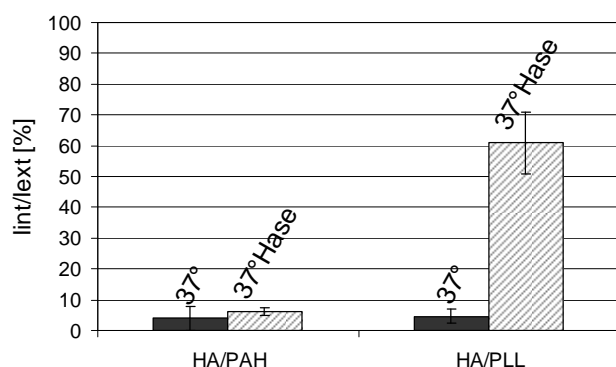


Figure 4.30. Degradation of cross-linked capsules (EDC 200mM) in contact with hyaluronidase at 37°C overnight, dextran-4 were used to check permeability. Dextran^{FTIC} (2g/L) and Hase (500U/mL) were dissolved in 0.02M MES at pH 6.5.

Compared to recent results published by Lee et al.³⁰ the release of BSA protein from cross-linked HA/PLL capsules was faster in contact with Hase starting from 10U/mL. However, the conditions used for the preparation of capsules were different (HA with M_w 64 000 g/mol). In the case of degradation of non cross-linked HA/CH planar films¹⁵, assemblies made of CH with $M_w = 100 \times 10^3$ g/mol were more resistant to degradation by Hase (500 U/mL) contrary to those containing CH with $M_w = 5 \times 10^3$ g/mol.

This work thus demonstrated that the stability and permeability properties of the HA capsules can be tuned by controlled chemical modifications of the shell. However, it should be noted that the physiological concentrations of Hase depend on the location in the body and other factors such as thermal degradation and attack by free radicals are also responsible for the degradation of hyaluronic acid.

4.4. Conclusion

In this chapter, we presented the formation of hollow capsules made from hyaluronic acid and three different cationic partners: PAH, PLL and QCH. In our conditions for capsule fabrication, only HA/PAH and HA/QCH showed stable mechanical properties, while the HA/PLL capsule morphology was disrupted during core dissolution. However, this could be overcome by cross-linking of the shell before template dissolution.

The permeability for different molecules is a key parameter of capsules to be controlled for drug delivery applications. In aqueous solution at low ionic strength, non cross-linked HA/QCH showed lower permeability than HA/PAH capsules due to the formation of a cohesive and well-packed film. The HA/PAH and HA/PLL capsules had to be cross-linked to improve their mechanical properties and decrease diffusion through the walls.

After optimizing the conditions to control permeability of capsules, we demonstrated the possibility to obtain capsules loaded with dextran-4. This hydrophilic drug model was shown to be released at various rates depending on the presence of salt and shell cross-linking. This release may be promoted by action of hyaluronidase, especially in the case of HA/PLL capsules.

While cross-linking of the HA/PLL shell was necessary to obtain capsules with suitable mechanical and permeability properties, the structure of HA/QCH assembly met these requirements without the need for covalent bridges in the multilayer assembly.

References:

- (1) Mak, W. C.; Cheung, K. Y.; Trau, D. *Chemistry of Materials* **2008**, *20*, 5475-5484.
- (2) Sei Kwang Hahna, A. S. H. *International Journal of Biological Macromolecules* **2005**, *37*, 227-231.
- (3) Zonghuan Lu, M. D. P., Zhanhu Guo, Vladimir O. Golub, Challa S. S. R. Kumar, and Yuri M. Lvov. *Langmuir* **2005**, *21*, 20042-22050.
- (4) Angelova, N.; Hunkeler, D. *Trends in Biotechnology* **1999**, *17*, 409-420.
- (5) Picart, C., Lavallo, Ph., Hubert, P., Cuisinier, Decher, G., Schaaf, P., and Voegel, J.-C. *Langmuir* **2001**, *17*, 7414-7424.
- (6) Akinc, A., Lynn, D. M., Anderson, D. G., and Langer, R. *J. Am. Chem. Soc.* **2003**, *125*, 5316-5323.
- (7) Dumitriu, S. *Polysaccharides. Structural diversity and functional versatility.*, Second edition ed.: Quebec, Canada, 2005.
- (8) Jaepyoung Cho, J. G., Micheline Piquette-Miller, and Christine Allen. *Biomacromolecules* **2006**, *7*, 2845-2855.
- (9) Laugel, N.; Betscha, C.; Winterhalter, M.; Voegel, J.-C.; Schaaf, P.; Ball, V. *Journal of Physical Chemistry B* **2006**, *110*, 19443-19449.
- (10) Schneider, A.; Picart, C.; Senger, B.; Schaaf, P.; Voegel, J.-C.; Frisch, B. *Langmuir* **2007**, *23*, 2655-2662.
- (11) Ludovic Richert, F. B., Philippe Lavallo, Jerome Mutterer,; Emmanuelle Ferreux, G. D., Pierre Schaaf,| Jean-Claude Voegel and Catherine Picart. *Biomacromolecules* **2004**, *5*, 284-294.
- (12) C. Porcel , P. L., G. Decher, B. Senger, J.-C. Voegel, and P. Schaaf. *Langmuir* **2007**, *23*, 1898-1904.
- (13) Richert, L., Lavallo, P., Payan, E., Stoltz, J.-F., Shu, X.Z., Schaaf, P., Voegel, J.-C., Picart, C. *Langmuir* **2004**, *20*, 448-458.
- (14) Kujawa, P., Moraille, P., Sanchez, J., Badia, A., Winnik, F.M. *J Am Chem Soc* **2005**, *127*, 9224-9234.
- (15) Picart, C.; Schneider, A.; Etienne, O.; Mutterer, J.; Schaaf, P.; Egles, C.; Jessel, N.; Voegel, J.-C. *Advanced Functional Materials* **2005**, *15*, 1771-1780.
- (16) Si-Ling Huang, P.-X. L., Tian-Min Zhang. *World Gastroenterol* **2007**, *13*, 945-949.
- (17) Schneider, A.; Francius, G.; Obeid, R.; Schwinte, P.; Hemmerle, J.; Frisch, B.; Schaaf, P.; Voegel, J.-C.; Senger, B.; Picart, C. *Langmuir* **2006**, *22*, 1193-1200.

- (18) Changyou Gao, S. L., Edwin Donath, Helmuth Mohwald. *J. Phys. Chem.B* **2000**, 104, 7144-7149.
- (19) Alexei A. Antipov, D. S., Yuri Fedutik, Alexander I. Petrov, Gleb B. Sukhorukov, Helmuth Mohwald. *Colloids and Surfaces A: Physicochemical and Engineering Aspects* **2003**, 224, 175-183.
- (20) Burke, S. E.; Barrett, C. J. *Biomacromolecules* **2005**, 6, 1419-1428.
- (21) Elbert, D. L.; Herbert, C. B.; Hubbell, J. A. *Langmuir* **1999**, 15, 5355-5362.
- (22) Qiu, X.; Donath, E.; Mohwald, H. *Macromolecular Materials and Engineering* **2001**, 286, 591-597.
- (23) Aurore Schneider, L. R., Gregory Francius, Jean-Claude Voegel and Catherine Picart. *Biomedical materials* **2007**, 2, S45-S51.
- (24) Engler, A. J.; Richert, L.; Wong, J. Y.; Picart, C.; Discher, D. E. *Surface Science* **2004**, 570, 142-154.
- (25) Picart, C., Senger, Bernard Sengupta, Khaya Dubreuil, Frederic, Fery, Andreas. *Colloids and Surfaces, A: Physicochemical and Engineering Aspects* **2007**, 303, 30-36.
- (26) Picart, C., Senger, B., Sengupta, K., Dubreuil, F., Fery, A. *Colloids and Surfaces A: Physicochem. Eng. Aspects* **2007**, 303, 30-36.
- (27) Schneider, A., Richert, L., Francius, G., Voegel, J.-C., and Picart, C. *Biomacromolecules* **2007**, 8, 139-145.
- (28) Schuetz, P.; Caruso, F. *Advanced Functional Materials* **2003**, 13, 929-937.
- (29) Antipov, A. A., Sukhorukov, G. B. *Advances in Colloid and Interface Science* **2004**, 111, 49-61.
- (30) Lee, H., Jeong, Yongho, Park, Tae Gwan. *Biomacromolecules* **2007**, 8, 3705-3711.
- (31) Koehler, K.; Sukhorukov, G. B. *Advanced Functional Materials* **2007**, 17, 2053-2061.
- (32) Peyratout, C. S.; Daehne, L. *Angewandte Chemie, International Edition* **2004**, 43, 3762-3783.
- (33) Schonhoff, M. *Current Opinion in Colloid & Interface Science* **2003**, 8, 86-95.
- (34) Alexei A. Antipov, G. B. S., H. Mohwald. *Langmuir* **2003**, 19, 2444-2448.
- (35) Weijun Tong, C. G., and Helmuth Mohwald. *Chemical Materials* **2005**, 17, 4610-4616.
- (36) Shiqu Ye, C. W., Xinxing Liu, Zhen Tong, Beye Ren, Fang Zeng. *Journal of Controlled Release* **2006**, 112, 79-87.

- (37) Ibarz, G.; Dahne, L.; Donath, E.; Mohwald, H. *Advanced Materials (Weinheim, Germany)* **2001**, *13*, 1324-1327.
- (38) Volodkin, D. V., Larionova, N. I., and Sukhorukov, G. B. *Biomacromolecules* **2004**, *5*, 1962-1972.
- (39) Cavalieri, F.; Ashokkumar, M.; Grieser, F.; Caruso, F. *Langmuir* **2008**, *24*, 10078-10083.
- (40) Hahn, S. K.; Park, J. K.; Tomimatsu, T.; Shimoboji, T. *International Journal of Biological Macromolecules* **2007**, *40*, 374-380.
- (41) Jung, B. D.; Hong, J. D.; Voigt, A.; Leporatti, S.; Dahne, L.; Donath, E.; Mohwald, H. *Colloids and Surfaces, A: Physicochemical and Engineering Aspects* **2002**, *198-200*, 483-489.
- (42) Robert Stern, G. K., Mark J. Jedrzejewski, Ladislav Šoltés. *Biototechnology Advances* **2007**, *25*, 537-557.
- (43) Jamal Alyoussef Alkrad, Y. M., Dieter Stroehl, Siegfried Wartewig, Reinhard Neubert. *Journal of Pharmaceutical and Biomedical Analysis* **2003**, *31*, 545-550.
- (44) Burdick, J. A., Chung, C., Jia, X., Randolph, M. A., and Langer, R. *Biomacromolecules* **2005**, *6*, 386-391.
- (45) Davies, C. L. H. a. M. J. *Free Radical Biology and Medicine* **1998**, *24*, 1396-1410.
- (46) Rinaudo, M. *Corrosion Engineering, Science and Technology* **2007**.
- (47) E.J. Menzel, C. F. *Cancer Letters* **1998**, *131*, 3-11.
- (48) Bollet, A. J., Bonner, W. M., and Nance, J. L. *The Journal of Biological Chemistry* **1963**, *238*, 3522-3527.
- (49) Sall, I.; Ferard, G. *Polymer Degradation and Stability* **2007**, *92*, 915-919.
- (50) Leach, J. B., Bivens, K. A., Patrick, C. P., Schmidt, C. *Biotechnology Bioengineering* **2003**, *82*, 578-589.

Conclusion (en)

Since their first introduction in 1998, polyelectrolyte multilayer microcapsules have attracted a great deal of interest due to the fact their properties such as composition, shell thickness, permeability, stability and surface functionality can be tailored fairly readily. Recent work suggested that these systems may contribute not only to the understanding of biological systems but also to the development of multifunctional drug delivery vehicles with designed surfaces and interior compositions as well as stimuli-responsive properties. However, there are still many challenges remaining for drug delivery applications, including the use of biocompatible materials and improvement of the drug release profile for a specific disease treatment. This clearly motivated this study. Based on previous work performed on the characterization and chemical modification of hyaluronic acid in CERMAV, we proposed to design and synthesize capsules from this natural polysaccharide. Little was known about its behavior in multilayer capsules. However, it has become clear that *in vitro*, the biological role of HA is related to its property to self-organize into strongly hydrated matrices in the extra- and pericellular space. Hydrogel-like pericellular layers seem to perform crucial functions, both in the general protection of the cell, and communication with its environment. The first question thus addressed in this work was if capsules could be obtained from HA and poly(allylamine) using the layer-by-layer technique. We found that the molecular weight of HA as well as the HA solution concentration used during deposition on carbonate particles used as biocompatible colloidal templates are crucial parameters influencing the multilayer structure. HA lead to dense structures for concentrations from five to ten times the critical overlap concentration during adsorption. Such conditions were found to be favourable for the formation of hollow shells. In the next step, we thus extended our methodology to produce capsules from HA using other polycationic polymers. We selected poly(L-lysine) and a quaternized derivative of chitosan as biocompatible polymers belonging to the families of polypeptides and polysaccharides, respectively. The behavior of these materials was shown to be very different during capsule fabrication. The weak nature of the HA/PLL complex resulted in the disruption of the multilayer assembly during core removal, whereas the HA/QCH system demonstrated good stability related to the formation of a cohesive and well-structured film. The chemical cross-linking of the HA/PLL shell was thus required to obtain hollow capsules. The optimization of conditions for production of impermeable capsules allowed us to encapsulate dextran as a model drug molecule. We finally showed that its

release may be modulated by changes in certain environmental conditions such as the presence of salt or enzyme capable to depolymerize HA. All these results thus established the possibility to obtain capsules in a reproducible manner. This provided the basis for the development of tailor-made capsules from selectively modified polysaccharides. One of the next challenges will be to engineer capsules able to transport hydrophilic and hydrophobic drugs. These capsules seem indeed to be stable despite of the absence of chemical cross-linking between layers. Such an approach would thus combine in the same material the unique biological properties of these natural polymers with their multifunctionality of capsules.

Conclusion (fr)

Depuis leur instruction en 1998, les capsules multicouches de polyélectrolytes suscitent un intérêt tout particulier lié à la possibilité d'ajuster assez facilement leur propriétés telles que leur composition, l'épaisseur de leur paroi, leur perméabilité, leur stabilité et la fonctionnalité de leur surface. Les travaux récents menés dans ce domaine indiquent que ces systèmes peuvent contribuer non seulement à progresser dans la compréhension des systèmes biologiques mais aussi à proposer de nouveaux systèmes transporteurs de médicaments multifonctionnels et stimulables. L'utilisation de ces capsules pour la libération de médicament demeure néanmoins un défi. Une telle application passe en effet par l'utilisation de matériaux biocompatibles et nécessite de maîtriser l'encapsulation et relargage du principe actif en fonction de la maladie à traiter. Ces aspects ont clairement motivé ce travail. Compte tenu des travaux antérieurs effectués au CERMAV sur la caractérisation et la modification chimique de l'acide hyaluronique, nous nous sommes proposés de concevoir et synthétiser des capsules à partir de ce polymère naturel. Il est désormais bien établi que dans l'organisme, le rôle du HA est lié à ses propriétés d'auto-organisation sous la forme d'une matrice fortement hydratée dans l'espace extra- et pericellulaire. Des couches de gels constituées de HA autour des cellules semblent jouer des rôles cruciaux à la fois dans la protection générale de la cellule mais aussi dans la communication avec son environnement.

Dans cette étude, la première question à laquelle nous avons cherché à répondre était l'accès à ces capsules en utilisant l'acide hyaluronique et la poly(allylamine) comme polyélectrolytes partenaires. Nous avons ainsi mis en évidence que la masse molaire du HA ainsi que sa concentration lors du dépôt sur des particules de carbonate utilisées comme supports colloïdaux étaient des paramètres cruciaux influençant la structure de la multicouche. Le HA a ainsi donné lieu à des structures denses pour des concentrations cinq fois plus élevées que la concentration critique de recouvrement lors de l'adsorption. De telles conditions se sont donc avérées favorables pour la préparation de capsules creuses.

Dans une deuxième phase, nous avons donc étendu cette méthodologie à la synthèse de capsules de HA en utilisant d'autres partenaires polycationiques. Nous avons choisi la poly(L-lysine) et un dérivé quaternisé du chitosane comme polymères biocompatibles appartenant aux familles des polypeptides et polysaccharides, respectivement. Le comportement de ces

matériaux s'est révélé très différent lors de la fabrication des capsules. Le film constitué par le complexe HA/PLL, faible, se trouve déstabilisé lors de la dissolution du cœur de carbonate contrairement au système HA/QCH qui montre une grande stabilité liée à la formation d'un film cohésif et bien structuré. La réticulation chimique de la paroi de HA/PLL s'est donc avérée nécessaire pour aboutir à des capsules. L'optimisation des conditions pour produire des capsules peu perméables nous a permis d'encapsuler de petites molécules de dextrane comme modèles de médicaments hydrophiles. Nous avons finalement démontré que leur libération pouvait être modulée par des changements des conditions environnantes telles que la présence de sel ou d'enzyme capable de dépolymériser le HA. Tous ces résultats ont ainsi montré la possibilité d'obtenir des capsules de manière reproductible. Ceci ouvre ainsi la voie vers des perspectives intéressantes dans le développement de capsules « sur-mesure » à partir de polysaccharides modifiés sélectivement. L'un des prochains défis consistera à concevoir des capsules multifonctionnelles à partir de dérivés d'acide hyaluronique et de chitosane, capables de transporter des molécules hydrophiles et hydrophobes. Ces capsules se montrent en effet stables même en l'absence de pontages covalents entre les couches. Une telle approche permettrait de combiner dans le même matériau les propriétés biologiques uniques de ces polymères naturels avec les propriétés multifonctionnelles des capsules.

List of Figures

Figure 1.1.	Build-up of the polyelectrolyte multilayer film by the consecutive adsorption of anionic and cationic polymers (multiple repetition of the steps for obtaining desired number of layer).....	6
Figure 1.2.	Areas of applications of polymer capsules.....	10
Figure 1.3.	Polyelectrolyte multilayer deposition process and subsequent core dissolution resulting in the formation of hollow capsules.....	11
Figure 1.4.	The illustration of different interactions within the LbL shell: electrostatic (a), hydrogen bonding (b), specific (c), covalent bonds (d), and (e) host-guest.....	14
Figure 1.5.	Different methods for encapsulating materials: (a) encapsulation of crystalline particles, (b) incorporation in porous materials, and (c) loading preformed capsules.....	16
Figure 1.6.	Swelling of the capsule in basic conditions due to electrostatic repulsion between negative charges of PSS.....	18
Figure 1.7.	a) Incubation of polyelectrolyte multilayer capsules in a solution of the desired compound, b) The mixture is heated until the capsules shrink so much that the shells become impermeable for the molecules leading to an entrapment; c) Removal of surrounding molecules by subsequent washing steps.....	19
Figure 1.8.	Phagocytosis of coated LbL microcapsules by dendritic cells, capsules made from PSS/PAH polyelectrolytes: (a) PSS-coated microcapsules; (b) PLL-g-PEG coated microcapsules. FITC labelled PAH was used for capsule synthesis to enable CLSM visualization. Arrows indicates the sites of capsule placement. Scale bare=50µm.....	21
Figure 1.9.	Model of the cells with a) and without b) “A33” antigen. Capsules with incorporated antibody are able to recognize only the cell with specific antigen.....	22
Figure 1.10.	Protocol for engineering virus functionality. The PSS/PAH coated particles were incubated in the liposome vesicles solution to accomplish the lipid membrane and incorporate viruses particles.....	22
Figure 1.11.	The capsules under laser irradiation.....	24
Figure 1.12.	Irradiation of capsules with laser pulses. SEM images of capsules: (a) before irradiation, (b) after radiant exposure.....	24

Figure 1.13.	Mechanism of the glucose-induced decomplexation of a polyelectrolyte bilayer. The red circles represent the negatively charged PSS, and the blue circles represent the amino groups with uncharged phenylboronic acid (green circles). After treatment with glucose the repulsion occurs as the result of negative charge of borate	25
Figure 1.14.	Release profile of insuline from (ALG/CHI) ₅ microcapsules coated with additional layers after loading.....	26
Figure 1.15.	Structures of the monomers used for the synthesis of polystyrene labelled with rhodamine B, reaction occurs inside the capsules.....	27
Figure 1.16.	Schematics of the shell-in-shell polyelectrolyte multilayer capsule and laser induced inter-compartmentalized mixing and above their equivalent CLSM images.....	28
Figure 1.17.	Enzymatic formation of fluorescein within polyelectrolyte microcapsules catalyzed by an encapsulated bacterial alkaline phosphatase.....	29
Figure 1.18.	Biotin-functionalized system immobilized inside avidin-modified polyelectrolyte multilayer-covering nanoporous silica particles.By complexation with a DNA sequence complementary to the loop, a change of conformation occurred resulting in a fluorescent signal.....	30
Figure 1.19.	SNARF-loaded capsules change from red to green fluorescence upon internalization by cells. The capsules outside of the cells exhibit red fluorescence due to the basic pH of the environment. Capsules remaining in the cell medium retain their red fluorescence (red arrows). Capsules incorporated in the acidic endosome retain their green fluorescence (green arrows). Some capsules were incorporated in endosomal/lysosomal compartments inside cells which is indicated by their change in fluorescence from red to green (red to green arrows)	31
Figure 1.20.	SEM images showing satellite-like structures with central capsule core and porphyrin fibers (scale bar=2µm).....	32
Figure 1.21.	HA structure.....	38
Figure 1.22.	The repeating unit of HA with its functional groups.....	39
Figure 1.23.	Occurrence of HA in human body	41
Figure 2.1.	The hydrodynamic radius of FITC and FITC labelled dextran molecules at different M _w	58

Figure 2.2.	Scheme of principally obtainable images for a single suspended shell in the presence of fluorescent probes. The green color indicates regions of lower or higher fluorescent intensity according to the local concentration distribution of the probe (outside/shell wall/inside). Black regions mean the absence of fluorescent probes. The visualization is carried out by means of Confocal Laser Scanning Microscopy (CLSM).....	59
Figure 2.3.	Schematic diagram of a Scanning Electron Microscope.....	61
Figure 2.4.	Jeol JSM6100 at CERMAV, Grenoble.....	62
Figure 2.5.	Mechanism of fluorescence.....	63
Figure 2.6.	Schematic diagram of the optical pathway and principal components in a laser scanning confocal microscope.....	63
Figure 2.7.	Confocal Microscope Leica TCS SP2 AOBS.....	64
Figure 2.8.	Scheme of principal components of Transmission Electron Microscope (TEM).....	65
Figure 2.9.	Illustration of stretching and bending vibration.....	67
Figure 2.10.	A multiple reflection ATR system.....	67
Figure 2.11.	ITC cells and syringe. The syringe rotates during the ITC experiment. The system is controlled by computer and injects precise volumes of ligand.....	69
Figure 2.12.	A standard QCM-crystal with electrodes on the both side of the disc.....	70
Figure 2.13.	The typical graph of the frequency changes (Δf) and dissipation changes (ΔD) during adsorption process as a function of the time.....	71
Figure 2.14.	The QCM-D system.....	71
Figure 2.15.	Schematic distribution of ions around charged particle.....	73
Figure CR 3.1	HA/PAH capsule formation from different M_w of HA and concentrations below C^* and PAH of 2g/L. Polyelectrolytes were dissolved in 0.15M NaCl (pH 6.5). Citric acid (0.1M, pH 5.4) was used for core dissolution.....	96
Figure CR 3.2	HA820/PAH capsules (HA of 5g/L) after core removal using citric acid (a), EDTA (b).....	97

Figure CR 3.3.	HA200/PAH capsules after core removal using centrifugation a) and dialysis process b). Scale bare 10 μ m a) and 5 μ m b).....	97
Figure 4.1.	Calorimetric titration of a PAH solution (C _p =2g/L or 21.3 mM) in TRIS buffer (pH 7.4) containing 0.15M NaCl at 25°C. Raw ITC data (a) and integrated values of the enthalpy changes following injection of HA HA (C _p = 3g/L or 7.4 mM) (b).....	106
Figure 4.2.	Values of complexation enthalpy for HA200/PAH and HA820/PAH (a) and, HA820/PAH; HA820/PLL and HA820/CH (b) in TRIS buffer (grey columns) and TRIS + 0.15M NaCl (white columns). The error of subsequent measurements for one sample was in the range of 6 %.....	107
Figure 4.3.	QCM-D frequency shifts $-\Delta f/\nu$ during the alternate deposition PAH/HA, PLL/HA and QCH/HA multilayers obtained at harmonics 15 MHz (black line) , 25 MHz (red line) and 35 MHz (green line) as a function of time. HA820 at concentration 5g/L and polycations at concentration 2g/L were used for solution preparation.....	109
Figure 4.4.	QCM-D frequency shift $-\Delta f/\nu$ during the alternate deposition of PAH/HA, PLL/HA and QCH/HA obtained at harmonics 15 MHz (black squares), 25 MHz (red circles) and 35 MHz (green triangles) as a function of deposited layer, the points demonstrate the polyelectrolyte deposition after rinsing step. HA820 and the polycation were used at a concentration of 5g/L and 2g/L, respectively. Inset compares the PAH/HA film growth using HA200 at 1 g/L or 5 g/L.....	110
Figure 4.5.	Film thickness as a function of the number of layers estimated by QCM-D. Deposition of layers are represented by symbols: PAH/HA (black squares), PLL/HA (red circles), and QCH/HA (green triangles).....	111
Figure 4.6.	Variation of the ζ -potential value as a function of layer number during LbL coating of CaCO ₃ particles : a) HA/PAH, b) HA/PLL and c) HA/QCH bilayers.....	112
Figure 4.7.	Schematic representation of multilayer build-up using HA as a polyanion. (a) The semi-rigid character and entangled chains of HA (M _w = 820 \times 10 ³ g/mol) promote the formation of a thick and cohesive layer; (b) flexible small synthetic polyelectrolytes (PAH and PLL) can diffuse easily into the porous layer of HA; (c) semi-rigid high Mw QCH chains (M _w = 180 \times 10 ³ g/mol) can not penetrate into the HA layer.....	114
Figure 4.8.	CaCO ₃ particles alone and with <i>n</i> deposited layers of HA820 (c = 5g/L) and different polycations: PAH (M _w = 70 \times 10 ³ g/mol), PLL (M _w = 15 \times 10 ³ - 30 \times 10 ³ g/mol), QCH (M _w = 180 \times 10 ³ g/mol) at a concentration = 2g/L each. The first and outermost deposited layer is HA.....	115

Figure 4.9.	FTIR-ATR spectra of individual polymers: HA (black), PAH (red), PLL (green), QCH (blue) (a), and HA/PAH (red), HA/PLL (green) and HA/QCH (blue) capsules (b).....	116
Figure 4.10.	SEM images of dried HA/PAH, HA/PLL and HA/QCH capsules. All multilayer were composed of 4.5 bilayers (HA occurred as the first and the last deposited layer). Scale bare: 20, 5 and 2 μ m, respectively.....	117
Figure 4.11.	CLSM images of HA/PAH, HA/PLL and HA/QCH capsules as an aqueous suspension. The high intensity of green colour is the effect of fluorescent properties of FITC-dextran ($M_w = 4 \times 10^3$ g/mol) solution. FITC labelled dextran is adsorbed within the shells at high concentration allowing visualisation of capsules.....	118
Figure 4.12.	AFM image of a dried HA/PAH capsules with corresponding profile.	118
Figure 4.13.	Formation of the polyelectrolyte film on porous (a) and smooth (b) surface.....	120
Figure 4.14.	FTIR-ATR spectra of a) (HA/PAH) _{4,5} hollow dried capsules without cross-linking (thick line) and cross-linked with 50mM EDC (triangles), 200mM EDC (squares), 400mM EDC (circles). The difference between the two spectra (before and after cross-linking) is represented b).....	122
Figure 4.15.	FTIR-ATR spectra of (HA/PLL) _{4,5} hollow dried capsules without cross-linking (thick line) and cross-linked with 200mM EDC (green squares) (a) and (HA/QCH) _{4,5} hollow dried capsules without cross-linking (thick blue line) and cross-linked with 200mM EDC (blue squares) (b). Below, the differences between the two spectra (before and after cross-linking) are represented (dotted lines).....	123
Figure 4.16.	Structure of HA/QCH (a) and HA/PLL (b) multilayers with amide covalent bonds. Blue chains are from HA while the red ones are from polycations (QCH or PLL). Stars indicate the sites of amide bond formation.....	125
Figure 4.17.	SEM images of (HA/PAH) _{4,5} , (HA/PLL) _{4,5} , and HA/QCH non cross-linked (left) and cross-linked (right) hollow capsules.....	126
Figure 4.18.	CLSM images of (HA/PAH) _{4,5} , (HA/PLL) _{4,5} , and (HA/QCH) _{4,5} non cross-linked (left) and cross-linked (EDC 200mM) (right) hollow capsules incubated in fluorescent Dext-4 solution. Dext-4 dissolved in MES at pH 6.5.....	127
Figure 4.19.	HA/PAH and HA/PLL capsules cross-linked by means of 50, 200 and 400mM EDC. Scale bar =5 μ m.....	128

Figure 4.20.	AFM images of air-dried (HA/PAH) _{4,5} (up) and (HA/PLL) _{4,5} (down) cross-linked (EDC 200mM) capsules and corresponding to them thickness profiles.....	128
Figure 4.21.	CLSM images of non cross-linked HA/PAH capsules incubated in FITC-Dext -4, -500 and -2000 solutions, respectively.....	130
Figure 4.22.	Permeability of non cross-linked and cross-linked capsules. Permeability is expressed as the ratio of intensities by capsules interiors (I_{int}) and surrounding solution (I_{ext}) 20 min after mixing capsules and solutions of FITC-Dext-4. For HA/PLL the permeability was estimated only for cross-linked capsules. Cross-linking was performed using EDC at a concentration of 200mM. The average value was taken from 7-10 capsules.....	130
Figure 4.23.	Ratio of fluorescence intensities capsules interiors (I_{int}) and surrounding solution (I_{ext}) 20min after mixing capsules and solutions of FITC (squares) and FITC-dext molecules of different Mw (4 000 (rhomboids), 500 000 (triangles) and 2 000 000g/mol (turned triangles)) for HA/PAH (a) and HA/PLL cross-linked capsules (b). The covered points indicate the same permeability ratio.....	131
Figure 4.24.	Permeability of non cross-linked HA/PAH (red) HA/QCH (blue) capsules without salt (uniform columns) and with presence of salt (0.15M) (spotted dcolumns). FITC-Dext-4 were used for diffusion.....	133
Figure 4.25.	Permeability of cross-linked HA/PAH (a), HA/PLL (b) and HA/QCH (c) capsules in the absence (open squares) and in the presence (filled squares) of salt. Dextran ^{FITC} -4, dextran ^{FITC} -500, dextran ^{FITC} -2000 were used for diffusion throw HA/PAH and HA/PLL shells, while only dextran ^{FITC} -4 molecules for HA/QCH shells.....	133
Figure 4.26.	CaCO ₃ particles with adsorbed Dextr-4 (a) and Dextr-2000 (b).....	134
Figure 4.27.	CLSM images of non cross-linked (a) and cross-linked (b) (HA/PAH) _{4,5} microcapsules with encapsulated Dext-4 (top) supported with the fluorescent profile (bottom).....	135
Figure 4.28.	Permeability of the cross-linked HA/PAH and HA/PLL capsules without and in the presence of salt. Permeability was measured in two directions: diffusion of Dext-4 from external environment into interior of capsules (red columns), and liberation of encapsulated Dext-4 outside (blue columns).....	136
Figure 4.29.	Confocal and their transmission equivalent images of HA/PAH and HA/PLL non cross-linked capsules at 37°C solution and at 37°C in contact with hyaluronidase of 500 U/mL. Enzyme was dissolved in 0.02 MES solution at pH 6.5. The capsules were mixed with FITC-Dext-4 20min before observation.....	137

Figure 4.30. Degradation of cross-linked capsules (EDC 200mM) in contact with hyaluronidase at 37°C overnight. FITC-Dextr-4 were used to check permeability. FITC-Dext (2g/L) and Hase (500U/mL) were prepared in 0.02M MES at pH 6.5..... 138

List of Tables

Table 1.1.	Synthetic polymers for LbL film formation.....	7
Table 1.2.	Natural polymers used for LbL multilayer formation.....	8
Table 1.3.	Templates used for the preparation of hollow polyelectrolyte capsules...	12
Table 1.4.	Polysaccharides in LbL capsules.....	34
Table 1.5.	Occurrence of HA in different animal tissues and its content	40
Table CR 3.1	C* values of HA at various M_w	95
Table 4.1.	Molecular structures of used polycations used as partners of HA for the synthesis of microcapsules.....	103
Table 4.2.	Values of enthalpy changes for polyanion/polycation complexation measured by ITC. Concentrations: HA200=3g/L (7.4mM), HA820=3g/L (7.4mM) ; PAH=2g/L (21.3mM), PLL=2g/L (10mM), QCH=5 g/L (23mM) dissolved in TRIS or TRIS + NaCl.....	107
Table 4.3.	Values of the wall thickness of dried capsules determined by AFM and planar film thickness derived from QCM-D analysis. Capsules contain 9 layers and the planar films 8 layers.....	119
Table 4.4.	Literature data of the film thicknesses made from polysaccharides deposited on planar surface except (CH/Dext) ₂₀ deposited on the ibuprofen particles.....	121

Abbreviations

ADH	Adipic acid dihydrazide
Dextran^{FITC}	FITC labelled dextran
Dextran-4	Dextran at $M_w = 4 \times 10^3$ g/mol
DS	Degree of substitution
EDC	(<i>N</i> -(3-Dimethylaminopropyl)- <i>N'</i> -ethylcarbodiimide hydrochloride
EDTA	Ethylenediaminetetraacetic acid
FITC	Fluorescein Isothiocyanate
HA	Hyaluronic acid
HA^{FITC}	FITC labelled HA
Hase	Hyaluronidase enzyme
LbL	Layer-by-Layer
MES	2-(<i>N</i> -Morpholino) ethanesulfonic sodium buffer
PAH^{FITC}	FITC labelled PAH
PAH	Poly(allylamine hydrochloride)
PE	Polyelectrolyte
PLL	Poly(L-lysine) bromide
Sulfo-NHS	<i>N</i> -Hydroxysulfosuccinimide sodium salt
TRIS	Tris (Hydroxymethyl) Aminomethane buffer
QCH	Quaternized chitosan

Symbols

Δf	Frequency changes
M_w	Weight-average molecular weight
R_g	Radius of gyration
R_h	Hydrodynamic radius
ζ	Zeta Potential

List of Instruments

AFM	Atomic Force Microscopy
CLSM	Confocal Laser Scanning Microscopy
FTIR-ATR	Fourier Transform Infrared Spectroscopy with Attenuated Total Reflectance
ITC	Isothermal Titration Calorimetry
SEC	Size Exclusion Chromatography
SEM	Scanning Electron Microscopy
TEM	Transmission Electron Microscopy
QCM-D	Quartz Crystal Microbalance with Dissipation

ABSTRACT

Polyelectrolyte microcapsules prepared by the Layer-by-Layer deposition technique have attracted a great deal of interest for their potential applications in various fields such as drug delivery and biotechnology. The aim of this work was to develop new LbL microcapsules made from hyaluronic acid (HA) - biocompatible, biodegradable and non-toxic polysaccharide. First, optimization of conditions for preparing microcapsules from HA and poly(allylamine) (PAH) was carried out. In the second step, synthetic PAH was replaced by biocompatible cationic polymers: a polypeptide, poly(L-lysine (PLL) or a quaternized derivative of chitosan (QCH) from polysaccharide family. The influence of the polycationic partner on the morphology, stability, permeability properties and enzymatic degradation of microcapsules was analyzed. Those properties were then tuned by shell cross-linking. The encapsulation of dextran release as a model drug was demonstrated.

RESUME

Les microcapsules de polyélectrolytes préparées par de dépôt couche-par-couche suscitent depuis plusieurs années un intérêt croissant lié à leurs applications potentielles dans divers domaines, notamment ceux des biotechnologies et de la libération contrôlée de médicaments. L'objectif de ce travail était de développer de nouvelles microcapsules à base d'acide hyaluronique (HA), un polysaccharide biocompatible et biodégradable. La première partie de ce travail a consisté à optimiser les conditions de synthèse de microcapsules à partir de HA et de poly(allylamine) (PAH). Le PAH a par la suite été remplacé par des polymères biocompatibles : la poly(L-lysine (PLL), ou un dérivé de quaternisé du chitosane (QCH). L'influence du partenaire polycationique sur la morphologie, ainsi que les propriétés de stabilité, perméabilité et de dégradation enzymatique des capsules a été analysée. L'encapsulation d'un dextrane comme médicament modèle a par ailleurs été démontrée.